# THE ERBIA-HAFNIA SYSTEM

by

James Keith Johnstone

A Dissertation Submitted to the
Graduate Faculty in Partial Fulfillment of
The Requirements for the Degree of
DOCTOR OF PHILOSOPHY

Major Subject: Ceramic Engineering

Approved:

Signature was redacted for privacy.

In Charge of Major Work

Signature was redacted for privacy.

Head of Major Department

Signature was redacted for privacy.

Dean of Graduate College

Iowa State University
Ames, Iowa

1970

# TABLE OF CONTENTS

# INTRODUCTION

The oxides of the group IVA metals--Zr, Hf and Th--are among the most refractory and chemically inert oxides known. Their melting points are approximately 2700, 2800 and 3100°C, respectively. Unfortunately each oxide is excluded from general use by some characteristic fault. In the case of thoria ($ThO_2$), its general use is limited by its radioactive nature. While hafnia ($HfO_2$) and zirconia ($ZrO_2$) are not radioactive, they are characterized by a destructive crystallographic transformation that takes place at higher temperatures. The transformation is between the room temperature monoclinic form and the high temperature tetragonal form of these oxides and is accompanied by a unit cell contraction on the order of 3 volume percent. A further drawback to the general use of hafnia has been its scarcity. For this reason, the study and use of hafnia has been neglected in favor of the more plentiful zirconia.

The destructive transformation in zirconia can be eliminated by the addition of a second oxide of the form MO or $M_2O_3$. The most popular additions are CaO and $Y_2O_3$. The addition of the second oxide to zirconia causes the formation of a cubic solid solution of the fluorite[1] type ($CaF_2$, space group $Fm\bar{3}m$) and is usually characterized by a reduced unit cell

---

[1]In this thesis, fluorite will refer to the $CaF_2$ structure, and not to the mineral $CaF_2$.

volume. In this form, the zirconia is said to be stabilized. The cubic fluorite solid solution does not exhibit any crystallographic changes up to the melting point and the final result is an extremely useful super refractory material.

A further benefit is realized from the addition of a stabilizing oxide. A large number of vacancies are created on the anion sublattice brought about by the substitution of $Ca^{2+}$ of $Y^{3+}$ for $Zr^{4+}$ and the resulting decrease in oxygen content required to maintain electrical neutrality. Such a defect structure had been predicted by Wagner (1) and was confirmed by Hund (2,3). It was shown by Kiukkola and Wagner (4) that the zirconia with 15 m/o[1] calcia solid solution is an excellent solid electrolyte.

One disadvantage of stabilized zirconia is the progressive destabilization (5) which occurs on thermal cycling through the transformation temperature range (1000°C-1200°C). A natural alternative is stabilized hafnia because of its substantially higher transformation range (1600°C-1800°C) and because the smaller volume contraction (6) should provide a lesser driving force for destabilization. Furthermore, with the increased demand for zirconium metal in industry, and improved separation techniques, hafnia (since hafnium and zirconium occur together in nature) is becoming more readily available for general use.

---

[1]In this thesis, mole % will be written m/o.

Because of their inherent similarities, most of the comments made above concerning zirconia also apply to hafnia. In particular, hafnia is stabilized by addition of similar oxides and recent work (7) has shown that hafnia stabilized with 8 m/o yttria is also a solid electrolyte. The large thermal neutron capture cross section of hafnium combined with the chemical inertness of hafnia suggests possible nuclear applications. The extremes in thermal neutron capture cross section and high temperature stability of several rare earth oxides make them likely candidates for the oxide addition used to stabilize the hafnia. One such combination of interest[1] contains a large amount of erbia ($Er_2O_3$) in a composite stabilizer containing a mixture of rare earth oxides. Hafnia stabilized with yttria (a C-type rare earth) has recently been evaluated as a refractory coating for use in the Aerospace program and has proved to be more stable than calcia or magnesia-stabilized hafnia (8).

The hafnia-erbia system was chosen for this study primarily because of its possible nuclear applications. One goal was to determine the phase relations throughout the diagram. Because of its practical importance, the primary emphasis was placed on the single phase domain containing the fluorite solid solution. Since ordering within the solid solution

---

[1]Spink, D. R., Amax Specialty Metals, Inc., Akron, New York 14001. Characterization of rare earth pyrohafinate ($Re_2Hf_2O_7$). Private communication. 1967.

domain is of fundamental importance, the results were to be interpreted in terms of ordered and disordered structural models and related to anomalies in the electrical conductivity.

# STRUCTURES

## Structure of End Member Oxides

The two end member oxides of interest in this study are hafnia ($HfO_2$) and erbia ($Er_2O_3$). The crystal structure of monoclinic hafnia was recently determined by Ruh and Corfield (9) and found to be so similar to monoclinic zirconia ($ZrO_2$) (10,11) that the general aspects of the zirconia structure also apply to the hafnia structure. The structure belongs to space group $P2_1/c$ with 4 $HfO_2$ molecules in the unit cell. An interesting feature of the structure is the 7-fold coordination of Hf (9). The coordination polyhedron has been visualized by McCullough and Trueblood (11) as being derived from a cube. Four of the oxygen atoms are at each corner of the base of a cube in a planar array and one is at one of the upper corners. The remaining two oxygen atoms are at the midpoints of the cube edges connecting the unoccupied corners. The resulting polyhedron very closely resembles the basic $MO_8$ coordination group used in describing the fluorite structure (Figure 1). Smith and Newkirk (10) have discussed the spatial arrangement of $ZrO_7$ coordination polyhedra in detail and have noted several aspects that are very similar to the fluorite structure. Combining the relatively small variations in the lattice parameters a = 5.116Å, b = 5.172Å, c = 5.295Å and $\beta$ = 99°11' (12) with the structure similarities, it is not unreasonable to consider the monoclinic hafnia lattice as being

A

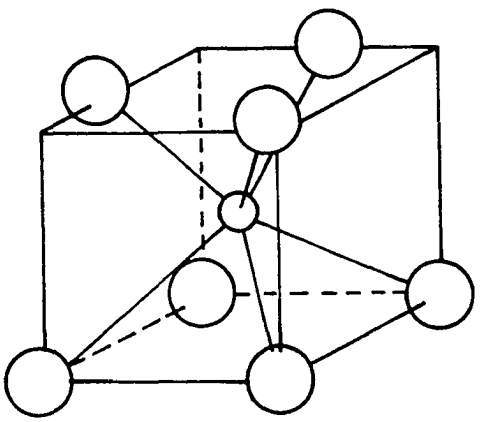

B

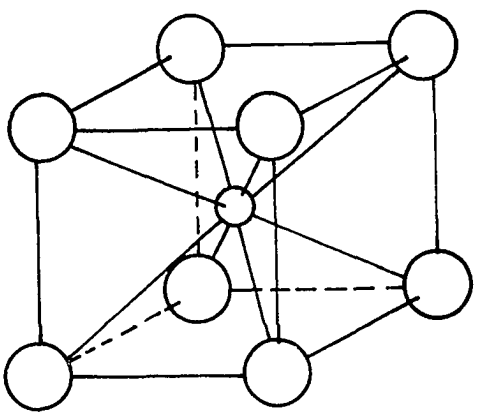

Figure 1. Oxygen coordination polydedra
A) Idealized $MO_7$ group characteristic of $HfO_2$ ($ZrO_2$) (11)
B) Basic fluorite $MO_8$ group

derived from a distorted fluorite lattice.

The monoclinic ⇌ tetragonal transformation in hafnia is a nonquenchable transformation which takes place over a temperature interval. The transformation is characterized by a hysteresis depending on whether temperature is being raised or lowered (13-16). Furthermore, at any constant temperature within the transformation range the relative proportions of the two phases do not change with time (13,14,16). Such behavior is characteristic of certain types of diffusionless transformations (13).

The transformation intervals in hafnia have been reported to occur over a wide range of temperatures and are listed in Table 1. All but one (15) of the studies used high temperature X-ray diffraction techniques. Wolten (13) noted the effects of the purity of the hafnia on the transformation ranges. The transformation occurred at higher temperatures for the sample of higher overall purity (although the sample contained the greatest $ZrO_2$ contamination). The effect of thermal history was demonstrated by Baun (14). He reported the lowest range of transformation temperatures for a sample that had not been presintered in an oxygen deficient atmosphere. When the sample was presintered at 1900°C in vacuum, the transformation temperatures on heating were raised approximately 200 and 300 degrees, respectively.

The structure of the tetragonal modification of hafnia has not been determined, while that of zirconia has been

determined by Teufer (17). However, because of their other similarities, the tetragonal forms of zirconia and hafnia are probably essentially the same (10). Thus, from analogy with tetragonal zirconia, the Hf are probably 8-fold coordinated by oxygen in tetragonal hafnia. The lattice constants of tetragonal hafnia at 1920°C have been reported by Curtis *et al.* (6) to be a = 5.14 and c = 5.25Å. The c/a ratio is near unity (= 1.002) and, combined with the probably 8-fold coordination, demonstrates the close similarity of the tetragonal phase with the fluorite structure.

A face centered cubic modification of pure hafnia has been reported by Boganov *et al.* (19) to exist at temperatures greater than 2700°C. In view of the foregoing, the cubic structure is most likely the fluorite type.

Erbia possess the cubic rare earth C-type structure (20) which belongs to space group Ia3 (21). There are sixteen sesquioxide ($Er_2O_3$) molecules per unit cell. Eight of the thirty-two erbium atoms are in position (b) (22). The remaining twenty-four erbium atoms are in position (d) and have one undetermined parameter. The forty-eight oxygen atoms are in the (e) positions with three undetermined parameters. The values of the unknown parameters have been determined for erbia by Fert (23) and are

$$x_{Er} = -0.033$$
$$x_{oxy} = 0.394$$
$$y_{oxy} = 0.149$$

Table 1. Literature values for monoclinic ⇄ tetragonal transformation in hafnia

| Purity | Monoclinic → tetragonal starting temp°C | Monoclinic → tetragonal completion temp°C | Tetragonal → monoclinic starting temp°C | Tetragonal → monoclinic completion temp °C | Reference |
|---|---|---|---|---|---|
| >99.8% | 1640 | <1920 | | | (6,18) |
| ~99.5% HfO 0.47% $ZrO_2$ | ~1620 | ~1770 | ~1700 | ~1550 | (13) |
| <99.5% HfO 30 ppm $ZrO_2$ | ~1510 | ~1690 | ~1590 | ~1460 | (13) |
| Spectrographic[a] grade | ~1480[b] | ~1600 | ~1550 | 1450 | (14) |
| | | | | | (14) |
| Spectrographic[a] grade | 1650[c] | 1900 | | | (14) |
| Nuclear grade[a] | 1593[d] | 1816 | 1638 | 1288 | (15) |
| ≥99.8% | 1900 | 2000 | | | (19) |
| Spectrographic[a] grade | 1620 | 1650 | 1620 | 1520 | (16) |

[a]Wah Chang Corporation.

[b]Not presintered in oxygen deficient atmosphere.

[c]Presintered in oxygen deficient atmosphere.

[d]Determined from thermal expansion dilatometer data.

$$z_{oxy} = 0.380.$$

The fluorite ($MO_2$) structure can be visualized as an array of cubic $MO_8$ coordination groups with the cation located at the center of the simple cubic anion cell (Figure 1B). The $MO_8$ groups share edges producing an overall face centered cubic symmetry. Hyde et al. (21) have described the C-type rare earth structure as a fluorite structure modified by having one fourth of the anion sites vacant to balance the trivalent cation charge with slight displacements of most ion positions. The resulting $MO_6$ groups share edges such that the vacant oxygen sites are arranged in non-intersecting strings along the four <111> directions of the cubic cell. This particular arrangement gives rise to two kinds of $MO_6$ groups in which the two vacant oxygen sites may be at the extremes of either a face-diagonal or of a body-diagonal (Figure 2). The resulting structure has a unit cell edge that is twice that of the fluorite unit cell and possesses body-centered-cubic symmetry. Aside from the slight displacement (<3% of the unit cell edge) of three-fourths of the cations, the cations occupy the same positions in both the C-type and fluorite structures. However, the most striking feature of the C-type structure as compared to the fluorite structure is the ordered arrangement of the highly defective anion lattice. For both structures the coordination number of the anions is four, with the cations located at the corners of a tetrahedron.

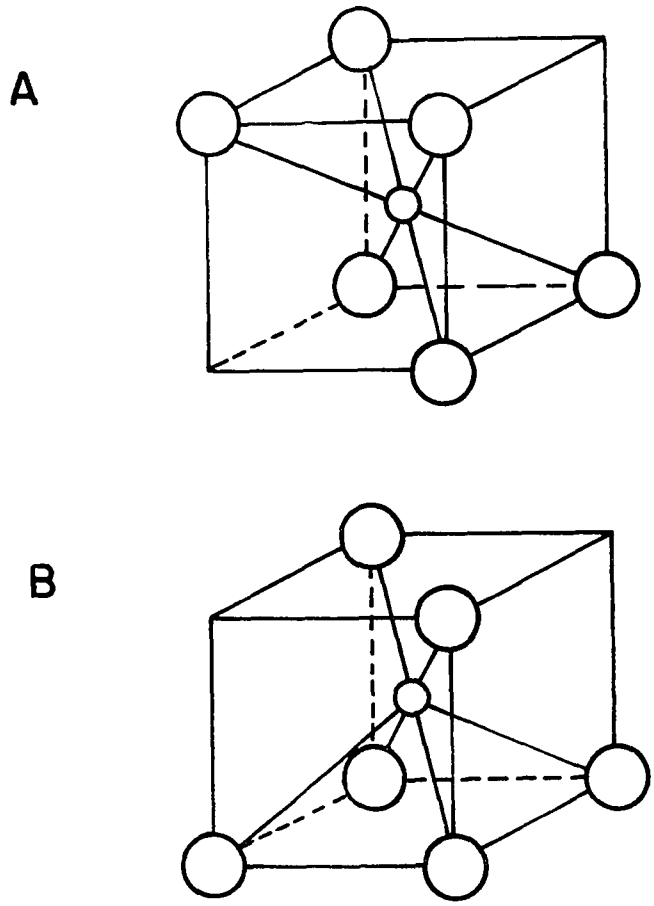


Figure 2. Idealized $MO_6$ coordination polyhedra characteristic of the C-type rare earth structure
A) Vacancies on body diagonal
B) Vacancies on face diagonal

Foex and Traverse (24) have reported the existence of a high temperature form of erbia which they designated H. The new form is probably hexagonal being related to the hexagonal A-type structure common to the lighter lanthanides at room temperature.

Since both hafnia structures are essentially distorted fluorite lattices, the structural relationship between hafnia and erbia are similar to that of fluorite and C-type rare earth oxides.

## The Pyrochlore Structure

Intermediate between the fluorite ($MO_2 = M_4O_8$) structure and the C-type ($M_2O_3 = M_4O_6$) structure lies the possible pyrochlore[1] ($M_4O_7$) structure. The pyrochlore structure may also be thought of as a distorted fluorite (25) with one-eighth of the anions missing. The structure formula is generally given as $A_2B_2X_6Y$. That the pyrochlore is a highly adaptive structure is demonstrated by its many possible compositions. According to Palache *et al.* (26), A can be Na, Ca, K, Mg, $Fe^{3+}$, $Fe^{2+}$, $Mn^{2+}$, $Sb^{3+}$, Pb(?), Ce, La, Dy, Eu, Y, Th, Zr, and U. B may be Nb, Ta, Ti, Sn, $Fe^{3+}$, and W(?) and more recently Hf (27) and Zr (25,27,28). X is generally oxygen. Only in a few cases (25,29) have substitutions been reported for oxygen

[1]In this thesis, pyrochlore will refer to the structure of the pyrochlore mineral type (26).

in this position. In these cases, it was possible to substitute for only one of the six oxygen, and the compounds were formed only under artificial, laboratory, conditions. Y can include $O^{2-}$, OH, F and Cl (25).

The space group of the pyrochlore structure is Fd3m (30) and there are eight molecules per unit cell. As in the C-type structure, the unit cell edge is approximately twice that of the fluorite unit cell. The sixteen A atoms are in position (c) of the space group. The sixteen B atoms are in the position (d), the forty-eight X atoms are in position (f) which contains one unknown parameter, and the eight Y atoms are in position (a). The eight vacant oxygen sites are in position (b). If the pyrochlore compound existed in the $Er_2O_3$-$HfO_2$ system, it would have the composition $Er_2O_3 \cdot 2HfO_2$. The structure would be described by letting A = $Er^{3+}$, B = $Hf^{4+}$, and X = Y = $O^{2-}$.

The pyrochlore structure differs from the fluorite structure by having an ordered alternation of cations in the fluorite cation positions and an ordered arrangement of the vacant anion sites. Another important difference also exists. The ordering described results in two kinds of coordination groups, $AO_8$ and $BO_6$. The most important of these is the $BO_6$ octahedra. The structural framework is composed strictly of a three-dimensional array of $BO_6$ octahedra sharing corners. The one unknown parameter, x, in the (f) set determines the shape of the octahedra and is a measure of the departure of

these oxygen from the fluorite positions. The x parameter also indicates the degree of relaxation of the oxygen toward the vacant oxygen sites. In Figure 3, the effect of various x values[1] on the shape of the octahedra is demonstrated. x = 0.25 corresponds to a fluorite-type unit with highly distorted $BO_6$ octahedra, while x = 0.312 yields regular $BO_6$ octahedra.

The A ions and the (a) set anions occupy the open spaces in the $BO_6$ framework, and it is essential that the (a) set anions should not take part in the building up of the framework (30). Thus, in contrast to the fluorite and C-type structures in which all ions participate in the network by sharing edges of coordinating polyhedra, the pyrochlore structure contains ions that are not essential to the network formation. In addition, the structure forming polyhedra share corners rather than edges.

Paradoxically, the pyrochlore structure is closely related to the fluorite structure. Although ordered, the cations in the pyrochlore structure occupy (with no displacements) positions which are precisely geometrically equivalent to the cation sites in the fluorite structure. The same is true for the (a) set anions. The only displacement occurs in the anion (f) set. As in the fluorite and C-type structures, each anion is coordinated by four cations.

---

[1]The values of x reported in this thesis are consistent with a unit cell whose origin is at $\bar{4}3m$ (22, p. 340).

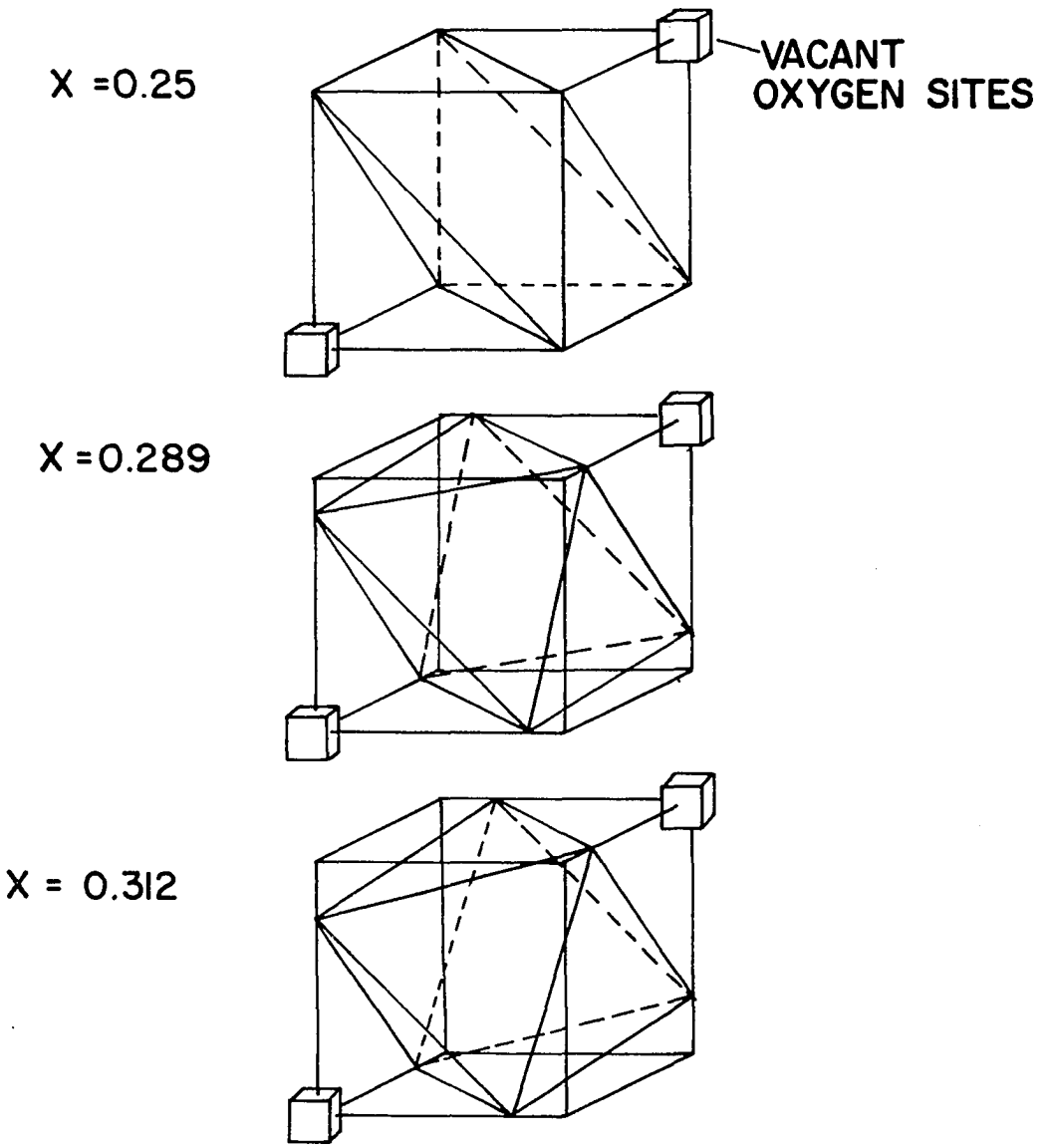


Figure 3. Effect of the (f) set x parameter on the shape of the octahedra characteristic of the pyrochlore structure

# LITERATURE REVIEW

While there is an abundance of literature on zirconia systems, there are very few comprehensive studies on hafnia systems. Reference will be made to selected zirconia systems when they may aid the discussion by providing useful analogies. After reviewing the very limited work involving erbia as the stabilizing oxide, the survey will focus on systems in which hafnia is stabilized into the cubic defect fluorite structure by other oxides. Particular emphasis will be placed on the question of ordering and compound formation (pyrochlore structure) within the fluorite solid solution region.

## Stabilized Hafnia Systems

The most comprehensive study to date involving erbia as a stabilizing additive was carried out by Rouanet (31) who determined the high temperature (>1800°C) phase relations and the liquidus curve for the $ZrO_2$-$Er_2O_3$ system. The resulting phase diagram is shown in Figure 4. The predominant feature is the nearly complete solid solution across the diagram. For compositions less than 60-70 m/o erbia, the solid solutions possess a fluorite (F) structure. For compositions greater than 60-70 m/o erbia, the solid solutions possess the C-type rare earth (C) structure. The transition from one solid solution to the other is apparently continuous, with no intermediate two-phase region. The sloping line at 60-70 m/o

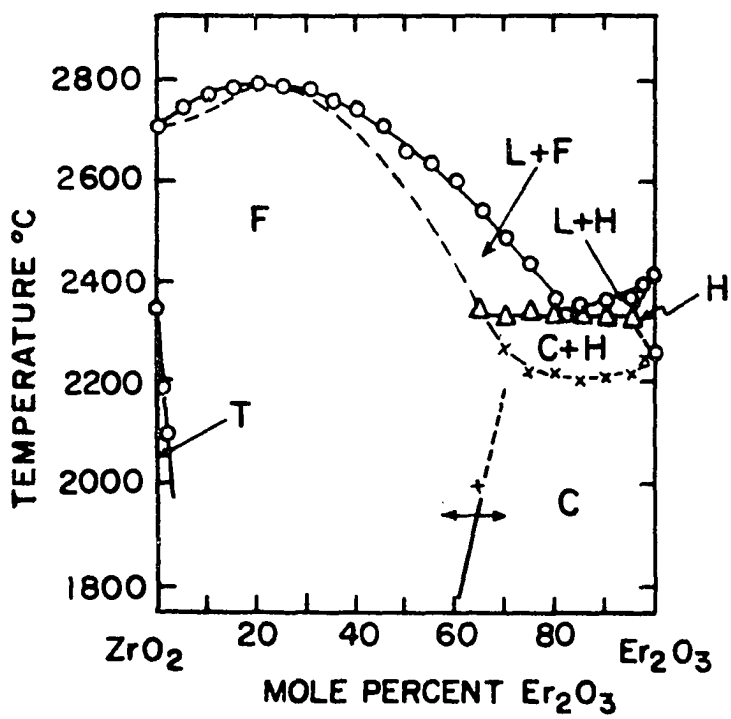


Figure 4. High temperature phase diagram for the $ZrO_2$-$Er_2O_3$ system (31)
T) Tetragonal $ZrO_2$ solid solution
F) Fluorite solid solution
C) C-type solid solution
H) Solid solution based on H modification of erbia (24)

erbia signifies the appearance of the first faint superlattice lines characteristic of the C-type structure. The domain of the H modification of erbia (24) is defined along with the two-phase region at the erbia-rich side of the diagram. The tetragonal modification of zirconia is designated T.

Stewart and Hunter (32) have reported that about 7 m/o $Er_2O_3$ completely stabilizes $ZrO_2$ in the fluorite structure. Spitsbergen and Houpt (33) were able to completely stabilize $ZrO_2$ with 4 m/o $Er_2O_3$. Kalinovskaya et al. (34) have indicated that at least 20 m/o $HfO_2$ is soluble in C-type $Er_2O_3$ forming a solid solution having the C-type structure. Neither Radzewitz (35) nor Klee and Weitz (27) were able to detect the pyrochlore structure in $Er_2Hf_2O_7$ using X-ray diffraction techniques. Only reflections characteristic of the fluorite structure were present. Klee and Weitz, however, detected some residual order in $Er_2Hf_2O_7$ from the infrared spectrum.

Some of the first studies on hafnia were carried out by Curtis et al. (6). They reported cubic hafnia solid solutions for CaO contents up to 40 m/o for samples calcined at 1800°C. However, their data, the lattice parameter vs composition relation in particular, indicate that the solid solution domain exists between 8 and 20 m/o CaO.

More recently, Delamarre and Perez y Jorba (36) have studied the $HfO_2$-CaO system at temperatures above 1000°C from 0-50 m/o CaO. A limited fluorite solid solution region was

found to exist above 1450°C. Even at 2000°C the cubic phase field only extends from 11 to 20 m/o CaO. These limits are in good agreement with the implied solid solution domain determined by Curtis et al. (6). For applications at temperatures below 1450°C the fluorite phase would be metastable, the equilibrium phases being $HfO_2$ + $CaHf_4O_9$ ($CaO \cdot 4HfO_2$). Such a tendency to destabilize would appear to limit the usefulness of calcia-stabilized hafnia.

The $HfO_2$-$Sc_2O_3$ system, where $Sc_2O_3$ has the C-type rare earth structure, has been studied by Kalinovskaya et al.(34). An extremely narrow (~1 m/o) region of disordered fluorite solid solution was found about 14 m/o $Sc_2O_3$. No pyrochlore compound was observed. However, several compounds whose structures are derived from the fluorite cubic cell were formed in the hafnia rich regions. The solubility of $Sc_2O_3$ in $HfO_2$ is less than 2 m/o. However a large single phase region of $HfO_2$ dissolved in $Sc_2O_3$ was reported. Solubilities extended to about 17 m/o $HfO_2$ at 1200°C and to 22 m/o $HfO_2$ at 2000°C.

Komissarova et al. (37) have studied the $HfO_2$-$La_2O_3$ system where $La_2O_3$ has the A-type (hexagonal) rare earth structure (20). The system exhibited the pyrochlore compound, $La_2Hf_2O_7$ which melted congruently at about 2300°C. The homogeneous solid solution based on $La_2Hf_2O_7$ ranges in composition from 30 to 40 m/o $La_2O_3$ at 1300°C. The range increases slightly with temperature, spanning from 30 to 43 m/o $La_2O_3$ at 1800°C. $La_2O_3$ was reported soluble in $HfO_2$ up to a maximum of

5 m/o $La_2O_3$, while from 5 to 10 m/o $HfO_2$ dissolves in $La_2O_3$.

The $HfO_2$-$Sm_2O_3$ system from 0 to 50 m/o $Sm_2O_3$ was studied by Isupova et al. (38) between 1000 and 1700°C. Samaria can exist in both the high temperature B-type (monoclinic) and low temperature C-type rare earth structures (20,39). The transformation temperature is about 880°C (39). A maximum solubility of samaria in hafnia of 2 m/o existed at 1000°C and decreased to 1 m/o at 1700°C. An extensive fluorite solid solution was observed in the system. At 1100°C the fluorite solid solution region extended from about 15 m/o $Sm_2O_3$ through 50 m/o $Sm_2O_3$ which was the maximum composition studied. At 1700°C the lower boundary was approximately 8 m/o $Sm_2O_3$. A pyrochlore compound, $Sm_2Hf_2O_7$, was reported to exist at 1000°C but it was observed only after the samples had been subjected to long time anneals.

The $HfO_2$-$Gd_2O_3$ system was studied by Spiridinov et al. (40) and Isupova et al. (41) at temperatures ranging from 1000 to 2300°C. Similar to $Sm_2O_3$, $Gd_2O_3$ exists in two polymorphic forms, C and B. The C to B transformation takes place at about 1200°C (39). Spiridinov et al. (40) studied the entire system at temperatures from 1000 to 2300°C. The maximum solubility of $Gd_2O_3$ in $HfO_2$ is less than 2 m/o. The fluorite solid solution extends from 20 to about 55 m/o $Gd_2O_3$ at 1200°C and from 10 to 55 m/o $Gd_2O_3$ at 2000°C. However, within the solid solution region, there exists a subregion in which pyrochlore ordering takes place. The subregion extends

from 33 to 40 m/o $Gd_2O_3$ at 1200°C and 30 to 40 m/o $Gd_2O_3$ at 2000°C. The authors note that ordering is indicated by the appearance of weak superlattice lines in the X-ray patterns that are characteristic of the pyrochlore structure. Thus, as the $Gd_2O_3$ content is increased, there is a transition from the disordered fluorite structure to the ordered pyrochlore structure. The pyrochlore compound, $Gd_2Hf_2O_7$, melts congruently at 2440°C. There is, however, no indication of a two phase region, nor is there any discontinuity in the fluorite lattice parameter vs composition curve which would denote compound formation. The subregion represents a region of homogeneous solid solution based on the pyrochlore structure which may be considered as a fluorite with ordered defects (40). A similar development of ordered pyrochlore solid solutions was noted by Perez y Jorba (42) in $ZrO_2$-$RE_2O_3$ systems (RE = Sm, Gd, Dy). Hafnia acts as a stabilizer of C-type $Gd_2O_3$ at 1900°C. Only 7.5 m/o $HfO_2$ is soluble in B-type $Gd_2O_3$ at 2000°C.

Isupova *et al.* (41) studied the region from 0 to 33 m/o $Gd_2O_3$ in the $HfO_2$-$Gd_2O_3$ system. They confirm the low solubility (<2 m/o) of $Gd_2O_3$ in $HfO_2$. They fixed the lower boundary of the fluorite solid solution region at 15 m/o $Gd_2O_3$ at 1100°C and about 7 m/o $Gd_2O_3$ at 1900°C, in fair agreement with Spiridinov *et al.* (40). In contrast, Isupova *et al.* were unable to detect any evidence of the presence of a pyrochlore compound at 33.3 m/o $Gd_2O_3$, nor was there evidence of ordering

of any kind in the fluorite phase.

The partial $HfO_2$-$Y_2O_3$ system has been studied by several workers (7,43,44). $Y_2O_3$ has the C-type structure at normal temperatures (39). Caillet et al. (44) studied the system from 0 to 50 m/o $Y_2O_3$. They note that from 0 to 8 m/o $Y_2O_3$ the system is two phase, indicating that there is very little solubility of $Y_2O_3$ in $HfO_2$. The fluorite solid solution region extended from about 9 to about 40 m/o $Y_2O_3$. No evidence of a pyrochlore structure nor of ordering within the fluorite solid solution region were observed by standard X-ray techniques which is in agreement with Perez y Jorba (42).

Isupova et al. (43) studied the same system from 0 to 40 m/o $Y_2O_3$. They found the solubility of $Y_2O_3$ in $HfO_2$ to be less than 1 m/o at 1500°C and less than 2 m/o at 1800°C. The lower boundary of the fluorite solid solution region was fixed at 10 m/o $Y_2O_3$ at 1300°C and 3 m/o $Y_2O_3$ at 1800°C. The fluorite single phase region extended through 40 m/o $Y_2O_3$, the final composition of the series studied. There was no evidence of ordering of the pyrochlore type.

Schieltz (7) fixed the lower value of the fluorite phase boundary in the $HfO_2$-$Y_2O_3$ system at 8 m/o $Y_2O_3$ which is in good agreement with the above.

Although no X-ray superlattice lines characteristic of the pyrochlore structure were noted in these studies of the $HfO_2$-$Y_2O_3$ system, Caillet et al (44) and Besson et al. (45) have inferred the existence of $Y_2Hf_2O_7$ from other measurements.

In a study of the electrical conductivity as a function of composition between 900 and 1600°C, Besson et al. related a minimum in the conductivity and an abnormally low activation energy (44) at 33.3 m/o $Y_2O_3$ (the pyrochlore composition) to the possible existence of the compound, $Y_2Hf_2O_7$. Caillet et al. (44) noted both an anomaly in the fluorite lattice parameter and a maximum coefficient of thermal expansion at the pyrochlore composition. Combining these results with the earlier study (45) led them to conclude that the compound, $Y_2Hf_2O_7$, was present. Komissarova et al. (46) noted the same conductivity minimum in the $HfO_2$-$Y_2O_3$ system but, in the absence of X-ray proof of the pyrochlore compound, cautiously assume some ordering of the cations to take place.

Radzewitz (35) made a cursory study of several $HfO_2$-$RE_2O_3$ systems (RE = Nd, Eu, Ho) at 1500°C. The three rare earth oxides chosen represent the three possible $RE_2O_3$ structures, A-, B-, and C-type respectively (39). The $HfO_2$-$Nd_2O_3$ system was extremely similar to the $HfO_2$-$La_2O_3$ system (37). A pyrochlore-type compound was detected and a domain of homogeneous solid solutions based on this structure existed between 25 and 38 m/o $Nd_2O_3$.

A large fluorite solid solution region existed between 14 and 56 m/o $Eu_2O_3$ in the $HfO_2$-$Eu_2O_3$ system. Similar to the $HfO_2$-$Gd_2O_3$ system determined by Spiridinov et al. (40), an ordered domain of the pyrochlore type exists within the fluorite solid solution field.

The fluorite solid solution domain in the $HfO_2$-$Ho_2O_3$ system extended from 8 to 55 m/o $Ho_2O_3$. About 23 m/o $HfO_2$ was soluble in the C-type $Ho_2O_3$. There was no evidence of a pyrochlore compound nor of ordering within the fluorite phase (35).

Belyaev and Artamonova (47) have recently reported the existence of the compound $Ho_2Hf_2O_7$ (and $Ho_2Zr_2O_7$); however their work deserves some comment. Their X-ray data for $Ho_2Hf_2O_7$ are listed in Table 2. The question marks in the table are theirs. All of the quantities in parentheses have been added for easier comparison and are not a part of their original data. The data were obtained from powder samples using camera techniques. The authors describe the X-ray patterns as "fairly clear". The possible (48) Miller indices for the three lowest unknown reflections are included in the table next to the appropriate question mark. The lattice parameters ($a_o$) calculated from the d-values and supposed hkl's compare very poorly with the others in the table. There is no improvement of even a single reflection when the hkl's are allowed to apply to any of the three reflections. It does not appear that these unknown reflections correspond to any of the possible pyrochlore reflections.

A fourth unknown reflection exists between the 222 and 400 reflections (47). In the pyrochlore structure, there is no possible unique reflection that can occupy that position. However, the unknown reflection indexes very well as a $CuK_\beta$ reflection from the 400 planes. The calculated d-value for

Table 2.[a] X-ray diffraction data for the compound, $Ho_2Hf_2O_7$ (47)

| hkl | I | d | ($a_o$) |
|---|---|---|---|
| ? (111)[b] | 3 | 4.482 | (7.763) |
| ? (220) | 1 | 3.960 | (11.201) |
| ? (311) | 5 | 3.312 | (10.985 |
| | | (2.993)β | (10.368) |
| 222 | 9 | 3.014 | (10.441) |
| ? | 3 | 2.867 | |
| | | (2.591)β | |
| 400 | 5 | 2.597 | (10.388) |
| 331 | 4 | 2.333 | (10.169) |
| 420 | - | (2.333) | (10.433) |
| 440 | 9 | 1.842 | (10.420) |
| 622 | 9 | 1.565 | (10.381) |
| 444 | 4 | 1.503 | (10.413) |
| 800 | 3 | 1.301 | (10.408) |
| 662 | 3 | 1.192 | (10.392) |

[a]All quantities in parentheses were added for easier comparison and were not a part of the original data.

[b]Possible allowed Miller indices for the pyrochlore structure.

the β reflection is 2.591Å as compared to 2.597Å obtained for the 400α reflection. A similar conversion of the unknown reflection designated (311) yields a d-value of 2.993Å. This is not in particularly good agreement with the d-value (3.014Å) of the 222 reflection but, in view of the overall quality of the data, it should not be discounted. The two remaining unknown peaks (designated 111 and 220) do not lend themselves to simple interpretations and therefore remain unknown. With the exception of the 331 reflection, all of the other reflection indices in the table are merely twice the

corresponding fluorite values. The 331 reflection is the only indexed reflection that is unique to the pyrochlore structure. The calculated $a_o$ for the 331 reflection is in poor agreement with the others. If the reflection is indexed as a 420 line instead, the agreement is substantially improved. Unfortunately, the 420 reflection is not allowed by the pyrochlore structure (48). Nevertheless, in the compilation of the reflection data for the $Ho_2Zr_2O_7$ compound, not presented here, Belyaev and Artamonova report an observed 420 reflection which is very questionable. The 420 reflection is allowed in the C-type structure, but the calculated $a_o$ (10.433) does not compare favorably with the lattice parameter of $Ho_2O_3$ (10.606). Thus, the reflection does not appear to be associated with possible unreacted holmia. An attempt to index the 331 reflection as the $CuK_\beta$ reflection from the 440 planes did not provide an acceptable alternative and the origin of the "331" reflection remains in question.

In view of the foregoing, the data do not support the existence of the pyrochlore compound, $Ho_2Hf_2O_7$. It should be pointed out that while Klee and Weitz (27) inferred the existence of some residual order in the compound, $Ho_2Hf_2O_7$, from their study of its infrared spectra, they were unable to detect ordering in the X-ray patterns.

## Ordering in the Fluorite Phase

The question of compound formation and ordering within the fluorite phase of $HfO_2(ZrO_2)$-$RE_2O_3$ systems is not easily resolved as can be seen from the preceding discussion. Several studies restricted solely to identifying the pyrochlore compound have been performed. In a study of the behavior of the coprecipitated hydroxides by DTA and X-ray methods, Komissarova *et al.* (49,50) have determined the formation of the pyrochlore compound $RE_2Hf_2O_7$ for RE = La and Nd. Only solid solutions of the fluorite type were found for Re = Y and Yb. Radzewitz (35) and Klee and Weitz (27) have studied the formation of the pyrochlore compound in all the $HfO_2(ZrO_2)$-$RE_2O_3$ systems. Limiting this discussion to $HfO_2$-based systems, Radzewitz found that the compound was formed for the rare earths ranging from La to Gd while only fluorite solid solutions were formed from Tb to Lu. Combining X-ray diffraction and infrared spectroscopy, Klee and Weitz determined the existence of pyrochlore compounds for rare earths ranging from La to Tb or Dy, the uncertainty arising from the rather arbitrary boundary established by the infrared analysis. The remaining rare earths formed fluorite solid solutions. However, some residual order in the $Ho_2Hf_2O_7$, $Er_2Hf_2O_7$, and $Tm_2Hf_2O_7$ compositions was detected in the infrared spectra. In general, it is found that the rare earths with larger ionic radii form pyrochlore compounds, while the rare earths with

smaller ionic radii form fluorite solid solutions.

Unfortunately, the question of order vs disorder is not settled that easily. As discussed earlier, the ordered pyrochlore structure is very similar to a disordered fluorite structure. Several of the studies presented above (35,38,40) have reported the formation of an ordered structure of the pyrochlore type within the fluorite solid solution domain. Perez y Jorba (42) studied this ordering in $ZrO_2$-$RE_2O_3$ systems. He identified the beginning of ordering by the appearance of superlattice lines in the X-ray diffraction patterns that were characteristic of the pyrochlore structure. He found that the superlattice lines were very faint at first, but that the intensity increased to a maximum as the composition approached that of the pyrochlore compound (33.3 m/o $RE_2O_3$). Further increases in the $RE_2O_3$ content caused the intensity of the superlattice reflections to decrease until they vanished leaving only the disordered fluorite solid solutions. Perez y Jorba also found for certain $ZrO_2$-$RE_2O_3$ systems (RE = Sm, Gd) that ordering existed within a domed domain characterized by a critical ordering temperature occurring at 33.3 m/o $RE_2O_3$. The critical temperature was found to be lowest for Gd, the rare earth with the smaller ionic radius of the two studied. It should be emphasized, that the ordered structure domain is a homogeneous region. Perez y Jorba was unable to detect the presence of intermediate two-phase domains and concluded that the transition was of the order-disorder type. Thus, the

similarity of the fluorite and pyrochlore structures is demonstrated on a practical basis.

In addition to the above, Perez y Jorba demonstrated a similar relation between the fluorite and C-type structures. In $ZrO_2$-$RE_2O_3$ systems where RE = Gd, Dy, and Yb, he noted the continuous transition from the fluorite solid solution to the solid solution based on the C-type structure.

Indirect evidence indicates that some degree of order exists in systems where direct X-ray methods are unable to detect it. Two such cases have already been discussed in Radzewitz's infrared spectroscopy study (35) and the study of the $HfO_2$-$Y_2O_3$ system (44,45) involving electrical conductivity, lattice parameters and coefficient of thermal expansion.

Several authors have interpreted anomalous behavior in electrical[1] conductivity (resistivity) of certain systems in terms of order-disorder phenomena in the fluorite phase. The systems $ZrO_2$-CaO and $ZrO_2$-$Y_2O_3$ have received the most attention in terms of ordering phenomena. Tien and Subbarao (52) detected a deviation from the exponential[2] behavior of the electrical conductivity of calcia-stabilized zirconia. They

---

[1]For the materials to be discussed here, the electrical conductivity has been shown to be ionic, or can be inferred to be so by comparison to similar systems (51).

[2]The temperature dependence of the electrical conductivity in most cases can be described by an Arrehnius type equation, $\sigma = Aexp(-Q/RT)$, where A is a constant, Q is the activation energy, R is the gas constant, and T is temperature ($^oK$).

found that the change depended on the heat treatment of the specimen. For temperatures below 1100°C, they found that electrical conductivity of a sample that had been annealed at 1000°C for one week was less than that of the same sample that had been annealed at 1400°C. Above 1100°C, the samples that had been previously annealed at 1000°C showed a change in slope in the log $\sigma$ vs 1/T plot and became more conductive, the electrical conductivity approaching that of the 1400°C annealed sample. Tien and Subbarao also detected the presence of extra reflections in the X-ray patterns of the 1000°C annealed samples. They indexed the lines in terms of a supercell with a cell edge four times that of the normal fluorite cell.

The dependence of these results on heat treatment was interpreted by Tien and Subbarao as indicating a reversible order-disorder transition, where the supercell and lower conductivity are indicative of the ordered state achieved in the low-temperature anneal. Upon heating above approximately 1100°C, the ordered phase became disordered. The conductivity anomaly (as well as the intensity of the X-ray superlattice lines) is more prominent with higher CaO content.

Subbarao and Sutter (53) combined those facts with conductivity vs time studies to ascribe the ordering phenomena primarily to the cation lattice. These authors argued against the decomposition of the cubic phase (i.e. precipitation of a second phase) as an alternative to ordering, because the two supposed second phases were monoclinic (tetragonal) $ZrO_2$ and

$CaZrO_3$. They were unable to detect either of these phases by X-ray or optical microscopy methods. Furthermore, they argued that the kinetics of the transformation were too fast to permit phase segregation. However, recent work has suggested the existence of an intermediate compound, $CaZr_4O_9$, at 20 m/o CaO (54). Pyatenko (55) has shown that the structure of the analogous hafnia-based compound, $CaHf_4O_9$, is derived from a very slight rhombohedral deformation of a fluorite cell. Thus precipitation and growth of a second phase may not be necessary, and the order-disorder transformation may be related to the compound, $CaZr_4O_9$.

While the anomaly in the log $\sigma$ vs 1/T plots has been observed by others (56,57), Carter and Roth (58) were unable to observe the X-ray superlattice lines for samples that had been annealed for three months.

Strickler and Carlson (57) noted a conductivity anomaly similar to that described by Tien and Subbarao (52) in yttria-stabilized zirconia. The anomaly was observed only in samples containing 20 and 25 m/o $Y_2O_3$ which had been annealed at 900°C for two weeks. As before, the anomaly occurred at about 1100°C. Strickler and Carlson have interpreted the anomaly as indicative of an order-disorder transformation. They suggest that the degree of ordering increases with $Y_2O_3$ content, attaining a maximum at about 33.3 m/o $Y_2O_3$--the pyrochlore composition. According to (57), in low yttria compositions (10 to 15 m/o $Y_2O_3$) the degree of ordering is very low, while

in high yttria compositions (>30 m/o $Y_2O_3$) the degree of ordering is high and an anomaly in the conductivity would not be detected for these extremes in ordering. Intermediate compositions would show the conductivity anomaly since the degree of ordering can be varied by annealing. They further argue that a composition dependent ordered phase would explain why the activation energy increases as the $Y_2O_3$ content increases.

Strickler and Carlson (57) were unable to detect the presence of the pyrochlore compound, $Y_2Zr_2O_7$, by X-ray methods. In a neutron diffraction study, Smith (59) was unable to detect the compound $Y_2Zr_2O_7$, but did find evidence of partial cation ordering. It should be pointed out, however, that the lowest temperature heat treatment used by Smith was 1600°C, well above the order-disorder transformation temperature of about 1100°C noted by Strickler and Carlson.

Bauerle and Hrizo (60) have related an observed curvature (distinct from the anomaly noted above) in the resistivity vs temperature curve to two possible mechanisms. One model explains the curvature in terms of a vacancy trapping mechanism where the yttrium ions act as traps for the oxygen vacancies. The second model postulated the existence of a grain boundary layer richer in $Y_2O_3$ than the bulk material. A rough calculation indicates that the layer is about 500Å thick. The activation enthalpy for conduction in the grain boundary layer is 1.17 eV as compared to 0.68 eV in the bulk grains. They

consider both models equally likely.

Another distinct characteristic of the systems discussed so far is that the conductivity of the fluorite phase decreases as the amount of the stabilizing oxide increases. Further, Strickler and Carlson (51) have noted the same behavior in $ZrO_2$-$RE_2O_3$ systems where RE = Sm, Y, Tb, and Sc. Since the conductivity is primarily due to oxygen migration through the vacancies in the anion lattice, and since the vacancy concentration increases as the amount of stabilizer increases, it would be expected that the conductivity should increase. Nevertheless, the conductivity is usually a maximum at the lower boundary (minimum stabilizer content) of the fluorite domain.

Strickler and Carlson (51) have suggested three possible explanations for this conductivity behavior:

(i) interaction or clustering of the vacancies

(ii) ordering of the vacancies (and/or cations)

(iii) formation of a second phase.

Barker (61) has argued strongly against the concept of vacancy clustering. He suggests that even the formation of a double vacancy complex (i.e. a vacancy with another vacancy as a nearest neighbor) gives rise to cations with energetically highly unstable environments. Thus, even in random solid solutions, the degree of randomness is limited.

In random (subject to the restriction just mentioned) fluorite solid solutions, Tien and Subbarao (52) have related

the decrease in conductivity primarily to the large ionic radius of the dopant cation--in this case Ca. They suggest that in migrating from site to site, the oxygen ion must pass between cation complexes of the type $Zr^{4+}$-$Zr^{4+}$, $Zr^{4+}$-$Ca^{2+}$ and $Ca^{2+}$-$Ca^{2+}$. Because of the larger ionic radius of $Ca^{2+}$ (0.99Å vs 0.78Å for $Zr^{4+}$), the energy necessary for an oxygen ion to squeeze between two $Ca^{2+}$ ions will be the greatest while that for the case of two $Zr^{4+}$ ions is the least. As the CaO content increases, the probability of encountering a cation complex containing $Ca^{2+}$ will increase. There will be an attendant increase in activation energy of conduction and an accompanying decrease in conductivity.

Substantial support to the foregoing is provided by the study of $ZrO_2$-$RE_2O_3$ systems (RE = Sm, Y, Yb and Sc) conducted by Strickler and Carlson (51). They found that the conductivity varied almost linearly with the $RE^{3+}$ ionic radius, the highest conductivity being associated with the smallest dopant ionic radius.

Another model, based on compositional fluctuations in the disordered phase, has been proposed by Carter and Roth (58) to explain the conductivity-composition dependence in calcia-stabilized zirconia. The conductivity vs composition relation is different for this case than that observed earlier. In the preceding, the conductivity was reported to be a maximum near the assumed cubic phase boundary at about 13 m/o CaO. However, the reported location of the cubic phase boundary varies from

author to author over a range from 10 to 13 m/o CaO (56). If the boundary is placed at 10 m/o CaO, the conductivity in the fluorite phase increased with increasing CaO content to a maximum around 13 to 15 m/o CaO. With a continuing increase in CaO content the conductivity decreases as described before. Carter and Roth (58) undertake to explain this second conductivity-composition relationship. Using neutron diffraction techniques, they were able to detect zones of ordered oxygen polyhedra at all temperatures. The size of the zones grows near 1000°C. From X-ray and electron diffraction coupled with electron microscopy studies, they were able to estimate that the order-disorder zones are at least 600Å in size. This compares very favorably with the 500Å thick grain boundary layer proposed by Bauerle and Hrizo (60) for the $ZrO_2$-$Y_2O_3$ system. Further evidence of order-disorder phenomena were obtained from ac and dc conductivity studies.

Carter and Roth (58) interpret their results in terms of compositional fluctuations in the disordered phase. They suggest that these "syntactic" zones are coherent and may form continuous two-dimensional sheets or networks characterized by a periodic variation in composition (i.e. spinodal decomposition). Thus, the "syntactic" zone model described calcia stabilized zirconia as composed of an interlocking network of coherent phases with differing conductivities.

From the total preceding presentation, it can be seen that the mechanism of ordering in stabilized hafnia and zirconia

systems is not resolved. While various anomalies have been interpreted in terms of order-disorder phenomena, there is little agreement as to what form of ordering is taking place; that is, whether ordering is due to compound formation, phase segregation, or cation-vacancy association. Nevertheless, the apparent sensitivity of electrical conductivity to structural changes suggests a method of detecting order.

# EXPERIMENTAL EQUIPMENT AND PROCEDURES

## Materials

The erbium sesquioxide (erbia) used in this study was supplied by the Ames Laboratory as the oxide clinker resulting from the calcination of hydrated erbium oxalate. An emission spectrographic analysis of the erbia is given in Table 3.

Table 3. Emission spectrographic analysis of $Er_2O_3$ powder

| Element | Concentration (ppm) |
|---|---|
| Al | <30 |
| Ca | 10 |
| Cr | <40 ND[a] |
| Dy | 200 |
| Fe | <40 |
| Ho | <<100 |
| Mg | <30 ND |
| Ni | <30 ND |
| Si | 500 |
| Ta | <300 ND |
| Tm | <<100 |
| W | <300 ND |
| Y | <100 |
| Yb | <50 |

[a]Not detected.

The hafnium oxide was obtained in the form of spectrographic grade hafnium oxychloride (Lot SP 10684B) from Wah Chang Corporation (Albany, Oregon). An emission spectrographic analysis of the hafnium oxychloride supplied by the manufacturer is given in Table 4. A comparative analysis of

these materials after being subjected to the sample preparation procedures described hereafter indicated that no appreciable amount of additional impurities were introduced during sample preparation.

Table 4. Emission spectrographic analysis of hafnium oxychloride

| Element | Concentration (ppm) |
|---|---|
| Al | <25 |
| B | <0.2 |
| Cb | <100 |
| Cd | <1 |
| Co | <5 |
| Cr | <10 |
| Cu | <40 |
| Fe | <50 |
| Mg | <10 |
| Mn | <10 |
| Mo | <10 |
| Ni | <10 |
| Pd | <5 |
| Si | <40 |
| Sn | <10 |
| Ta | <200 |
| Ti | <20 |
| V | <5 |
| W | <20 |
| Zr | 64 |

## Sample Preparation

The various sample compositions were prepared by coprecipitating acid solutions of the two starting materials. The hafnium oxychloride was dissolved in distilled water with the $HfO_2$ concentration determined by standard gravimetric tech-

niques. The standardization of the hafnia solution based on six determinations was 0.0958 gm. $HfO_2$/ml. solution.

The erbia was dissolved in boiling 4N HCl. The concentration of the erbia solution based on three determinations was 0.0320 gm. $Er_2O_3$/ml. solution. The concentration of a second solution prepared after the first was used up was 0.0502 gm. $Er_2O_3$/ml. solution based on five determinations.

The samples were formulated to yield 3-4 grams of final material. The desired compositions were achieved by combining the appropriate amount of each solution in a Pyrex beaker. The volumes of the individual solutions were measured either with various volumetric pipets or with 50 ml. burets. To insure intimate mixing, the combined solutions were mixed vigorously with a magnetic stirrer for at least one hour. The cations in solution were precipitated as hydroxides by adding the solution slowly to an excess of concentrated ammonium hydroxide which was being stirred vigorously with a magnetic stirrer. The hydroxide precipitate was of a gelatinous nature, so the precipitate was mixed for at least 1/2 hour to insure complete reaction. At the conclusion of each coprecipitation, the liquor was tested with litmus paper to be sure that it was still basic and thereby insure that the coprecipitation was complete. The speed of filtration was increased by allowing the coprecipitate to settle for at least an hour before filtering. The gelatinous nature of the coprecipitate seems to preclude any segregation.

The precipitate was filtered in a semiquantitative manner through a moderately retentive filter paper (Carl Schleicher and Schuell Co. No. 589 White Ribbon filter paper) and washed with distilled water. There was no evidence of any of the precipitate passing through the filter paper with the filtrate.

Following filtration, the filter paper containing the precipitate was removed from the funnel, the tops were folded loosely shut, and it was placed in a beaker and dried at 130°C in a drying oven over night. Upon completion of drying, the sample was removed from the filter paper, placed in a clean porcelain crucible and calcined at 1000°C for at least 3 hours. A thermal gravimetric study showed that the conversion to the oxides is rapid and irreversible at 1000°C.

The calcined clinker was ground to -325 mesh with a Diamonite mortar and pestle (Diamonite Products Manufacturing Co., Shreve, Ohio). Samples to be used for determining phase relations were pressed into pellets in a 3/8 in. diameter tungsten carbide lined steel die to 45,000 p.s.i. Samples used for electrical conductivity and open circuit emf studies were pressed in a 1/2 in. diameter tungsten carbide die to 5,000 p.s.i. then isostatically pressed to 50,000 p.s.i. The pellets were placed in a covered erbia crucible (2 or 3 at a time) with rhenium or tungsten sheet used to separate the individual pellets within the crucible. The pellets were then annealed in a resistance tungsten heating element furnace (Centorr Associated, Inc., Suncook, New Hampshire) operating

in an inert atmosphere of flowing argon. All samples were subjected to identical annealing cycles of one hour at 1900 to 1950°C. Generally, samples were furnace cooled from the annealing temperature to 1000°C in less than 4 minutes. The erbia-hafnia compositions were varying shades of gray after the high-temperature anneal, depending on their composition. Samples with low erbia content were light gray while samples with high erbia content were nearly black. This was attributed to reduction by the furnace atmosphere (7). The dependence of the degree of reduction on the erbia content is consistent with the gross reduction in pure erbia observed by Berard et al. (62). Annealing the disks for several hours in air at 1000°C restored the samples to their initial color (various shades of pink depending on the erbia content).

The sintered disks to be used for electrical conductivity measurements were surface ground on a polishing wheel until the two surfaces were parallel within ± 0.005 mm. The disks were fixed to the end of an aluminum rod with Loc-Wax-20 (Geoscience Instruments Corp., Mount Vernon, New York) and mounted in a small laboratory lathe. In this arrangement, the disks were formed into regular right cylinders by machining with a diamond tipped tool. The general dimensions of samples treated in this manner were 9.5 to 10.5 mm. in diameter and 1 to 2 mm. thick. The exact dimensions were taken with a micrometer and measured to the nearest 0.01 mm. The L/A ratios were calculated from these values and used to convert

the measured conductances to conductivities.

Densities were determined by the water immersion technique. Following density determinations, the samples to be used for the determination of phase relations and melting points were ground to -325 mesh.

Various samples were subjected to long time anneals and varying quenches. In all cases these samples had been subjected to the initial 1900°C anneal for one hour. The anneals were conducted in air in either a silicon carbide resistance furnace or a Pt-40% Rh resistance furnace. Annealing temperatures were 1400 to 1450°C and 1000°C. Times were 24, 72, and 170 (one week) hours. The samples were either furnace cooled, or quenched in an ice bath.

## Room Temperature X-ray Diffraction

Lattice parameters and phase identification at room temperature were determined using diffractometer and film techniques. The diffractometer was a Norelco Wide Range Diffractometer (Philips Electronic Instruments, Mount Vernon, New York) with the associated Mark III Data Control and Processor electronics system. Cu radiation was employed using a standard β-filter of Ni. The diffracted radiation was detected with a proportion counter. The pulse height analyzer (PHA) option in the data control panel was engaged. The PHA had a resolution time of 2 μsec.

The goniometer was carefully aligned mechanically and the

alignment was checked periodically using a polycrystalline silicon standard sample provided by the manufacturer.

The -325 mesh powder samples were carefully pressed into a 10 mm x 20 mm x 0.4 mm cavity which had been milled into 1/8 in. thick aluminum. The samples were scanned at a rate of $1^{\circ}$ $2\theta$/min., always in the direction of increasing $2\theta$. $1^{\circ}$ divergent and antiscatter slits and a 0.006 in. receiving slit were used for all ranges $2\theta$.

Powder photographs were obtained using a Debye-Scherrer camera with Straumanis mountings. Ni filtered $CuK_{\alpha}$ radiation was used. In one case, Fe filtered $CoK_{\alpha}$ radiation was used. Exposure times ranged from 7 to 30 hours. The films were read using precision techniques.

The lattice parameters were calculated using the analytical method of Hess (63) as modified for diffractometer data and programmed for computer solution by Vogel and Kempter (64). The error function used was $\cos\theta \cot\theta$. No correction was made for variations in ambient temperature. Both $CuK_{\alpha_1}$ and $CuK_{\alpha_2}$ Bragg reflections greater than $60^{\circ}$ $2\theta$ were used in the determination.

## Structure Determinations

The integrated intensities of the Bragg reflections were obtained for comparative structure determinations. The same experimental configuration described above for the diffractometer was used in these experiments except that the depth of

the sample holder was increased to 0.8 mm. The integrated intensities were found using a continuous scan technique and were recorded by the Data Processor unit of the Mark III Data Control and Processor system. According to the manufacturer, the Data Processor could operate in excess of 200,000 counts/sec. The scan times through a Bragg reflection ranged from 144 to 480 sec. The background intensities were obtained on each side of the Bragg reflection using 100 sec. count time intervals. The net integrated intensity was obtained by assuming a linear relation between the two background counts and subtracting the resultant total background from the total integrated intensity. Intensity data were gathered for 10 reflections.

The net observed intensities were converted to structure factors, $|F_o|$, through Equation 1

$$|F_o| = [I_o/(LP \cdot j)]^{\frac{1}{2}} \qquad (1)$$

where $I_o$ is the observed intensity, LP are the Lorentz and polarization factors, and j is the multiplicity. The combined Lorentz and polarization factors were calculated for each reflection with Equation 2

$$LP = (1+\cos^2 2\theta)/(\sin^2\theta \cos\theta). \qquad (2)$$

The multiplicities were obtained from Cullity (65).

The structure refinement was made using the least squares crystallographic program of Busing et al. (66). The atomic scattering factors given by Cromer and Waber (67) were used

for $Hf^{4+}$ and $Er^{3+}$ and those given by Tokonami (68) were used for $O^{2-}$. The anomalous dispersion corrections given by Cromer (69) were used. The refinement was based on the structure factors.

## High Temperature X-ray Diffraction

The high temperature X-ray diffraction studies were made with a MRC (Materials Research Corporation, Orangeburg, New York) Model X-86-N3 high temperature X-ray diffractometer attachment for the Norelco Wide Range Goniometer. The furnace attachment is based on the design of Intrater and Hurwitt (70) and has been discussed in detail elsewhere (71). The furnace attachment is capable (manufacturer's claim) of operating at temperatures from -120 to 2500°C and in vacuum or controlled atmospheres. This work was performed at temperatures from 1050 to 1950°C in vacuum.

The furnace attachment consists of a water-cooled, cylindrical chamber fabricated from highly polished aluminum and is designed such that the cylinder axis is mounted coincident with the goniometer axis. A specimen stage composed of heating electrodes and alignment gearing is mounted in the furnace chamber. A very thin layer of sample is spread on a metal resistance strip heater that is clamped between water-cooled

brass[1] electrodes. The curved surface of the furnace chamber is fitted with vacuum tight, 10 mil thick beryllium windows which pass the incident and diffracted X-ray beam with a minimum of absorption. The beryllium window permits a diffraction range of $0^{\circ}$ to $160^{\circ}$ $2\theta$. The specimen stage can be adjusted in elevation, azimuth rotation and translation under operating conditions without loss of temperature or vacuum. The elevation is controlled by a micrometer screw which provides for fine adjustment. A port in the chamber cover allows optical temperature measurements. The sight angle is approximately 50 to $55^{\circ}$ from the normal to the sample surface.

The furnace attachment was provided with a power supply capable of automatic proportional control through a silicon controlled rectifier or manual control through a rheostat. Because of the high temperatures required, the power was controlled manually in this work.

---

[1]Brass is a poor material to use for the electrodes when the furnace is to be used at high temperatures (>1700°C). It was found during initial experiments that the zinc and lead components tended to distill out of the brass and coat the inside of the chamber at high operating temperatures. While it was not difficult to clean the furnace chamber, it was, nevertheless, a mess. The problem was solved by baking the system at temperatures above those to be attained in normal use. Some distillation still occurred, but it was very slight and did not interfere in any way with the experiments. Still, it is felt that copper would be a better choice for the electrode material.

A conventional 1 1/2 in. vacuum system incorporating a mechanical pump, an air-cooled oil diffusion pump and a liquid nitrogen cold trap was designed for use with the furnace attachment. All but the mechanical pump were mounted on a mobile chassis that was constructed to be in alignment with the vacuum port in the furnace chamber and which could be wheeled into place as needed. The mechanical pump was mounted on a separate platform to eliminate vibrations that could disturb the furnace alignment. The furnace attachement was fitted with an ordinary rotating O-ring seal. The furnace was coupled to the vacuum system through a flexible stainless steel bellows. Easy access to the furnace was achieved by using Heraeus-Engelhard Quick-Flange vacuum fittings. The system routinely achieved vacuums of $5 \times 10^{-5}$ torr. The same vacuum system was coupled with the furnace used for melting point determinations which is described in the next section.

The furnace attachment was mounted on the goniometer which had previously been carefully aligned. The elevation, azimuthal, translation and 2θ alignments were carried out at $0^{\circ}$ 2θ using a 1 mil slit provided with the equipment. The alignment was checked with a special standard silicon sample fabricated for mounting in the furnace. In the course of the experiments, it was found that once the furnace attachment was properly aligned, the alignment did not change from run to run. Nor was it found necessary to adjust the alignment at operating temperatures. Nevertheless, the $0^{\circ}$ 2θ alignment was

checked with the alignment slit between each run.

A photograph of the two types of heaters used with the sample in place is given in Figure 5. Pt-40% Rh (5 mils thick) was used to form the specially shaped heater (71) on the left of Figure 5. The tungsten heater and sample arrangement normally used in this work is shown on the right of Figure 5.

The tungsten heating elements were formed in the shape of an inverted flat-bottomed U from a 1 1/2 x 5/16 x 0.002 in. strip of tungsten sheet. The flat surface available for sample placement was 5/16 x 3/8 in. A new heating element was used for each sample.

The sample was mounted on the heater by first placing a small amount of -325 mesh sample on the heater surface. A small camel hair brush that had been dipped in a concentrated water solution of Carbowax 4000 (Carbide and Carbon Chemical Co., New York, New York) was used to wet the sample and spread it evenly across the heater surface after which the slurry was allowed to dry. The dried wax adhered tightly to the heater surface. The binder also formed a protective, wax-like crust which permitted rather casual handling of the heater/sample combination. With some practice, it was possible to consistently obtain uniform samples that were less than 2 mils thick.

Once dry, the edges of sample were trimmed with a glass slide so that the remaining sample was centered within the uniform hot zone of the heater (72). The final sample size

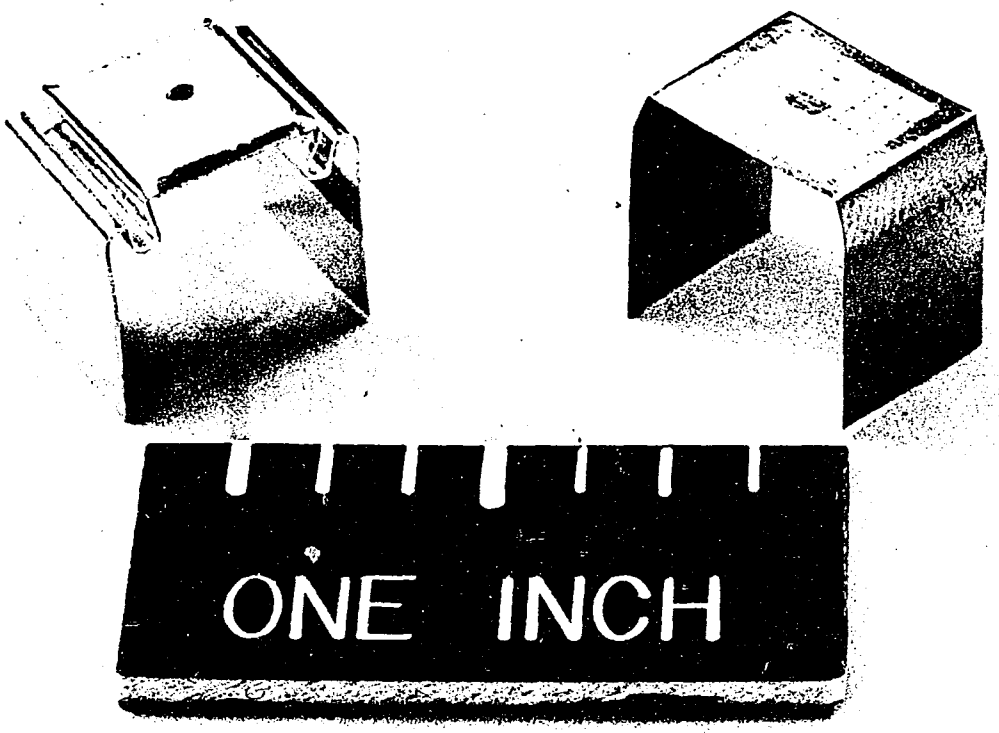


Figure 5. Photograph of the heater/sample configurations used in the high temperature X-ray furnace. Left side: Pt-40% ribbon; Right side: Tungsten ribbon

was approximately 1/4 x 5/16 in. A small area in the center was scraped clean of sample to expose the tungsten surface for temperature measurements. The sample surface was scored in a grid configuration to relieve stresses within the sample caused by sample shrinkage due to sintering and heater expansion. The grid also served to improve temperature uniformity.

The combined heater/sample was mounted in the furnace and aligned relative to the X-ray beam with the alignment slit. The wax binder protecting the sample greatly improved and simplified the alignment procedure since it was not necessary to worry about disturbing the sample. The protective coating made it possible to clamp the heater/sample to the alignment slit thus insuring correct alignment while the legs of the heater were being clamped in the electrodes.

Once fastened in place, the sample was scanned with X-rays to confirm the alignment. The X-rays were shut off, and then the binder was removed by passing sufficient current through the tungsten heater to melt and burn off the wax. This process was carried out in air. An added benefit was the tendency of the melting process to further even out any irregularities in the sample surface. When the binder was completely removed, the current was shut off, and the furnace chamber was sealed and evacuated. The alignment was again checked with X-rays before heating was begun.

The samples were scanned at $1^{\circ}$ $2\theta$/min. with nickel-filtered $CuK_{\alpha}$ radiation using $4^{\circ}$ divergence and antiscatter

slits and a 0.006 in. receiving slit. A special removable nickel filter was constructed of 0.35 mil nickel foil. The filter was fitted to the inside perimeter of the furnace chamber such that it lay between the heater and the beryllium windows. In this configuration, X-rays had to pass through the filter both upon entering and leaving the furnace chamber. Besides serving as a $CuK_\beta$ filter, the nickel foil acted as a heat shield and protected the beryllium windows from contamination by vapor deposits.

Temperatures were measured optically with a Pyrometer Instrument Co. Model No. 95 disappearing filament micro-optical pyrometer. The micro-optical pyrometer was calibrated against a NBS standard lamp. To eliminate errors that could be caused by varying surface conditions, varying sample composition and possibly the tungsten substrate (73), the temperatures read were those of the tungsten surface. Due to the angle of observation ($\sim 53^\circ$) and the smooth surface of the tungsten ribbon, it was not possible to apply normal emissivity corrections to the observed temperatures. It was necessary instead to calibrate the micro-optical pyrometer against melting points of standard materials. A small amount of material was placed on the tungsten ribbon and heated slowly under experimental conditions. The filament of the micro-optical pyrometer was focused on the tungsten ribbon adjacent to the standard material and the observed melting temperature noted. The materials used and the corresponding temperature observations are given

in Table 5.

Table 5. Calibration points of the micro-optical pyrometer for the X-ray furnace attachment

| Material | Observed melting point °C | True melting point °C (74) |
|---|---|---|
| Au | 989<br>990<br>993 | 1063 |
| Ni | 1335<br>1328<br>1328<br>1335 | 1453 |
| Pd | 1419<br>1400<br>1380<br>1410 | 1552 |
| Pt | 1615<br>1590<br>1612<br>1597 | 1769 |
| Rh | 1785<br>1775<br>1790<br>1796<br>1760<br>1772 | 1960 |
| $Al_2O_3$ | 1835<br>1835 | 2040 |

It should be pointed out that all calibration materials used except $Al_2O_3$ are fixed or secondary points of the International Temperature Scales (74). The method used to calibrate the micro-optical pyrometer includes the corrections for the fused quartz sight port. Due to the dependence of the observed

temperature on the angle of observation, care was taken during the course of the experiments to be sure that the temperature measurements were made in the same experimental configuration that was used for the calibration.

Three experiments that did not require temperatures greater than 1600°C were performed using Pt-40% Rh heating elements. A second calibration curve was determined for the micro-optical pyrometer. The bead of a Pt-13% Rh thermocouple was placed on the ribbon surface and the pyrometer focused next to it. The temperature was varied in 100°C increments on both heating and cooling. The calibration curve was obtained by plotting the thermocouple reading vs the micro-optical pyrometer reading.

The high temperature studies were made at five approximate temperatures; 1200, 1400, 1600, 1800, and 1900°C. The sample was brought to the desired temperature and 10 to 15 min. allowed for the temperature to stabilize. The major Bragg reflections were scanned immediately to detect any rapid changes. Scan intervals ranged between 26 and 53° 2θ which included the major peaks of all phases studied. Phase changes were noted by the appearance or disappearance of the characteristic Bragg reflections. Exact temperatures were determined at the beginning and end of each scan. Soak times at temperature ranged from 45 min. to 12 hrs. During the soaking time, the sample was continuously scanned with X-rays. If there was no change in the relative peak intensities of the various

phases present in a 45 min. to 1 hr. period, the temperature was raised to the next value.

Studies were normally made during the heating cycle. Upon cooling, parts of the sample had a tendency to come loose from the tungsten ribbon which caused large temperature gradients to exist. The loose part was much cooler. Nevertheless, it did not happen for all samples, and in some cases, studies could be made on cooling as well as on heating.

Temperature gradients in the plane of the sample surface were measured with the micro-optical pyrometer. For correctly fabricated samples, the gradients were found to be less than 25°C and tended to decrease at higher temperatures.

## Melting Point Measurements

A modified version of the microfurnace used by Statton (75) was designed and built for determining the melting points of the various hafnia-erbia compositions. The primary design criteria were that the apparatus a) be capable of reaching temperatures in excess of 2900°C, b) provide for optical temperature measurement, and c) be operable in vacuum or inert atmospheres. Simplicity of operation was also an important consideration. Tungsten was chosen for the heating element because of the high temperatures required.

A schematic diagram of the apparatus is shown in Figure 6. The tungsten ribbon (G) served as both heating element and sample support. The ribbon was clamped between two copper

blocks (F) which were silver soldered on water-cooled electrodes (E). A single set of radiation shields (H) surrounded the heating chamber. The entire assembly was enclosed in a water-cooled copper housing (B). The housing was fitted with a port (D) that could be used to draw a vacuum or for operating in inert atmospheres. In general operation, the entire housing was removed between determinations to provide easy access to the tungsten ribbon. Power was supplied through a variable transformer connected in series with a high current transformer with a secondary rating of 10 volts and 500 amps. The maximum power required (2900°C) was approximately 0.96 KVa (8 volts and 120 amps.) for a 1 1/2 x 5/16 x 0.002 in. tungsten ribbon.

A fused quartz sight port (A) on the top of the housing provided a means for optical temperature measurement. The quartz window was mounted eccentrically over the port. This arrangement allowed the window to be rotated to a new position while taking temperature readings and eliminated errors which could be caused by vapor deposits. Added protection against vapor deposits was provided for the window by a shutter assembly (K and L) which was mounted in the top of the housing.

A gas feed-through could be substituted for the shutter control knob (L) which provided a means of introducing inert atmospheres. Although not shown in Figure 6, the flanges of the housing were drilled and tapped for bolts to provide a positive seal in case experiments were performed in inert

Figure 6. Schematic drawing of the furnace used for melting point determinations

A. Fused quartz sight port; eccentric mount
B. Copper housing
C. O-ring seal
D. Vacuum port
E. Water cooled electrodes
F. Copper blocks for clamping heating elements
G. Tungsten heating element/sample support
H. Radiation shields
I. Electrical insulating vacuum seal
J. Cooling coils
K. Sight port shutter
L. Sight port shutter control knob

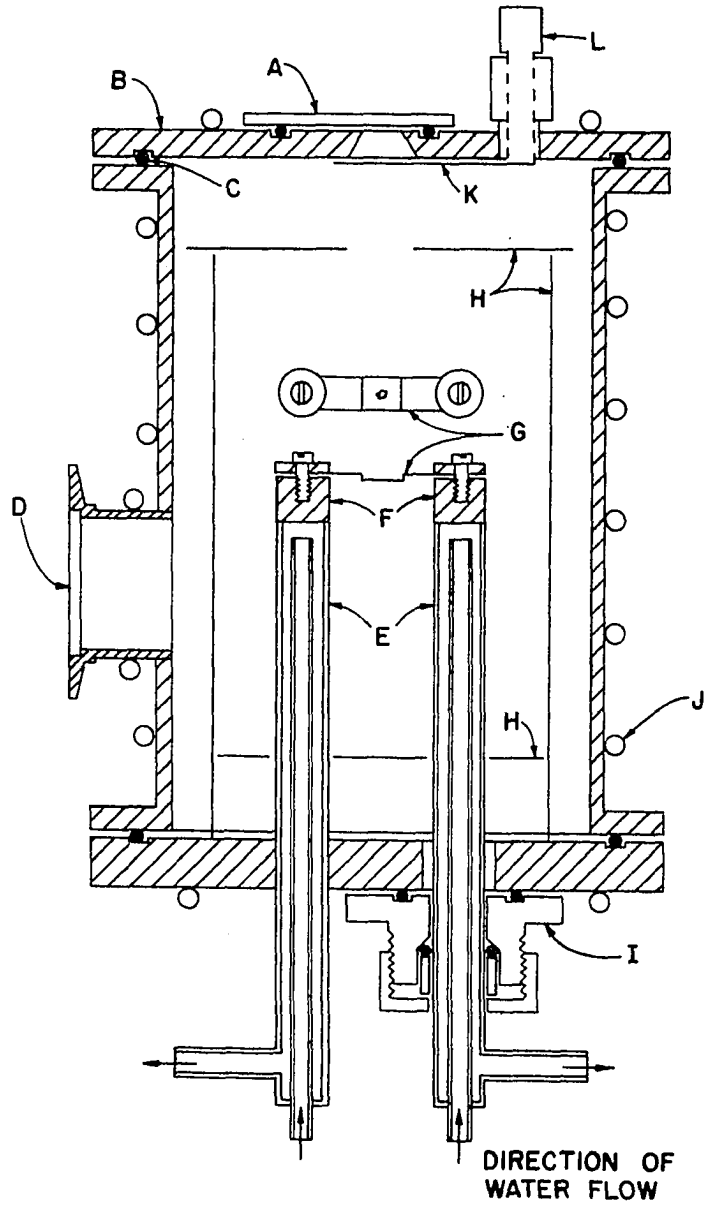
L
A
B
C
K
H
G
F
D
E
H
J
I
DIRECTION OF
WATER FLOW

atmospheres.

Temperatures were measured with the disappearing filament micro-optical pyrometer described in the section on high temperature X-ray procedures. The pyrometer was sighted normal to the surface of the tungsten ribbon. Observed temperatures were read from the surface of the ribbon. As noted before, this eliminated errors that could arise through variation in properties of different samples and related the temperatures of all determinations to the same reference material--tungsten.

The correction for absorption in the fused quartz window was obtained as a function of temperature in the following manner. The window to be used during the experiments was removed from the apparatus and another substituted. The tungsten ribbon was heated to a certain temperature that was measured by a pyrometer. Keeping the temperature fixed, the quartz window to be calibrated was inserted between the pyrometer and the ribbon and the decrease in the observed temperature noted. The temperature dependence was obtained by repeating the procedure at several temperatures. The corrections were applied to the observed temperatures which were then converted to true temperatures by applying the normal spectral ($\lambda = 0.65$ ) emissivity corrections for tungsten (76).

As an independent check on the calibration curve ($T_{true}$ vs $T_{observed}$), the melting points of several refractory materials were determined and compared with the literature values. The results of the determinations are given in Table 6. The

table shows that both the precision and the accuracy of the method are excellent.

Table 6. Melting points[a] of refractory materials measured with melting point apparatus and compared to literature values

| Material | Observed temp. | True temp. | Average true temp. | Literature value(s) (77) |
|---|---|---|---|---|
| $Al_2O_3$ | 1838 | 2033 | | |
| | 1838 | 2033 | 2020 | 2040- |
| | 1822 | 2020 | ± 9 | 2050 |
| $Y_2O_3$ | 2142 | 2412 | | 2410- |
| | 2137 | 2407 | 2410 | 2420 |
| Ir | 2158 | 2433 | | |
| | 2170 | 2447 | | |
| | 2182 | 2460 | | |
| | 2163 | 2438 | 2444 | 2443 |
| | 2168 | 2440 | ± 16 | |
| Mo | 2315 | 2635 | | |
| | 2290 | 2602 | | |
| | 2308 | 2625 | | |
| | 2303 | 2620 | 2621 | 2610- |
| | 2306 | 2623 | ± 14 | 2630 |
| $ZrO_2$ | 2365 | 2703 | | |
| | 2354 | 2689 | | |
| | 2366 | 2705 | | |
| | 2338 | 2670 | 2687 | 2677- |
| | 2338 | 2670 | ± 18 | 2722 |

[a]All temperatures in °C.

All of the experimental values listed in Table 6 were determined in vacuum. The possible effect of the vacuum on the melting points of the standards and the hafnia-erbia compositions was checked by performing several determinations in

both flowing and static argon atmospheres. The observed melting points were identical to those observed in vacuum. Therefore, due to the greater simplicity of the procedure, all determinations were made in vacuum.

Melting points were determined by placing a small amount of sample (<1 mg) on the tungsten ribbon as shown in Figure 7. To prevent the sample from shifting around during the initial set up procedure, it was fixed to the ribbon with a drop of alcohol saturated with stearic acid. The heat shields and the furnace housing were set in place and the system evacuated to $10^{-4}$-$10^{-5}$ torr. Voltage was applied to the tungsten ribbon until a temperature of about 1400°C was reached. The stearic acid had volatilized well before this temperature was achieved. The temperature was held constant while the micro-optical pyrometer was aligned and focused. The U-shaped disappearing filament of the pyrometer was focused on the tungsten ribbon as close as possible to the sample. The sample was heated rapidly to within about 50°C of the expected melting point--the approximate value determined initially for each composition. The last 50°C were traversed as slowly as possible (but continuously) until the sample was observed to melt. Heating was stopped immediately, and the observed temperature was recorded. The quartz window was rotated and the temperature measured again. In all cases, there was less than 20°C difference in the two readings. Following the last temperature reading, the power was turned down and off and another sample

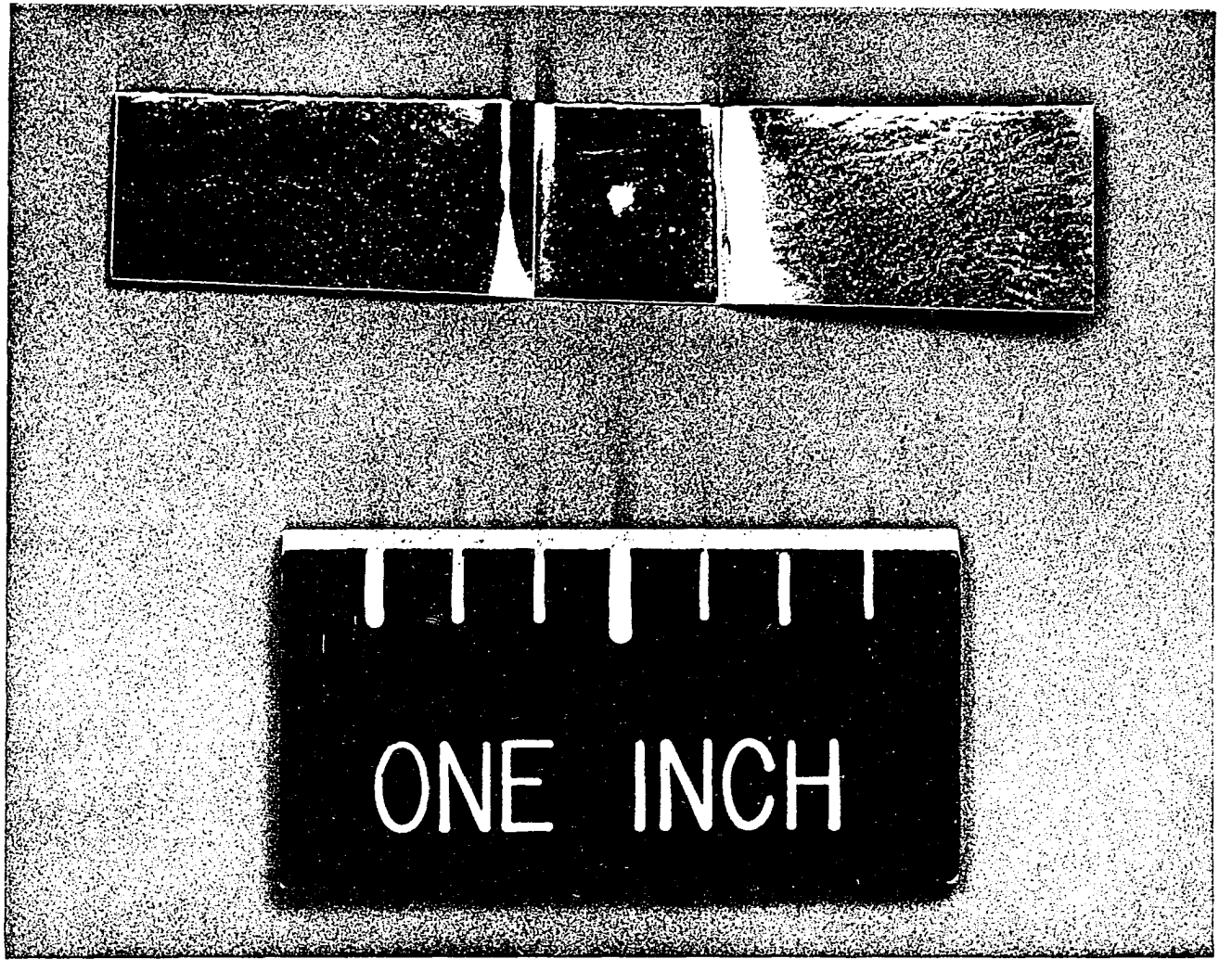


Figure 7. Photograph of a tungsten ribbon used in the melting point furnace. Note the sample in the depression

was prepared. As many as 5 or 6 determinations could be made on a single tungsten ribbon.

The melting point transition was always definite and could be easily observed. The transition was characterized by an abrupt increase in the brightness of the sample as it changed from solid to liquid. The pile of sample also exhibited a very obvious slump when melting took place.

## Electrical Conductivity Measurements

The apparatus and general procedures followed in electrical conductivity and emf studies has been described in great detail elsewhere (7). The ac electrical conductivities were determined using the two probe technique. The right cylinder disks were coated on the flat surfaces with porous platinum paste which in controlled atmospheres served as reversible electrodes. Successive coatings were applied until less than 0.5 ohm resistance existed between any two points on a surface. Each coating was fired at about 1000°C for at least one hour. The samples were backed with platinum electrodes fabricated from 1 mil platinum foil.

An experimental assembly (cell) consisted of three samples stacked one on top of another with the platinum foil electrodes sandwiched between. The cell was placed on a vertical alumina support pedestal and held in place by a spring loaded alumina cap. The cap also helped maintain good electrical contact throughout the cell. An air-tight chamber

was obtained by surrounding the entire assembly with a closed-end impervious alumina tube. The open end was sealed with a conventional O-ring seal. The platinum electrodes were connected to platinum leads which in turn exited the chamber through vacuum tight feedthrough connectors.

A Nichrome, noninductively-wound Marshall furnace was used to attain temperatures up to 1000°C. Temperatures were controlled to within ± 1°C with a West stepless silicon controlled rectifier coupled with a West proportional controller. The furnace maintained a three inch hot zone about the cell with a maximum temperature gradient of 2°C (7). Induced voltages were eliminated by placing a grounded Inconel shield between the furnace windings and an impervious alumina tube that enclosed the cell.

Once the cell and furnace were in place, the system was evacuated with a mechanical pump to about 25μ and the system baked out at 200°C for several hours. The temperature was then raised to 1000°C and the desired atmosphere introduced. The atmosphere was maintained at a very slow flow rate to insure uniformity around the cell. The ac conductivity measurements were made with a Wayne-Kerr Model 221 Universal bridge at a frequency of 1592 Hz. The measurements were repeated periodically until the conductance changed by less than 1% in a one hour interval. The temperature was lowered in 50 or 100°C increments and a conductance measurement made after each increment. At 800°C, temperatures were raised in

equal increments back to 1000°C. The increments were staggered so that only the 1000°C measurement overlapped.

Conductances were measured at 1000°C in six different controlled atmospheres. These atmospheres had oxygen partial pressures of 1, $10^{-1}$, $10^{-2}$, $10^{-7.8}$, $10^{-10}$, and $10^{-14}$ atmospheres of oxygen. The first three partial pressures were obtained from pure oxygen or He-$O_2$ gas mixtures. The oxygen partial pressure of $10^{-7.8}$ atm corresponds to purified helium. (The partial pressure was measured under experimental conditions with an oxygen gage (7)). The lowest two partial pressures were obtained with $CO_2$-CO gas mixtures. The desired mixtures were obtained by passing the gases through a Matheson Gas Proportioner.

The atmospheres within the cell chamber were changed by first evacuating the chamber to about 25μ. The new atmosphere was allowed to fill the chamber and flow vigorously through it for several minutes. The chamber was evacuated again, and the process repeated. The flushing procedure was carried out three times before the final flowing atmosphere was admitted.

## Open Circuit Emf Measurements

Open circuit emf measurements were made on selected samples in cells of the type

Pt, Ni-NiO/sample/Cu-$Cu_2O$, Pt

where the metal-metal oxide mixtures serve both as electronic leads and as reversible electrodes to fix different oxygen

chemical potentials (oxygen partial pressures) at the sample faces. The metal-metal oxide mixtures for the electrodes were compounded in a 10/1 molar ratio of metal to metal oxide. The powders were mixed and pressed in a 3/8 in. tungsten carbide lined die at 3000 p.s.i. and then isostatically pressed to 50,000 p.s.i. The electrodes were placed on either side of the sample, the platinum leads attached and the cell mounted in the furnace as described before. Normally it was possible to construct a double cell and run two samples at a time.

The measurements were performed in purified, static helium under a positive pressure. The cell was outgassed and flushed as described before. The purified helium was obtained by passing tank helium through activated BTS Catalyst at 180°C; a mixture of activated alumina, Drierite, and Anhydrone; Ascarite; and a liquid nitrogen cold trap, in that order. The open circuit emf measurements were made with a Leeds and Northrup 7554 Type K-4 potentiometer coupled with either a Hewlett Packard 419A DC Null Voltmeter or Keithley 610B Electrometer employed as the null detector. The measurements were made at 1000, 900 and 800°C.

# RESULTS AND DISCUSSION

## The $HfO_2$-$Er_2O_3$ System

### Room temperature X-ray diffraction studies

The phase relations after anneals at 1900 and 1450°C were studied by diffractometer and film techniques. Phase boundaries were determined by the appearance or disappearance of the diffraction lines characteristic of a particular phase, and from the lattice parameter vs composition relation. In general, the lattice parameters were determined from the diffractometer data, primarily for convenience. Comparisons with lattice parameters determined by film techniques agreed within 0.0005Å. The standard deviation of the lattice parameter calculated by the computer program (64) using the Bragg reflections of a given sample was less than 0.0002Å for fluorite solid solutions. It was less than 0.0005Å for erbia solid solutions. Values of the lattice parameters determined for standard materials (Si and W) checked within 0.0005Å of the ASTM values.

Reproducibility of the lattice parameter of a particular sample, as a rule, checked within 0.0010Å. This limit applied to determinations on the same sample as well as to determinations on newly-formulated samples of the same composition. There were two exceptions to the rule. The first was for compositions near a phase boundary. These patterns generally exhibited poorly-defined diffraction peaks which were diffi-

cult to read accurately, thereby introducing larger error. The second exception was for samples with the pyrochlore composition (33.3 m/o erbia) and will be discussed later. In view of the foregoing, the lattice parameters reported in this study are considered accurate within $\pm$ 0.0010Å.

Perhaps of greater importance is the possible error in sample composition. Due to the chemical stability of these materials, particularly those with high hafnia contents, the chemical analyses were difficult to perform. In general, the material balance associated with the chemical analysis was 100 $\pm$ 2 m/o. However, the estimated maximum error associated with the method of sample preparation is only $\pm$ 1 m/o, depending on the composition. The true error is probably within these limits but closer to the $\pm$ 1 m/o value.

The relation between lattice parameters ($a_o$) and composition (m/o erbia) is shown in Figure 8. The plot defines the presence of four distinct phase fields. A two-phase field consisting of monoclinic hafnia and fluorite solid solution exists up to about 6 m/o erbia. From 6 to 50 m/o erbia, there exists a homogeneous single-phase fluorite solid solution. A two-phase region composed of fluorite and erbia solid solutions extends from 50 to approximately 73 m/o erbia. For erbia compositions greater than about 73 m/o, there exists a single phase erbia solid solution.

No solid solutions of erbia in monoclinic (or tetragonal) hafnia were observed. For erbia contents as low as 1 m/o, a

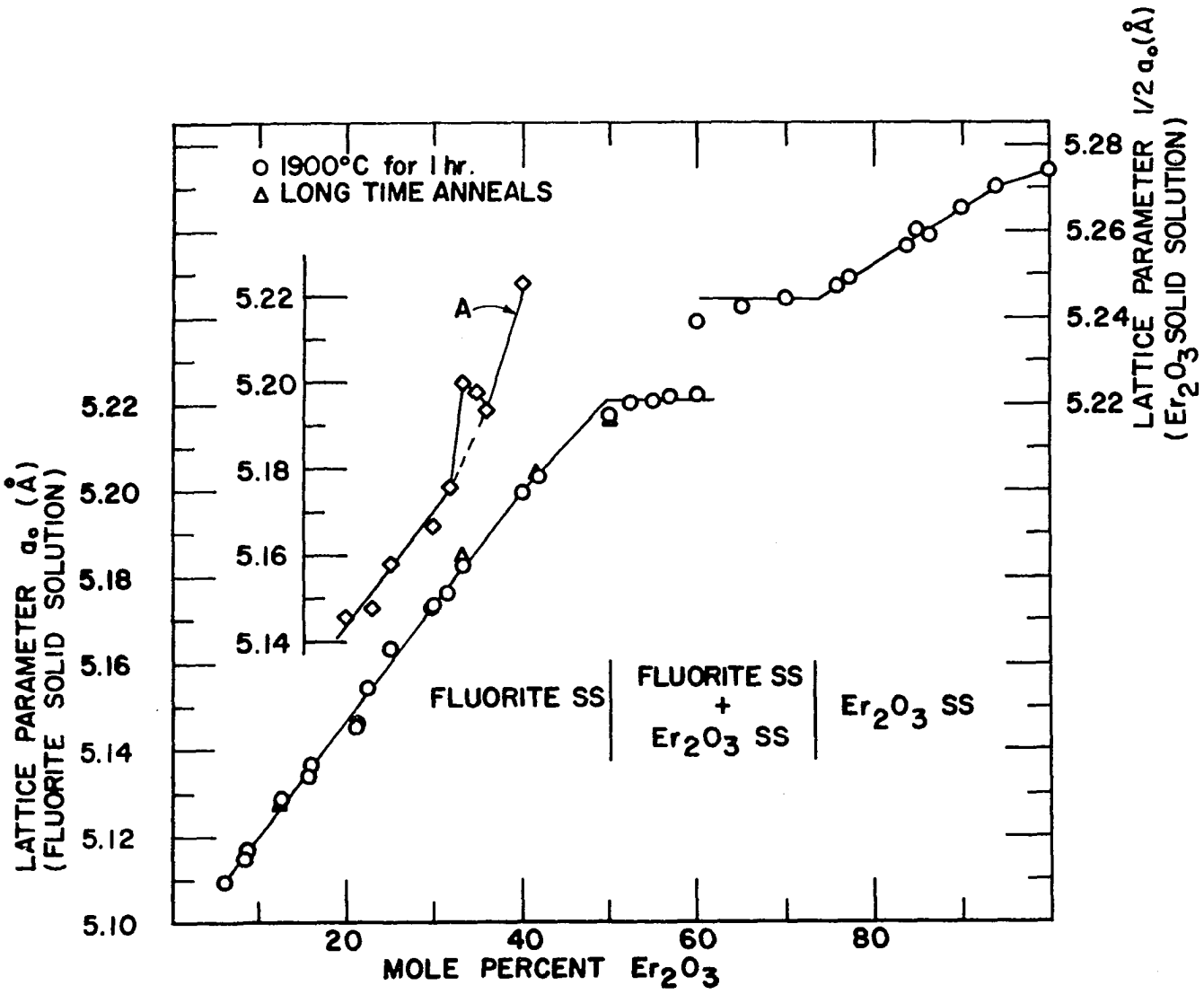


Figure 8. Relation between lattice parameter and composition
A. $HfO_2$-$Y_2O_3$ system

well-developed two-phase field was present. At 6 m/o erbia, very broad diffuse peaks of the fully-stabilized fluorite structure were the only reflections present. This was the case for both the calcined hydroxide and the 1900°C annealed sample. After annealing at 1450°C for 24 hours, weak monoclinic hafnia peaks (hkl = $11\bar{1}$ and 111) were present in the 6 m/o erbia sample. The 8.6 m/o erbia sample showed well-defined patterns of the fluorite type, although there was some deterioration in the line quality in the back reflection region. Faint monoclinic hafnia lines were also revealed by long-exposure of the 8.6 m/o erbia sample that had been subjected to the 24 hour 1450°C anneal. At 12.5 m/o erbia, only reflections characteristic of the fluorite structure were present for all heat treatments.

Within the fluorite solid solution domain, the diffraction patterns were sharp and well defined. Of particular interest is the nearly linear relation (Vegard's law (78, p. 76)) between the lattice parameter and composition shown in Figure 8. For comparison, the lattice parameter data reported by Caillet *et al.* (44) for the hafnia-yttria system are included in Figure 8 (curve A). Their data show an anomalous increase in the lattice parameter at 33.3 m/o yttria--the pyrochlore composition. There is no indication of such a drastic change in the hafnia-erbia data.

In an effort to induce ordering, two 33.3 m/o erbia

samples were subjected to various heat treatments as listed in Table 7. The two samples differ only in that they were prepared separately from the standard solutions. All of the samples were calcined at 1000°C for several hours to convert the mixed hydroxides to the oxides, and all but IIC were annealed at 1900°C for one hour. If the lattice parameter for a particular heat treatment was determined more than once, it is listed in the table, and the average lattice parameter of the set is also listed. If the average values of the lattice parameter for each heat treatment are in turn averaged, an overall value of the lattice parameter of $5.183_6$Å is obtained. The overall value is in good agreement with Klee and Weitz (27) and Radzewitz (35) who obtained values for this composition of $5.182_5$ and $5.183_5$Å respectively.

Samples IA and IIA served as the starting materials and show excellent agreement in lattice parameters. With one exception, the lattice parameters increased after the long time anneals. Sample IIC, which had not been preannealed at 1900°C, also exhibited an increase in lattice parameter. The increases range from about 0.0010 to 0.0025Å. The noted exception is IIB which showed a slight decrease in lattice parameter after annealing.

In general, the changes were very small; not being much greater than the estimated accuracy of $\pm$ 0.0010Å. The increases in $a_o$ were varied and did not reproduce a single value. In any case, as noted before, an increase on the order

Table 7. Lattice parameters of two 33.3 m/o erbia samples (I and II) subjected to various heat treatments

| Sample | $a_o$ Å | | Heat treatment[a] (in sequence) |
|---|---|---|---|
| IA | $5.182_7$ | | 1000-S[b]; 1900-1 |
| | $5.182_9$ | | |
| | $<5.182_8>$ | | |
| IB | $5.184_2$ | | 1000-S; 1900-1; 1450-72 |
| | $5.184_8$ | | |
| | $5.185_1$ | DS[c] | |
| | $<5.184_7>$ | | |
| IC | $5.185_5$ | DS | 1000-S; 1900-1; 1450-72; |
| | $5.185_3$ | DS | 1000-170 (1 week) |
| | $<5.185_4>$ | | |
| IIA | $5.182_9$ | | 1000-S; 1900-1 |
| | $5.182_4$ | | |
| | $<5.182_6>$ | | |
| IIB | $5.182_1$ | DS | 1000-S; 1900-1; 1450-72 |
| IIC | $5.184_0$ | DS | 1000-S; 1450-72 |
| Average $a_o$ | $5.183_6$ | | |

[a]The data are tabulated in terms of temperature in °C and number of hours at temperature. For example, 1900-1 = 1900°C for 1 hour.

[b]S means several hours.

[c]DS means $a_o$ determined from a Debye-Scherrer film, otherwise $a_o$ was determined from diffractometer data.

of that reported for the hafnia-yttria system (44) is not present.

No superlattice lines characteristic of a pyrochlore compound were observed in any of the diffraction patterns. To determine if such lines should be visible, a theoretical intensity diffraction pattern for the pyrochlore compound, $Er_2Hf_2O_7$ was calculated using the computer program of Yvon et al. (79). The program was slightly modified to accommodate the analytical forms of the atomic scattering factors given by Cromer and Waber (67). The intensities were calculated for $a_o = 10.366\text{Å}$, B (temperature factor) = $1.52\text{Å}^2$, and the x parameter for the oxygen in the (f) positions equal to 0.289. A partial listing of the calculated intensities is given in Table 8. The intensities are based on 100 for the most intense reflection.

Table 8. Theoretical intensities calculated for the compound $Er_2Hf_2O_7$

| hkl | I | hkl | I |
|---|---|---|---|
| 111 | 0.8 | 331 | 0 |
| 200 | NA[a] | 420 | NA |
| 220 | 0 | 422 | 0 |
| 311 | 1.2 | 511/333 | 0.5 |
| $222_F$[b] | 100.0 | 440 | 41.0 |
| $400_F$ | 34.0 | 531 | 0 |

[a]Not allowed because of extinction rules of the pyrochlore structure.

[b]hkl values subscripted with an F correspond to two times the equivalent fluorite reflection.

Only the 111, 311 and 511/333 superlattice reflections exhibit theoretical intensities greater than 0.5%. Of these, the most intense is the 311 reflection with an intensity of 1.2%. However, detection of the 311 reflection could be seriously impaired because it lies at the base of the 100% 222 reflection. The separation between the 311 and 222 reflections is about $1.3^{\circ}$ $2\theta$ for copper radiation.

Film exposures of up to 30 hours with copper radiation were made in an attempt to enhance the possible superlattice reflections. Cobalt radiation was used in an effort to increase the angular separation between the two peaks thereby improving the resolution of the 311 reflection. In neither case were any superlattice lines observed in the films.

The upper boundary (erbia-rich compositions) of the fluorite solid solution domain was found to exist at approximately 50 m/o erbia. Very faint superlattice lines were revealed by long-exposure of a 50 m/o erbia sample that had been annealed at $1450^{\circ}C$ for 24 hours. There was no evidence of superlattice reflections for the $1900^{\circ}C$ annealed sample.

As the erbia content increased above 50 m/o, corresponding to increased penetration into the two-phase region, the superlattice reflections increased in intensity. However, more than just superlattice lines should appear if the region is two phase. The erbia solid solution should also produce reflections similar to the fluorite reflections, but indexed in terms of a unit cell that is twice that of the fluorite

cell. Thus, consistent with the analogy between the fluorite and C-type structures, the C-type structure should exhibit the common fluorite lines as well as the extra (superlattice) lines allowed by the shift from fcc to bcc symmetry. Therefore, in addition to the superlattice lines observed, there should also be an erbia solid solution 222 reflection next to the fluorite 111 reflection, a 400 next to the 200, and so on. In general, this was not observed. The only sample that showed any indication of splitting of the fluorite peaks contained 60 m/o erbia. Even in this case, the resolution was poor. Annealing at 1450° for 24 hours did not improve the patterns.

In a study of $ZrO_2$-$RE_2O_3$ systems, Perez y Jorba (42) reported the gradual appearance of the rare earth superlattice lines in the systems where RE = Gd, Dy and Yb. This led him to propose that the transition from fluorite to C-type solid solutions is continuous, with no two-phase domain interposed. This contention does not appear to extend to the hafnia-erbia system. Although two distinct phases were not positively identified, the behavior of the lattice parameter vs composition relation between 50 and 73 m/o erbia is indicative of the presence of two phases.

The high-erbia boundary of the two-phase domain was determined by the lattice parameter vs composition relation in Figure 8. A single-phase region containing the C-type structure extended from approximately 73 to 100 m/o erbia.

The diffraction patterns of the erbia solid solutions were generally of good quality. The boundary at 73 m/o erbia is in fair agreement with Kalinovskaya et al. (34) who reported erbia solid solution existing at least as low as 80 m/o erbia. However, they did not report an actual boundary, so the comparison is rather indefinite.

High temperature X-ray diffraction studies

Selected compositions spanning the phase diagram were studied by high temperature X-ray diffraction techniques. Emphasis was placed both on the effect of erbia additions on the hafnia monoclinic $\rightleftharpoons$ tetragonal crystallographic transformation and also on the boundaries of the fluorite solid solution region. A cursory study of erbia-rich compositions was made to determine possible domains of ordering based on hexagonal structures as reported by Perez y Jorba (42) for $ZrO_2$-$RE_2O_3$ systems.

The method of temperature measurement has already been described. The temperature variation from the beginning to the end of a diffractometer scan (up to 25 min.) was at most 20°C. The precision of the temperature measurements was $\pm$ 5°. The accuracy is estimated to be $\pm$ 20°C. Considering the method used to determine temperatures--measuring the temperature of the tungsten ribbon surface with a micro-optical pyrometer--the measured temperature should be slightly greater than the true sample temperature. Nevertheless, because of the very thin (<2 mils) uniform samples utilized, the error is

probably not large and is well within the estimated accuracy.

Initial studies were made of the monoclinic to tetragonal transformation in pure hafnia. The pure hafnia was prepared from the standard solution in a manner identical to the method used to prepare mixed samples. Diffractometer traces depicting the transformation are shown in Figure 9.

The onset of the transformation is marked by the appearance of the characteristic 111 reflection of the tetragonal phase which lies between the monoclinic $11\bar{1}$ and 111 reflections. As the transformation proceeds with increasing temperature, other tetragonal reflections appear at the expense of the corresponding monoclinic peaks. Finally, the transformation of the last bit of monoclinic phase is denoted by the disappearance of the monoclinic $11\bar{1}$ and 111 peaks.

The transformation range on heating was found to be from 1580 to 1825°C. This is in good agreement with the range for pure hafnia reported by Wolten (13) and in excellent agreement with Ohnysty and Rose (15) (see Table 1). The change in the relative amounts of the two phases was represented by the changes in the relative peak intensities. The changes were found to take place very rapidly. No changes in the relative amounts of the two phases were observed as a function of time which is in agreement with others (13,14,16). The reverse (tetragonal to monoclinic) transformation could not be observed because the samples broke away from the heating element on cooling.

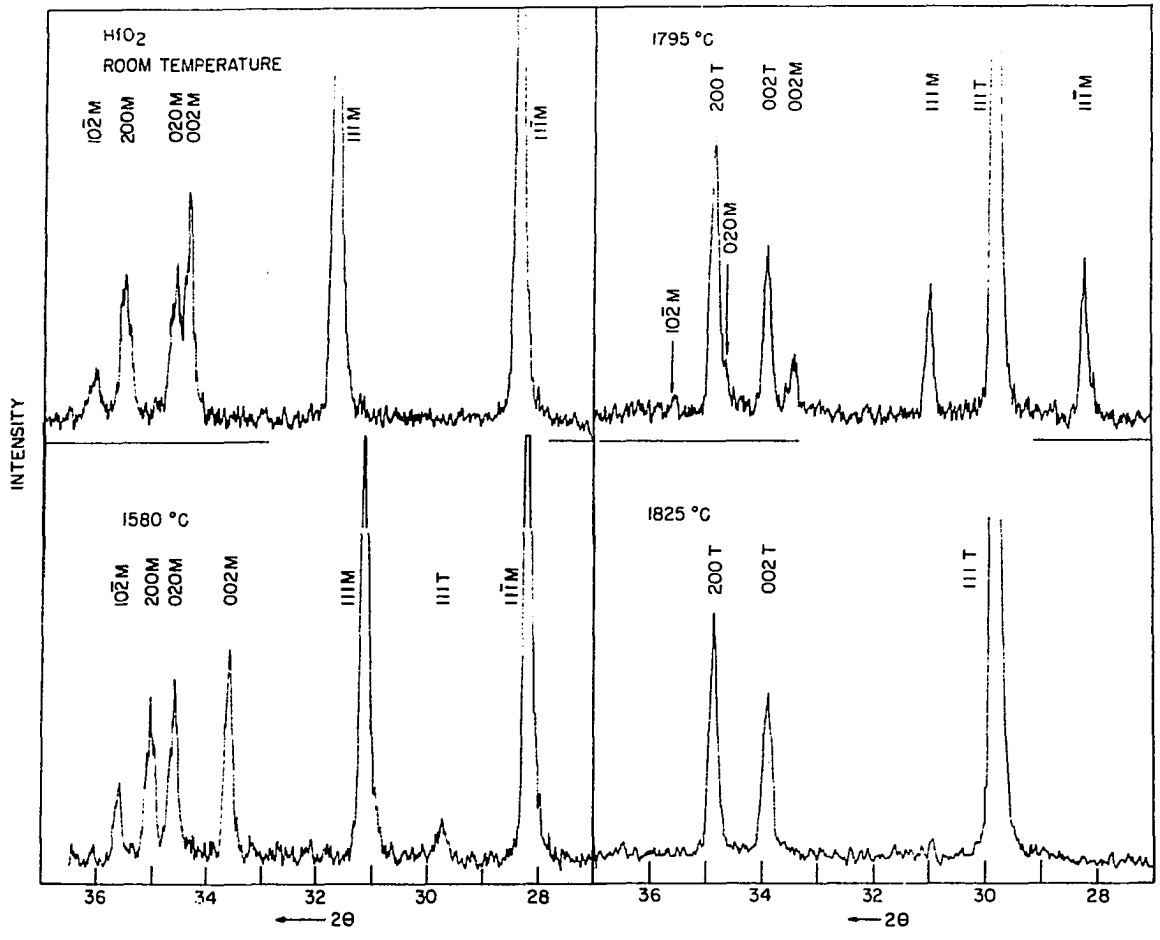


Figure 9. Diffractometer traces depicting the monoclinic to tetragonal transformation in pure $HfO_2$

As noted earlier, no single-phase hafnia monoclinic solid solutions were observed, i.e., two phases were present in samples containing 1 m/o erbia. However, even the slight solubility of erbia in hafnia which does occur was observed to lower the transformation temperature. It was not possible to observe the appearance of the first tetragonal phase because the fluorite 111 peak completely overlapped the tetragonal 111 peak. However, the disappearance of the last monoclinic phase--which defines the upper temperature limit of the transformation--was easily observed. The upper temperature limit of the monoclinic to tetragonal transformation was studied in samples containing 1, 2.5 and 4.4 m/o erbia. The upper limit was found to decrease from 1825°C observed in pure hafnia, to approximately 1725°C--a decrease of 100°C. Figure 10 shows diffractometer traces obtained for the transformation in the two-phase field. In the figure, M = monoclinic phase, T = tetragonal phase and F = fluorite phase. As before only data for the heating cycles were obtainable.

As reported above, the 6 m/o erbia sample was found to lie in either the two-phase (monoclinic + fluorite) region or in the single-phase (fluorite) region depending on the heat treatment. The transition from the two-phase to the single phase domain is shown in Figure 11. The last monoclinic phase was observed to disappear at 1715°C which is in good agreement with the upper monoclinic to tetragonal transformation limit. However, there was no evidence of the tetragonal phase, only

Figure 10. Diffractometer traces depicting the monoclinic to tetragonal in the two-phase domain at 4.4 m/o $Er_2O_3$

M = monoclinic phase;

T = tetragonal phase;

F = fluorite phase

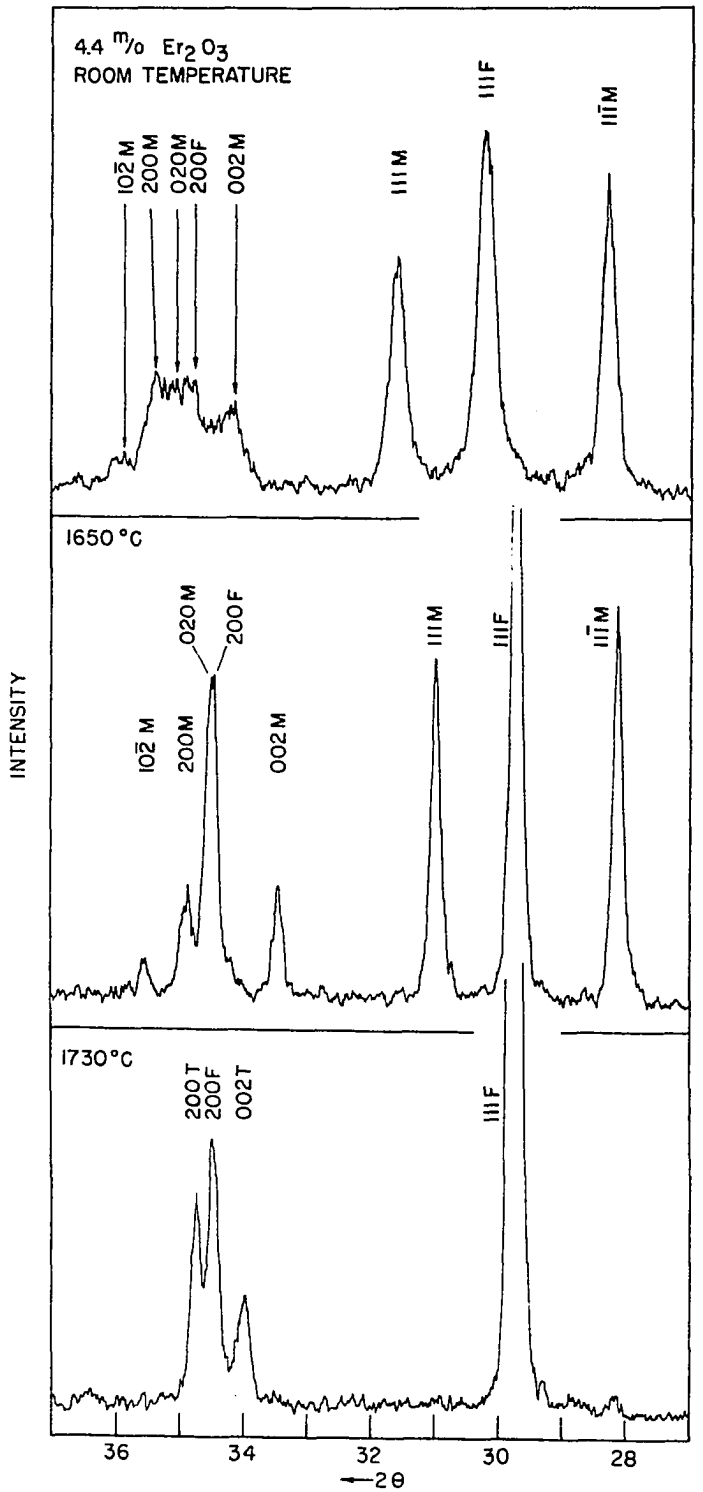
4.4 m/o Er2O3
ROOM TEMPERATURE
10$\bar{2}$ M
200 M
020M
200F
002 M
111 M
111F
11$\bar{1}$M
1650 °C
020 M
200F
10$\bar{2}$ M
200M
002 M
111M
111F
11$\bar{1}$M
1730°C
200T
200F
002T
111F
INTENSITY
36
34
32
30
28
←2θ

Figure 11. Diffractometer traces showing transition from two phase domain to single phase domain at 6 m/o $Er_2O_3$

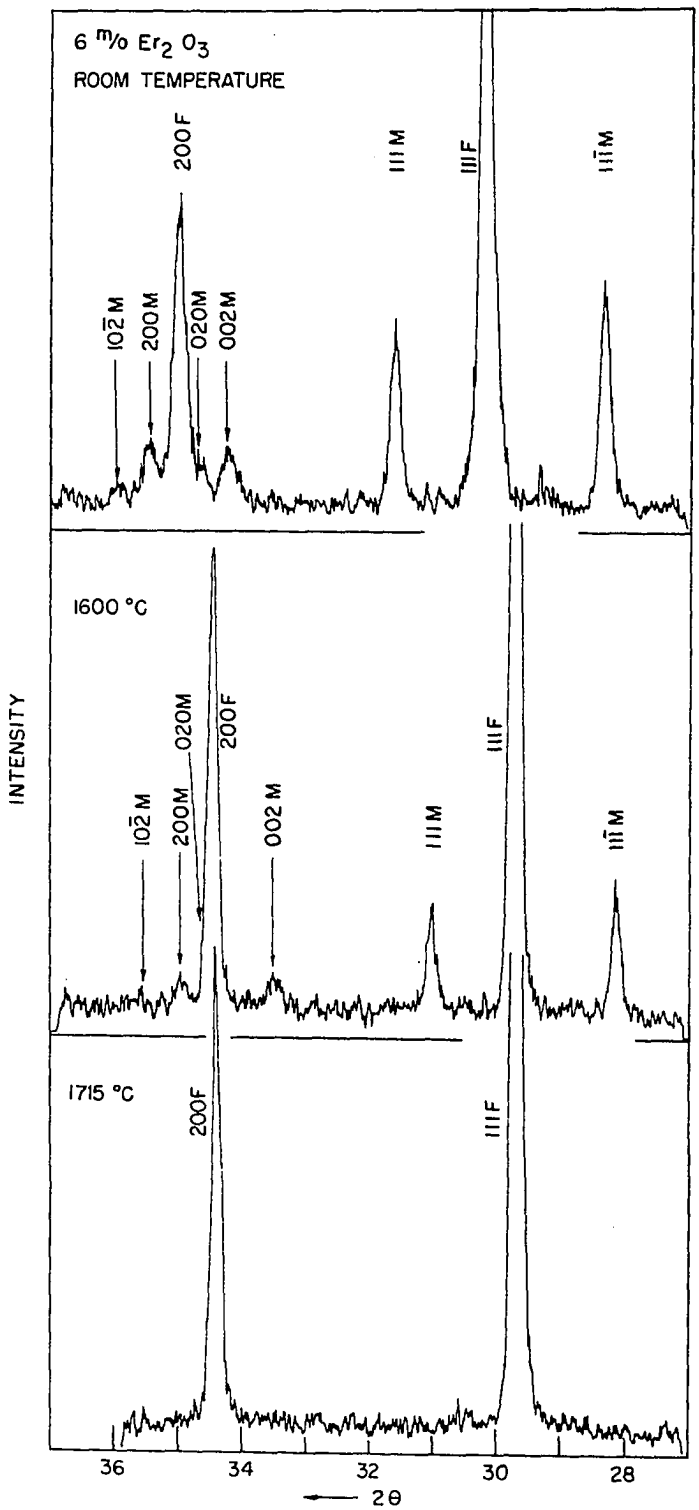
6 m/o Er2 O3
ROOM TEMPERATURE
200F
111M
111F
11$\bar{1}$M
10$\bar{2}$M
200M
020M
002M
1600 °C
020M
200F
111F
10$\bar{2}$M
200M
002 M
111M
11$\bar{1}$M
1715 °C
200F
111F
INTENSITY
36
34
32
30
28
2θ

reflections characteristic of a well-developed fluorite phase being present in the diffraction patterns. Upon cooling to about 1500°C and holding at that temperature for 12 hours, the monoclinic phase reappeared, although the characteristic reflections ($11\bar{1}$ and 111) were very weak.

The results of the study of the two-phase domain are summarized in Figure 12. The addition of erbia is assumed to decrease the lower limit of the monoclinic to tetragonal transformation by the same temperature increment as that observed for the upper limit. Note that the diagram does not represent equilibrium in a binary system in the ordinary sense of the phase rule. Wolten (13) has argued that the monoclinic $\rightleftharpoons$ tetragonal phase change possessed many of the characteristics (such as athermal characteristics, broad hysteresis and nonquenchability of the transformation) associated with diffusionless martensitic transformations of the Fe-Ni type. While the transformation in hafnia has not been proven to be diffusionless, Fehrenbacher and Jacobson (80) have presented conclusive evidence of the diffusionless nature of the analogous transformation in zirconia. If by analogy, the transformation in hafnia is diffusionless, Wolten argues that an additional determinative variable, strain energy, must be included with temperature and pressure in the phase rule. With this modification, the phase rule permits the transformation regions in Figure 12.

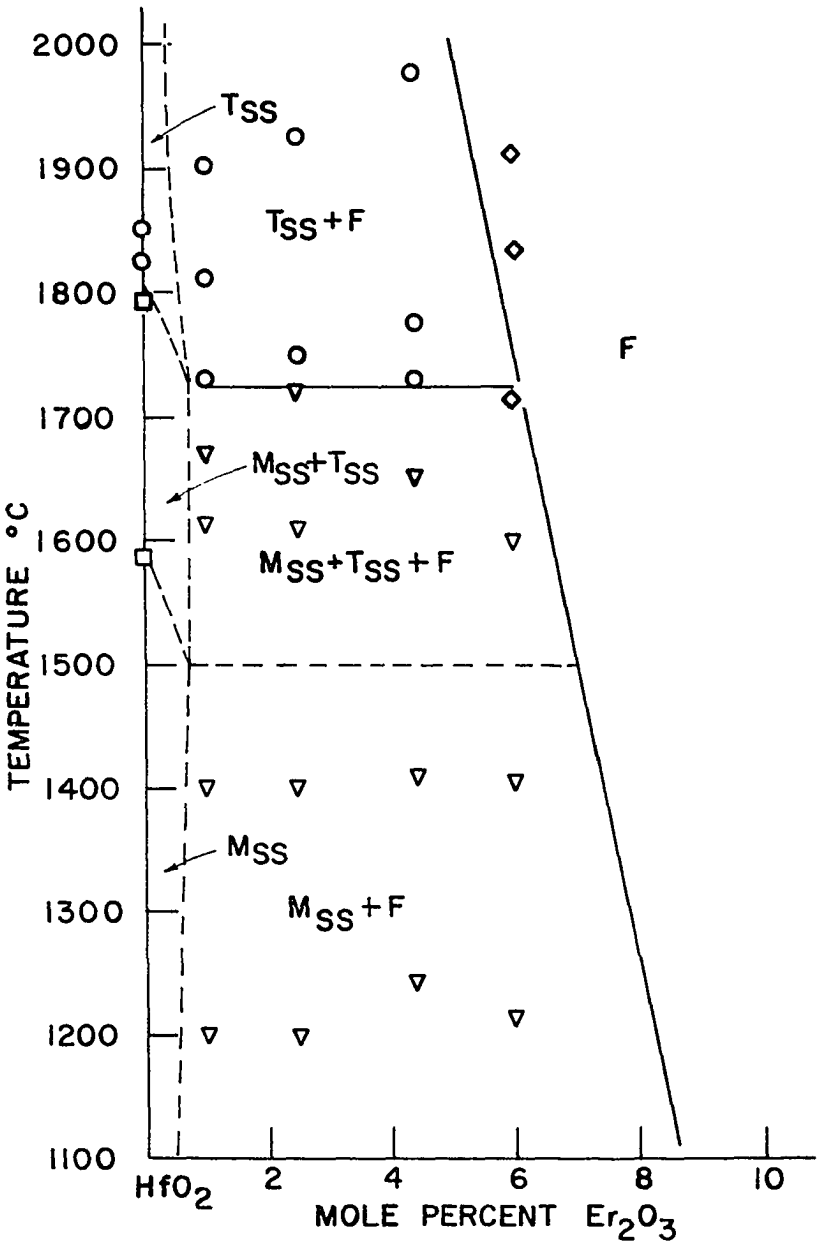


Figure 12. Phase relations in the hafnia-rich region of the hafnia-erbia system

In the fluorite domain, high-temperature X-ray studies were carried out on samples containing 12.5, 33.3 and 50 m/o erbia. Except for the normal temperature dependence of the reflections, the diffraction patterns remained unchanged throughout the temperature range. In particular, there was no evidence of ordering at high temperatures at the pyrochlore composition (33.3 m/o erbia). Thus, the fluorite domain is described by a continuous solid solution within the limits of this study.

The temperature-composition relation for the phase boundary separating the fluorite domain from the two-phase region was studied with samples containing 57 and 60 m/o erbia. Because of the absence of the major C-type rare earth peaks, the erbia solid solution was marked by the presence of the 411 and 510 C-type superlattice reflections. As the temperature was increased, the intensity of the C-type peaks decreased until they were completely absent from the patterns. The disappearance of the 411 and 510 reflections was taken to imply that the phase boundary had been traversed and that the composition now lay in the single-phase fluorite region. For the 57 m/o erbia sample, the transition from the two-phase to the one-phase fluorite domain occurred between 1600 and 1830°C. In the 60 m/o erbia sample, the transition occurred between 1795 and 1920°C.

Two other samples, containing 65 and 70 m/o erbia, which lay within the two-phase domain, were studied. In these

samples, the C-type superlattice lines were present at all temperatures (through 1920°C). However, at higher temperatures ($\geq$ 1800°C) the major peaks (111-222, 200-400, 220-440) in the 65 m/o erbia sample were observed to improve in overall quality. That is, they became sharper, better defined, and slightly increased in intensity. Since these major peaks are apparently composed of both fluorite and C-type reflections, their improved definition may denote the passage from the two-phase into a one-phase region. In this case, since the C-type superlattice reflections are still present, the single phase would be that of erbia solid solution. No major improvement in the overall quality of the peaks was observed in the sample containing 70 m/o erbia, but the peak quality in this sample was fairly good at the start.

High-temperature X-ray studies were made on samples within the erbia solid solution region in search of evidence of hexagonal ordering of the type reported by Perez y Jorba (42) in zirconia-rare earth systems. Samples containing 75, 85, and 90 m/o erbia were used. A sample of pure erbia was also studied. No evidence of ordering was observed. The diffraction patterns were characteristic of the C-type structure at all temperatures.

A reaction took place between the tungsten heater and samples containing 85, 90, and 100 m/o erbia. The reaction occurred between 1300 and 1600°C and was detected as additional diffraction peaks. There was no visible reaction that could

be observed through the optical pyrometer. Four additional diffraction peaks were observed. A low intensity peak appeared on the low angle side of the 222 peak. The 222 peak itself was observed to split, with a lower intensity peak appearing on the high angle side. Two poor-quality, low-intensity satellite peaks appeared, one on each side of the 440 erbia solid solution peak. The peaks were most prominent at about 1400°C. As the temperature increased, the intensities gradually decreased, until at 1600°C they were completely absent from the diffraction patterns. Upon further heating, there was no evidence of the unknown peaks nor did they reappear on cooling. At first, it was thought that the unknown peaks represented the hexagonal ordering. However, they were also observed for a pure erbia sample, and erbia is known to exist only in the C-type structure at these temperatures (20, 39). To determine if the reaction was attributable to the tungsten ribbon, a heating element was fabricated from Pt-40% Rh and the experiments repeated. None of the unknown reflections were observed in these studies.

The unknown structure produced with the tungsten heater was quenched by heating the sample to 1400°C, holding until the structure was well formed, and then shuting off the power to the heater. A room temperature X-ray scan showed the unknown peaks to be present at the same relative intensities as at 1400°C. Visual observation of the sample showed that it was a dull gray color rather than the characteristic pink

color. Attempts to index the unknown lines were unsuccessful, and, at present, their origin remains unknown.

A summary of the results of the X-ray investigations of the phase relations in the hafnia-erbia system are presented in Figure 13. The fluorite (F) domain extends from about 9 to about 50 m/o erbia at 1400°C. At 1900°C, it extends from 6 to about 60 m/o erbia. The two-phase domain composed of fluorite and erbia (C) solid solutions is constructed as a domed region based partially on the limited evidence discussed earlier and partially on the shape of the liquidus curve to be discussed in the next section. Similar domains have been reported by Perez y Jorba (42) in zirconia-rare earth systems. The uncertainty in the boundary on the erbia-rich side of the two-phase region is represented by a dashed line.

Melting point determinations

The results of the melting point determinations for the various compositions are included in Figure 13. In general, 3 or 4 determinations were made for each composition. The precision in temperature measurement was excellent, even at the highest temperatures. The variation in separate determinations was a maximum of $\pm$ 20°C.

As discussed before, melting was abrupt and easily observable, but it was not possible to obtain a prolonged equilibrium state between the solid and liquid even though it was not unusual to observe the remaining solid floating in the liquid. Thus, the melting points probably lie between the solidus and

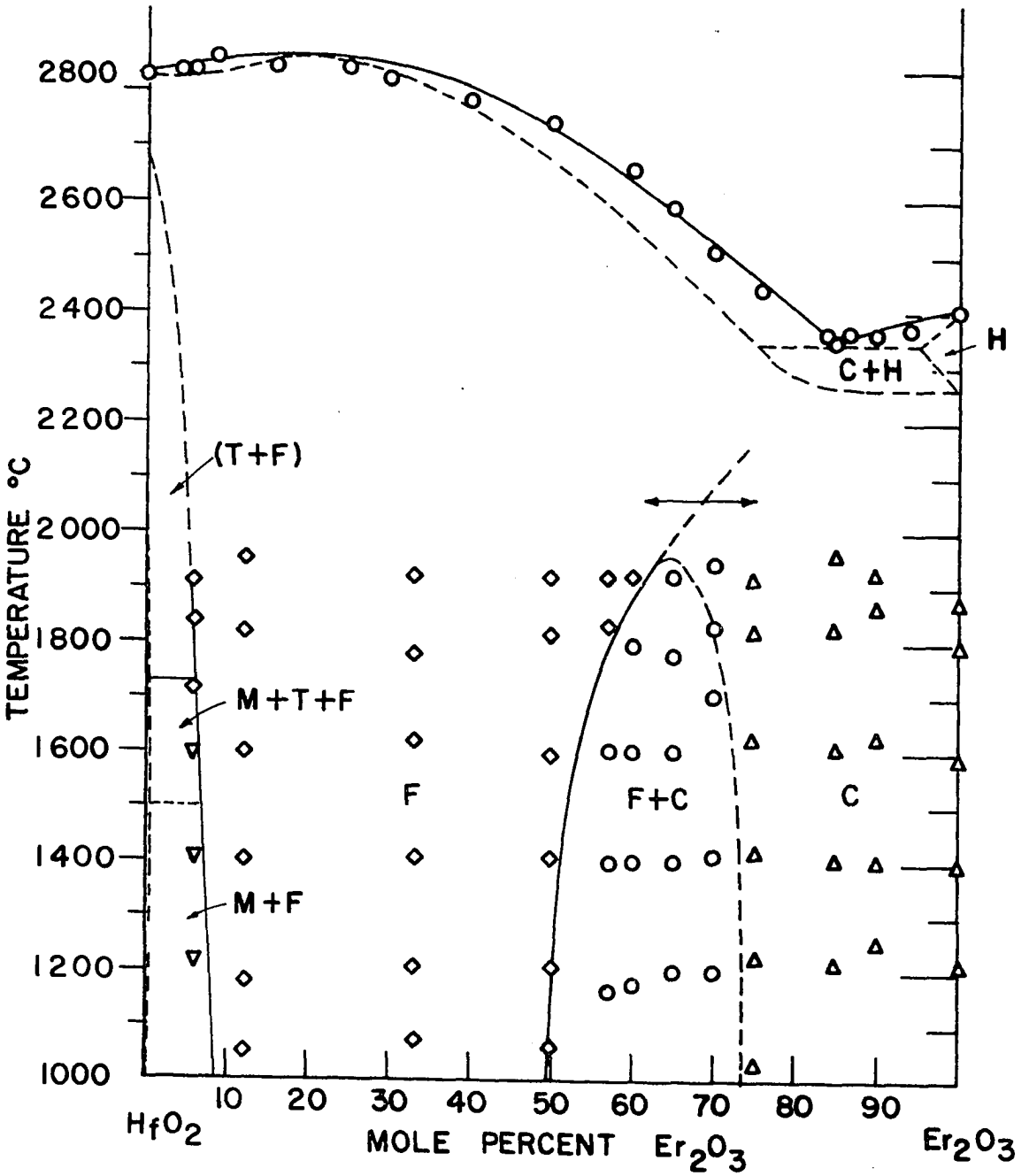


Figure 13. Proposed phase diagram for the hafnia-erbia system

liquidus boundaries of the diagram. Because there was relatively little fine control of the power input, it was not possible to adjust the temperature to preserve the two-phase relation. A more serious problem, however, was the very high vapor pressure of the solid and liquid at the temperatures in question (2400 to 2825°C). Once melted, the sample in the liquid state evaporated rapidly. As the liquid evaporated, additional solid melted and vaporized, until the entire sample disappeared. The entire process did not take more than 30 sec.

The melting points were found to be independent of the heating rate, with one qualification. If the heating rate was too slow, the solid completely sublimed before the melting point was reached. Experiments showed, however, that the sublimation had no effect on the melting point since any remaining sample melted at the same temperature as the bulk material.

The melting points of the end member oxides were found to be 2825 $\pm$ 20°C for hafnia and 2400 $\pm$ 20°C for erbia, in good agreement with the literature (77,81,82). The eutectic temperature is about 2340°C and the eutectic composition is approximately 85 m/o erbia. The liquidus curve, derived from the melting point data and shown in Figure 13, is nearly identical in general shape to that reported by Rouanet (31) for the zirconia-erbia system (Figure 4). The maximum in the liquidus curve is not as conspicuous in the hafnia-erbia system, the maximum increase in liquidus temperature being not more than

15 or 20°C compared to approximately 100°C in the zirconia-erbia system (31). There is no indication in the liquidus curve in Figure 13 that the two-phase domain extends to the liquidus. In fact, the shape of the liquidus supports the X-ray data in suggesting that the two-phase domain is a domed region.

The high-temperature portion of the hafnia-erbia system in Figure 13 is constructed in a manner after Rouanet (31). The diagram is dominated by a nearly continuous solid solution region that is partitioned by a hypothetical dotted line delineating the transition from fluorite to erbia solid solutions (42). The transformation temperature of tetragonal to cubic hafnia is that reported by Boganov et al. (19); whereas, regions containing the H modification of erbia (24) are constructed after Rouanet (31) (Figure 4).

Defect structure of fluorite and erbia solid solutions

As erbia is added to hafnia in the fluorite domain, electrical neutrality is preserved by one of two defect structures. Either the cation sublattice remains completely filled and the positive charge deficiency is balanced by vacancies on the anion sublattice (anion vacancy model), or the anion sublattice remains filled and the negative charge excess is balanced by cations occupying interstitial sites (cation interstitial model). In a similar manner, two possible defect models exist for the erbia solid solutions as hafnia is added to erbia. If the cation sublattice remains filled in this

case, electrical neutrality is preserved by anions occupying interstitial sites (anion interstitial model). If the anion lattice remains filled instead, then the neutrality is preserved by vacancies in the cation sublattice (cation vacancy model). By expressing each model in terms of a composition dependent theoretical unit cell population, the theoretical X-ray densities can be calculated using the experimentally determined lattice parameters in the manner prescribed by Hund (2,3).

The comparison between the theoretical and the measured apparent densities is shown in Figure 14. Samples containing less than 70 m/o erbia, while extremely porous, contained virtually no closed porosity, and, therefore, their apparent densities should be very close to their true densities. These samples show excellent agreement with the anion vacancy model for the fluorite solid solutions, a result which is in agreement with others for analogous systems (3,7). In contrast, samples containing 70 m/o or more erbia sintered to extremely high densities and in fact, routinely sintered to translucency. The transition from the open pore to the closed pore condition is graphically portrayed in Figure 14 by the discontinuous decrease in the measured densities at 70 m/o erbia. While the closed porosity within these samples causes larger deviations from the theoretical curve, the defect structure of the erbia solid solutions is concluded to be of the anion-interstitial type. Similar defect structures have been found by others for

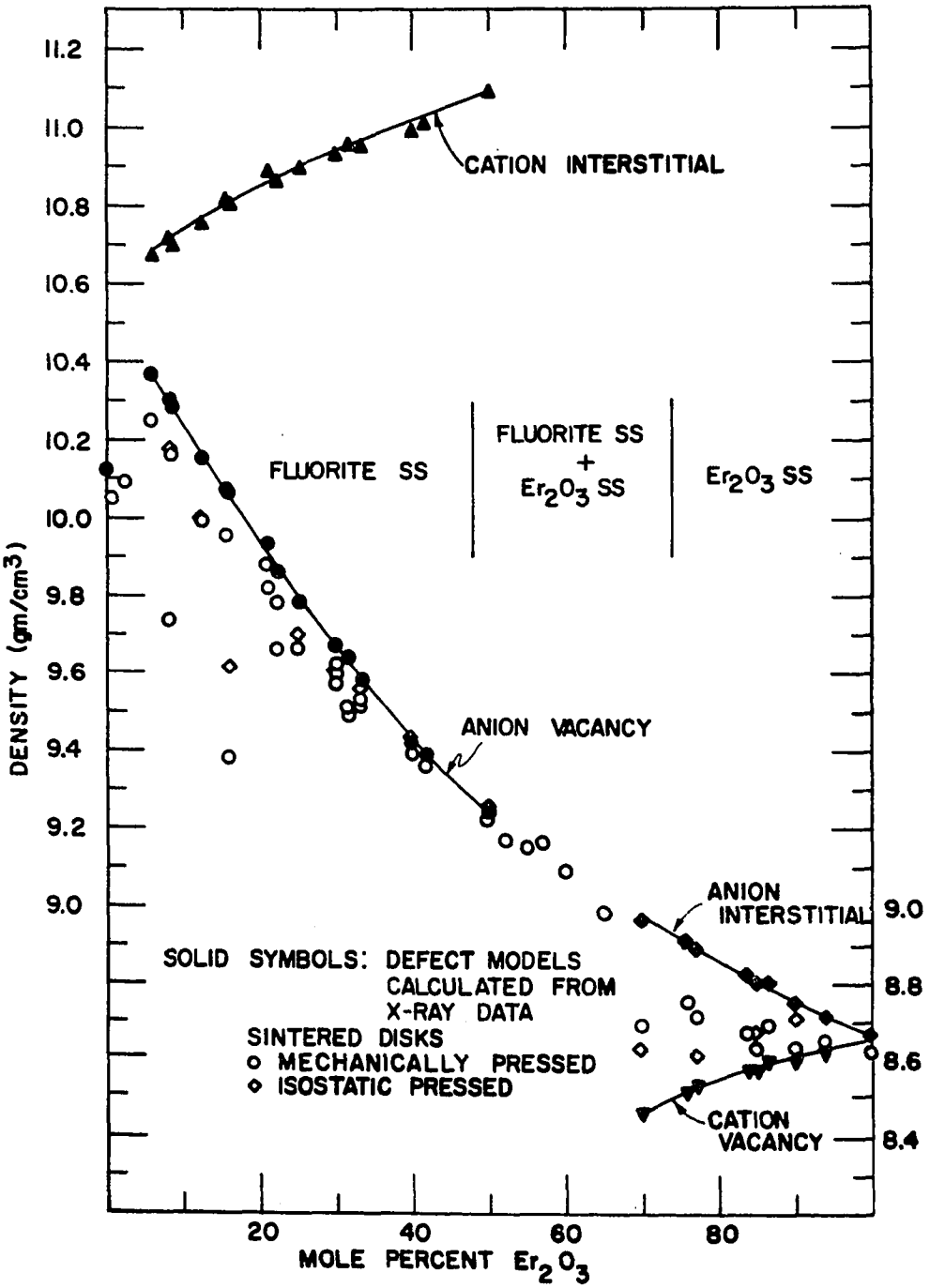


Figure 14. Theoretical and measured apparent densities of fluorite and erbia solid solutions

analogous systems (83,84).

As shown in Figure 14, the same density-composition curve results from the anion vacancy model of the fluorite structure and the anion interstitial model of the C-type structure. While the terminology used to describe the defect structure in each case is different, the defect structures themselves are identical. This arises from the fact that the C-type structure is derived from a massively defective fluorite cell in which all $M^{4+}$ cations have been replaced by $N^{3+}$ cations. It is correct to consider the fluorite structure and the C-type structure as distinctly different host lattices. However, by changing the reference structure from the fluorite to the C-type, the solute cation is also changed; from $N^{3+}$ to $M^{4+}$. This change in reference structure gives rise to the different terminology used to describe the defective anion sublattice.

## Ordering in the Fluorite Phase

### X-ray structure determinations

While the density measurements in the previous section identified the defects in the fluorite phase as anion vacancies, that technique is incapable of differentiating between a random or an ordered structure. The method of X-ray structure analysis was used in an effort to detect ordering within the fluorite phase. In this technique, the calculated structure factors for a given structural model are compared to the experimentally measured structure factors. The model struc-

ture factors are calculated from Equation 3

$$F = \sum_n f(s)_n \exp[-2\pi i \bar{G}\cdot\bar{r}_n]\exp[-B_n s^2] \qquad (3)$$

where $f(s)_n$ is the scattering factor of atom n, $s = \sin\theta/\lambda$, $\bar{G}$ is a reciprocal lattice vector, $\bar{r}_n$ is the position vector for atom n in the unit cell, and $B_n$ is the temperature factor for atom n. The "goodness of fit" for a particular model is expressed in terms of the disagreement factor, R, given in Equation 4

$$R = \frac{\sum_i \left||F_o|_i - |F_c|_i\right|}{\sum |F_o|_i} \qquad (4)$$

where $F_o$ is the experimentally observed structure factor and $F_c$ is the structure factor calculated from the model. The smaller the value of R, the better the correlation between the calculated and observed data.

In this study, experimental structure factors were determined for samples containing 8.3, 16, 30, 31.6, 33.3, and 41.8 m/o erbia which had been annealed at 1900°C for 1 hour. A second sample containing 33.3 m/o erbia which had been annealed at 1450°C for 72 hours was also studied. Because only 10 reflections were used, the variable parameters were limited to the scale factor and the overall temperature factor. All reflections were given unit weights. The results of these studies are expressed in terms of the R factor and are shown in Figure 15.

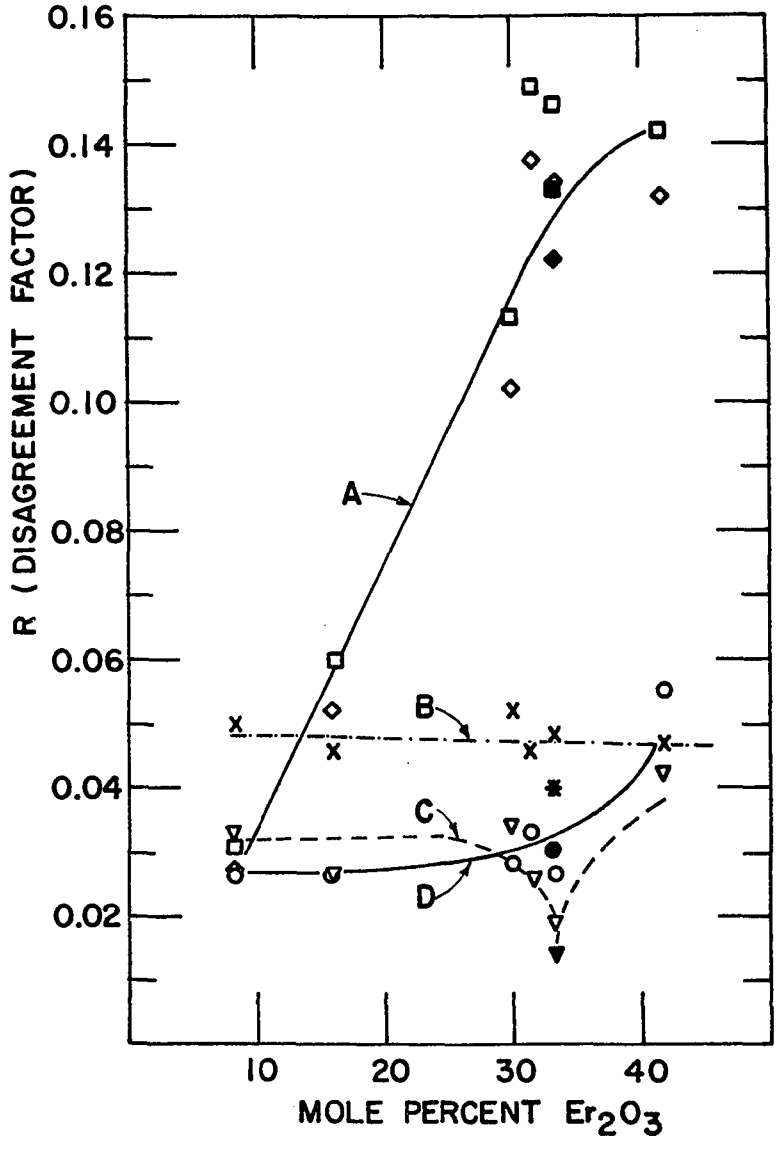


Figure 15. Crystallographic R factors for various structural models
A. □, ◇, fluorite, cation interstitial;
B. ×, x(f) = 0.312 pyrochlore;
C. ▽, x(f) = 0.289 pyrochlore;
D. ○, fluorite, anion vacancy and x(f) = 0.250 pyrochlore

An initial study was made to confirm the anion vacancy defect structure determined by the density measurements for the fluorite solid solution. In the anion vacancy model, calculations were based on the $Er^{3+}$ and $Hf^{4+}$ cations being randomly distributed on the cation sublattice. Similarly, the oxygen ions and vacancies were considered to be randomly distributed on the anion sublattice. In calculations for the cation interstitial model, two distributions were tried. In both cases, the interstitial cation was assumed to be located on the $\frac{1}{2}\frac{1}{2}\frac{1}{2}$ site. In the first case, both cations ($Hf^{4+}$ and $Er^{3+}$) were assumed to be randomly distributed on the cation and interstitial sublattices. In the second case, only the $Er^{3+}$ solute ions were allowed to occupy interstitial sites in a random manner.

The results of the structure fits are indicated in Figure 15 by (D) for the anion vacancy model and by (A) for the cation interstitial model. The rapid divergence of the R factors for the two models is immediately apparent. At 8.3 m/o erbia, the R factors are nearly the same. This is due to the small number of cations occupying interstitial sites. The divergence is a consequence of the increasing occupation of the interstitial sites. In contrast, the R factors for the anion vacancy model remain relatively constant throughout the composition range. At all compositions, the R factor for the $Er^{3+}$ interstitial model is less than that for the random

cation interstitial model. This is probably due to the smaller atomic scattering factor of the erbium ion. These data support the density data in confirming the anion vacancy model for the fluorite solid solutions.

The primary purpose of these structure studies was to try to detect ordering of the pyrochlore type within the fluorite domain. As discussed before, the unit cell edge of the pyrochlore structure is twice that of the fluorite unit cell. The cations are ordered in special positions as are the anion vacancies. However, the actual shape of the structural framework (composed of $Hf^{4+}O_6$ octahedra, Figure 3) is controlled by the value of the variable parameter in the (f) positions. Thus, various structures of the pyrochlore type can be constructed by assuming different values for the variable parameter, x(f).

Roth (48) has argues that x(f) is probably close to 0.250. Nevertheless, he obtained better qualitative agreement between observed and calculated X-ray intensities for $La_2Zr_2O_7$ and $Nd_2Zr_2O_7$ when x(f) = 0.289, an experimental value obtained by Bystrom (30) for $Cd_2Ta_2O_7$.

In this study, three trial values were chosen for x(f); 0.250, 0.289, and 0.312. The effect of these values on the $BO_6$ octahedra has been shown in Figure 3, however, it is worthwhile to discuss these pyrochlore structures in greater detail here. x(f) = 0.250 corresponds, in effect, to an ordered fluorite structure. The cations and vacant anion

sites order as before, but there is no relaxation of the (f) set oxygen ions towards the vacant sites. These oxygen ions remain at the corners of the basic fluorite $MO_8$ group. Each $Hf^{4+}$ ion is coordinated by 6 oxygen ions in highly distorted octahedra (Figure 3) and each $Er^{3+}$ ion is 8-coordinated by oxygen at the corners of a cube.

For x(f) = 0.289, a general relaxation of the 6(f) oxygen ions coordinating the $Hf^{4+}$ ion toward the vacant anion sites has occurred, resulting toward regularizing the $Hf^{4+}O_6$ octahedron (Figure 3). Simultaneously, the 8-fold coordination of the $Er^{3+}$ ion has undergone a subtle change. The relaxation of the 6 oxygen ions toward the vacant sites effectively increases the bond length of 6 of the 8 oxygen ions coordinating the $Er^{3+}$ ion, and the oxygen coordinating the $Er^{3+}$ ion is no longer described by a regular cube. The two unmoved oxygen ions belong to the (a) set. The $Er^{3+}$ ion and (a) set oxygen ions now exist in the holes between the octahedral structural units. A schematic diagram of the pyrochlore structure for x(f) = 0.289 is shown in Figure 16. The z coordinate is divided into 4 layers. The top fraction beside each layer corresponds to the oxygen plane and the second fraction corresponds to the cation plane above the base plane. Figure 17 is a clinographic projection of the pyrochlore structure constructed from Figure 16. The oxygen atom labeled A in the lower left hand corner is common to both figures and serves

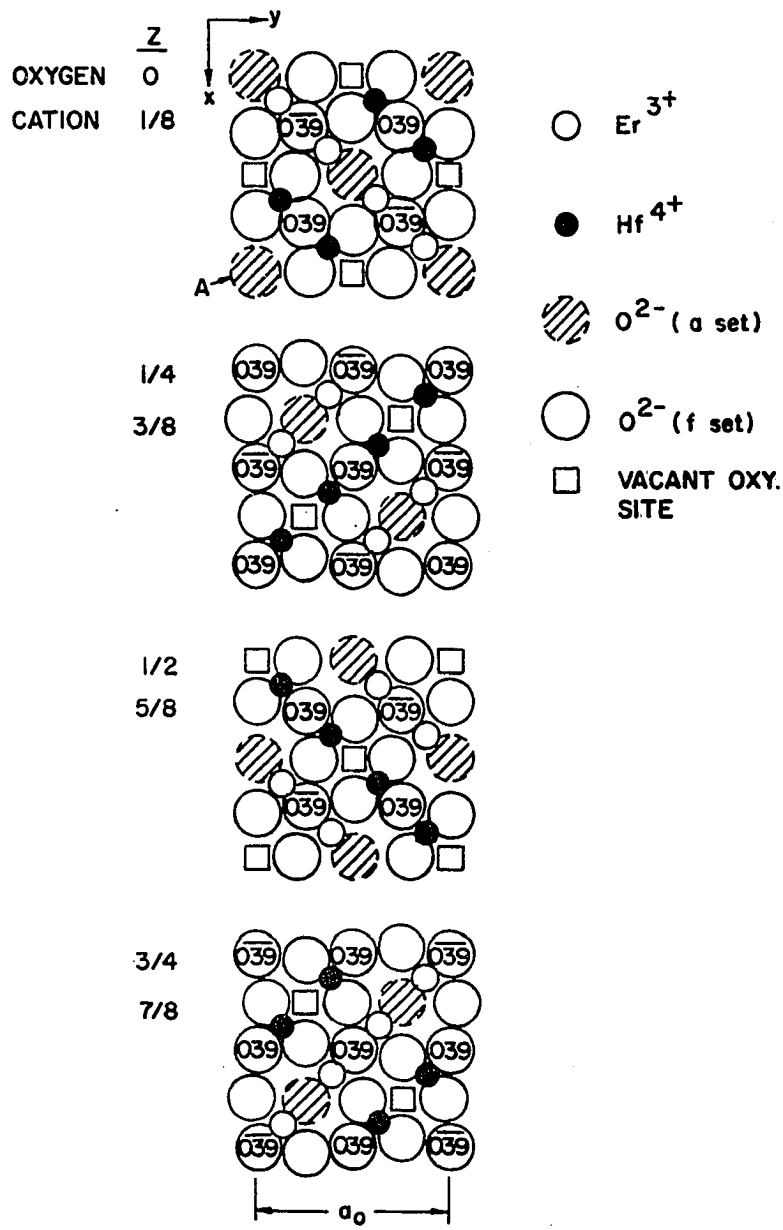


Figure 16. Pyrochlore structure for x(f) = 0.289

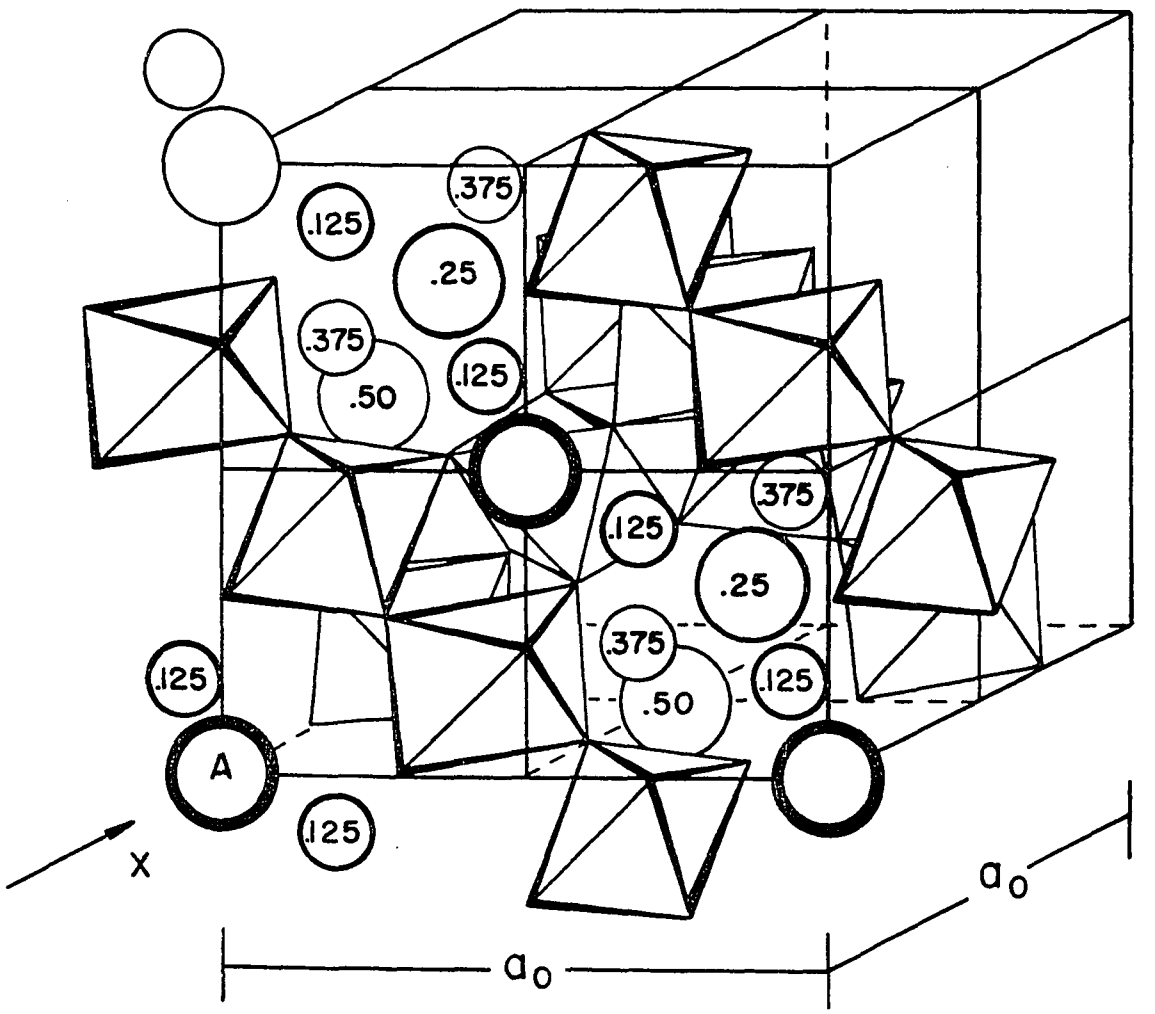


Figure 17. Clinographic projection of the pyrochlore structure in Figure 16, showing the $Er^{3+}$ cations and the (a) set oxygen ions located in the holes between the framework octahedra. The oxygen ion labeled A in the lower left hand corner is common to both figures

to orient one with respect to the other. Figure 17 shows the $Er^{3+}$ cations and (a) set oxygen ions in the holes between the $Hf^{4+}O_6$ octahedra.

The case x(f) = 0.312 represents a further relaxation of the (f) set oxygen ions and the formation of regular octahedra as discussed before. In general, the same comments made for x(f) = 0.289 apply here.

In calculating the structure fits for the various x(f) values, the structures had to be modified for compositions different than the pyrochlore composition, 33.3 m/o erbia. In keeping with the basic anion vacancy defect structure, the excess oxygen ions present for erbia contents less than 33.3 m/o were randomly distributed in the vacant anion sites of the regular pyrochlore structure. The cations were placed in their proper positions first and the excess in one kind of cation position were used to randomly fill the occupancy deficiency in the other cation position. In the case of lower erbia contents, the excess $Hf^{4+}$ ions were randomly distributed in the $Er^{3+}$ deficient (c) positions. For erbia contents greater than the pyrochlore composition, the oxygen deficiency was limited to the (a) positions. For this case, the excess $Er^{3+}$ ions were randomly distributed in the $Hf^{4+}$ deficient (d) positions.

The results of the structure fits as denoted by the R factors are given in Figure 15. Curves (D), (C) and (B) correspond to x(f) = 0.250, 0.289 and 0.312 respectively.

For all compositions the R factors for the random fluorite anion vacancy model and the x = 0.250 pyrochlore (ordered fluorite) are identical. This is not too surprising in that the cation ordering manifests itself in the calculation by either the difference or the sum of the respective atomic scattering factors. For the random fluorite vacancy model, each cation site, since it is treated as a composite cation, is represented by a composition-weighted atomic scattering factor with a value somewhere between those of $Er^{3+}$ and $Hf^{4+}$. For all the observed Bragg reflections (only those of the fluorite structure were present) the cation scattering factors add only. Therefore the contribution to the structure factor by the cations in each model will be identical. The same argument is valid for the anion lattice, but only for the x(f) = 0.250 pyrochlore, since here the oxygen ions occupy the ideal fluorite sites.

For the cases x(f) = 0.289 and 0.312 the cation contribution will be the same as above, since x(f) affects only certain oxygen positions. Therefore, the change in the R factors is due entirely to the positional shift of the (f) set oxygen. It should be pointed out that the effect of the oxygen ions on the structure factor will be significant although not large. While the atomic scattering factor of the oxygen ion is small compared to those of the cations, the unit cell contains about 64 atom % oxygen (at the pyrochlore composition) and its contribution to the structure factor is weighted accordingly.

For the x(f) = 0.312 pyrochlore model (curve B in Figure 15), the R factors are consistently greater than those for the random fluorite model at all compositions except 41.8 m/o erbia. There is very little scatter in the R factors.

The x(f) = 0.289 pyrochlore model (curve C, Figure 15) shows generally higher R factors compared to the random fluorite model, but the fit is better than that of the x(f) = 0.312 pyrochlore model. The area of most interest occurs about the pyrochlore composition, 33.3 m/o erbia. At 31.6 m/o erbia, the R factor for the x(f) = 0.289 pyrochlore has dropped below that for the random fluorite model, suggesting that the experimental data are better explained by the x(f) = 0.289 pyrochlore model. At 33.3 m/o erbia the same behavior is noted.

In an attempt to permit maximum ordering within the matrix, a sample containing 33.3 m/o erbia was annealed at 1450°C for 72 hours and furnace cooled. The results of the structure fits for this sample are represented by solid symbols in Figure 15. The separation between the R factors increased as a result of the heat treatment. The R factor for the random fluorite model increased slightly relative to the unannealed sample. At the same time, the x(f) = 0.289 pyrochlore R factor decreased relative to the unannealed sample. The result is a substantially improved fit to the experimental data with the x(f) = 0.289 pyrochlore model.

In general, the R factors are very low, and any one of them, taken by itself, would usually be sufficient to confirm a structure. Therefore, the significance of the differences noted was tested using the significance tests for crystallographic R factors developed by Hamilton (85). The test permits the determination of the level of significance at which one structure model may be rejected in favor of another by comparing the ratio of the respective R factors to a set of numbers that have been derived from the theory of linear hypothesis tests. The set of numbers are dependent on the number of experimental observations, the number of variables in the structure refinement and the significance level of interest. In general, a model is not rejected at a significance level greater than 0.05 (= 5%) (85). A significance level of 0.05, for example, corresponds to rejecting a true model 5% of the time.

The application of this test to the structural data leads to the following conclusions. The x(f) = 0.312 pyrochlore can be rejected relative to the best apparent model at a significance level of about 1%. For samples containing 8.3, 16 and 30 m/o erbia, the best apparent structure model is that of the random fluorite solid solution. For samples containing 31.6 and 33.3 m/o erbia, the best apparent structure is the x(f) = 0.289 pyrochlore. The x(f) = 0.312 pyrochlore is thus eliminated from further consideration.

It remains to compare the random fluorite model with the x(f) = 0.289 pyrochlore. According to the significance tests, neither of the models can be rejected at the acceptable (5%) significance level, with one exception. In the case of the 33.3 m/o erbia sample that was annealed at 1450°C for 72 hours, the random fluorite model can be rejected in favor of the x(f) = 0.289 pyrochlore at a significance level of 0.5%. While the significance test does not confirm either model for the other compositions, a second factor is present that the test cannot assess--a trend. By unambiguously rejecting the random fluorite model for the long-time annealed 33.3 m/o erbia sample, the significance test has legitimized the apparent trend toward ordering which is evident in the other compositions. Thus, this study confirms the existence of ordering within the fluorite domain and is in agreement with Klee and Weitz (27) who detected residual ordering in $Er_2Hf_2O_7$ from a study of its infrared spectra.

At 41.8 m/o erbia, both the x(f) = 0.289 and x(f) = 0.312 pyrochlore models appear to fit the data better than the random fluorite model. According to the significance test, none of the models can be rejected. Nevertheless, some order seems to persist. It should be pointed out that this composition lies between the $M_4O_7$ (pyrochlore) and the $M_4O_6$ (C-type) structure types. The ordering tendency depicted by this composition may reflect the tendency to maintain a structure based on $MO_6$ octahedra which are common structural units in

both structures.

It is not known why the pyrochlore superlattice lines are not observed in the diffraction patterns. One reason may be that, in spite of the predictions of the theoretical calculation (Table 7), the superlattice lines are too weak to be observed.

Electrical conductivity and ordering

The total electrical conductivities of selected compositions spanning the fluorite and erbia solid solution regions were measured as a function of temperature and composition. The purpose of these studies was to search for indications of ordering, particularly in the fluorite phase, similar to that reported by others (45,51,52,53,57,60). The temperature range over which these studies were made was from 800 to 1000°C. Equipment limitations prevented studies at higher temperatures.

Figure 18 is a plot of log $\sigma_T$ vs $1/T(^{\circ}K)$ for compositions from 8.6 to 90 m/o erbia in pure oxygen at 1 atm. The activation energies for conduction were calculated by a least squares linear fit of the data to an Arrhenius equation (see footnote 2, p. 29) and are included in Figure 18. Due to the temperature limitations, the anomaly in the electrical conductivity vs temperature relation reported by others (51,52, 53,57) could not be observed. However, in the course of the study an anomaly was noted in the activation energy vs composition relation shown in Figure 19. The anomaly is apparent as a plateau in the activation energy curve which appears between

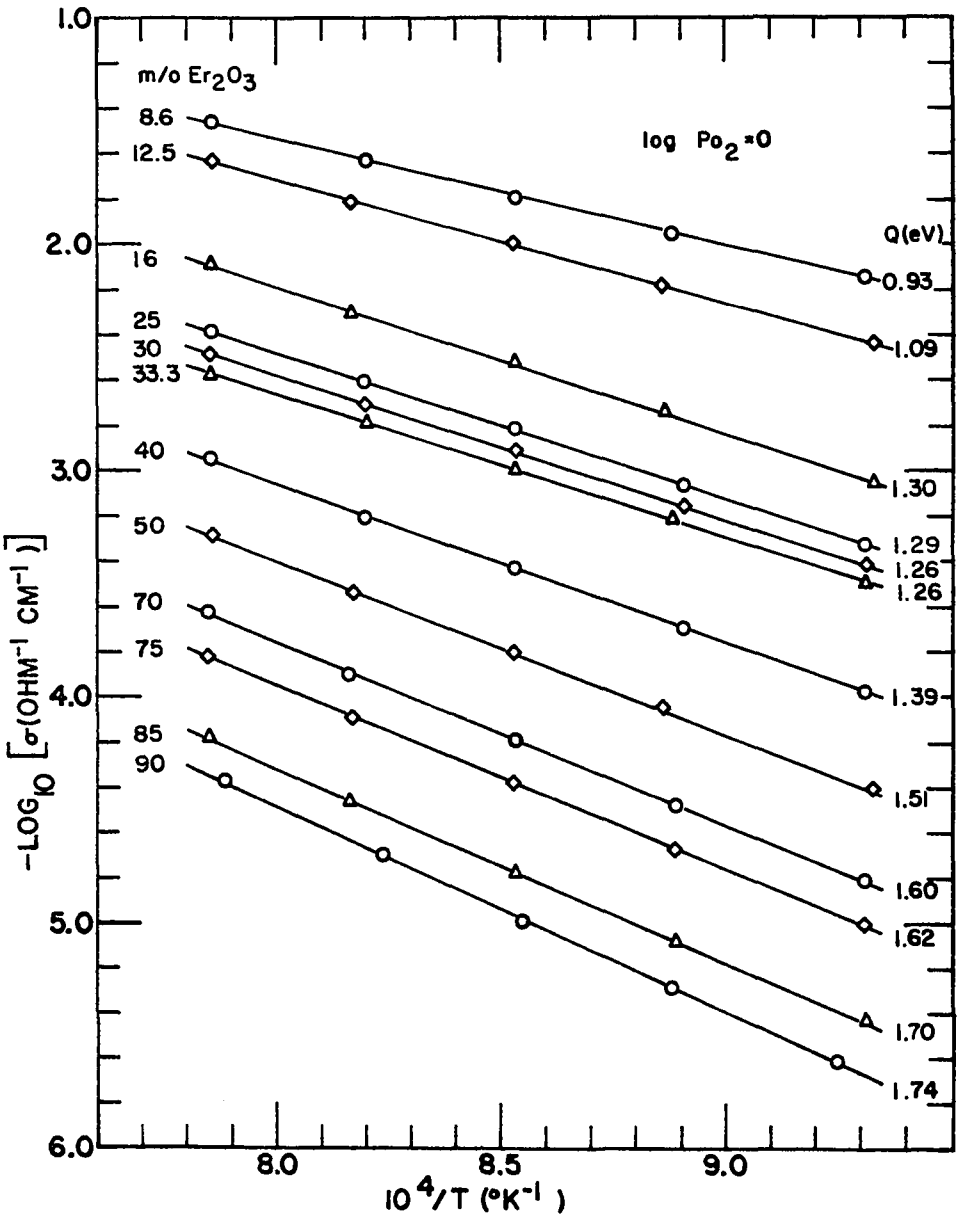


Figure 18. Total conductivity in pure oxygen as a function of temperature for selected compositions in the hafnia-erbia system

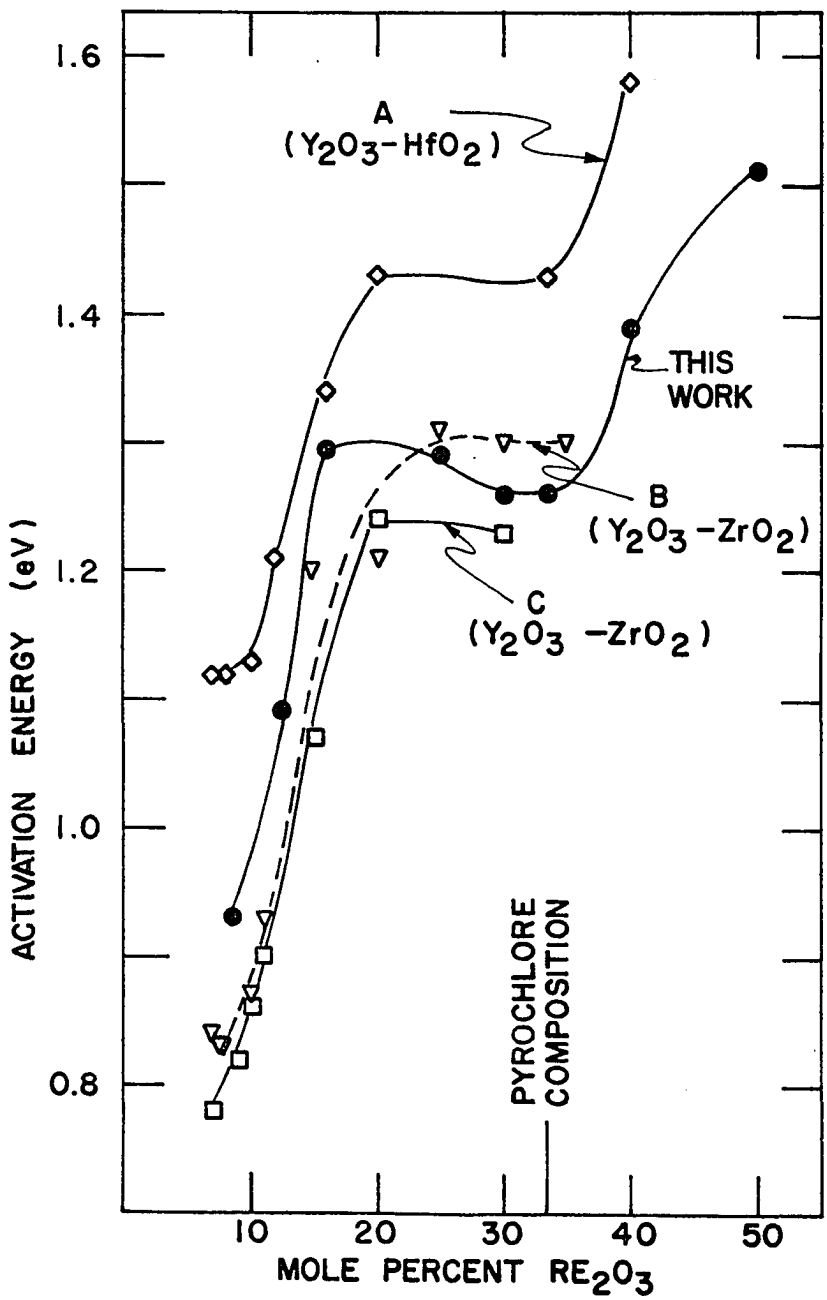


Figure 19. Activation energy for conduction as a function of composition
A. Besson et al. (45);
B. Strickler and Carlson (57);
C. Dixon et al. (56)

16 and 25 m/o erbia and extends through 33.3 m/o erbia. On either side of the plateau, the activation energy increases rapidly with increasing erbia content. A search of the literature disclosed that similar anomalies were recorded but not recognized (45,51,56,57) for analogous $HfO_2(ZrO_2)$-$RE_2O_3$ systems. Several of the activation energy vs composition relations are included in Figure 19. Only in one case (44), was there even mention that an abnormally low activation energy was observed at the pyrochlore composition. Moreover, all the data included in Figure 19 are reported for fluorite phases; there was no X-ray evidence of ordering. The initial increase in the activation energy with stabilizer content has been related by Tien and Subbarao (52) to the larger radius of the stabilizing cation and its effect on the activation complex. However, the activation energy plateau remains to be explained.

An anomaly was also observed in the conductivity vs composition plot shown in Figure 20. The conductivity decreases as erbia content increases, but an inflection is noted around 33.3 m/o erbia, the pyrochlore composition. Similar behavior was observed by Besson et al. (45) in the hafnia-yttria system. They related the anomaly to ordering of the pyrochlore type. Strickler and Carlson (57) did not observe this behavior in the zirconia-yttria system, but they studied samples containing only up to 35 m/o yttria.

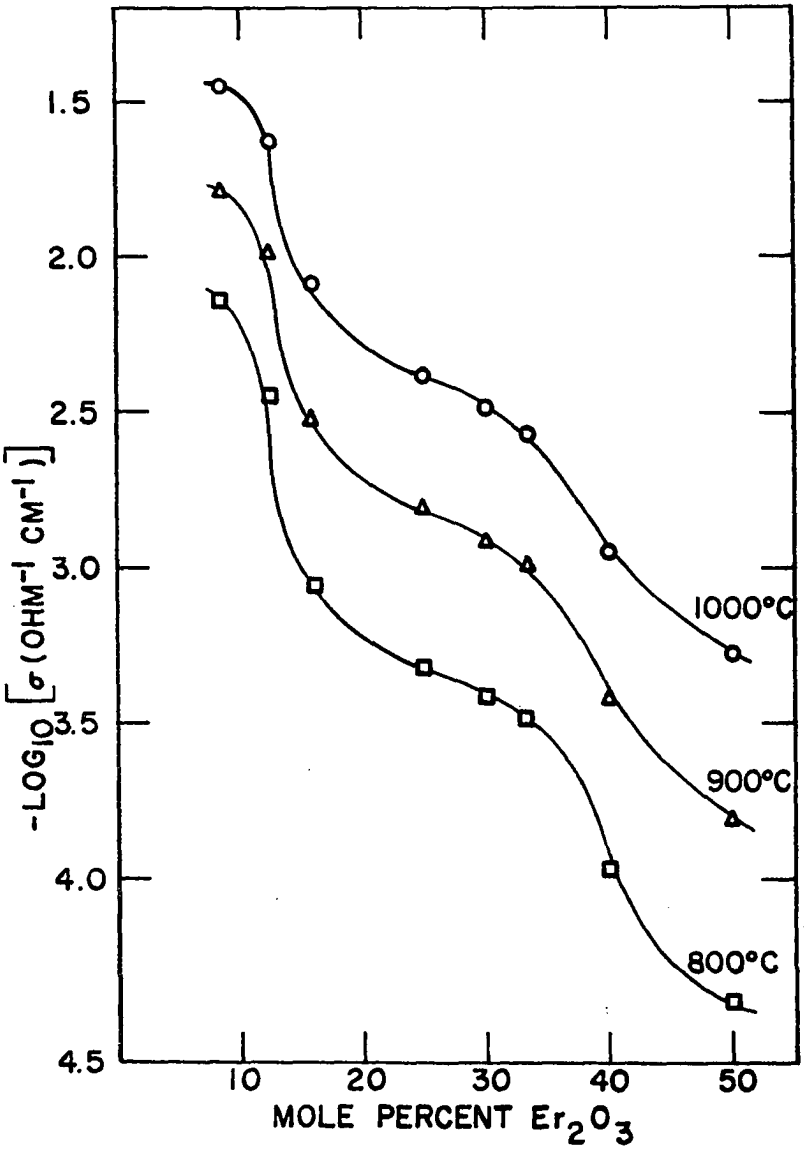


Figure 20. Total conductivity as a function of composition measured in pure oxygen at 1 atm pressure

In his study of the $ZrO_2$-$CaZrO_3$ system, Tien (86) observed both of the anomalies just mentioned. The general features of the anomalies in both Tien's and this study are identical. The important difference is that the anomalies in the $ZrO_2$-$CaZrO_3$ system occur as the sample composition passes from the single-phase fluorite region at 22 m/o CaO into the two-phase region composed of fluorite solid solution and $CaZrO_3$. Tien argues that such behavior should be expected in the two phase region since the composition of the fluorite solid solution is fixed and only the relative amounts of the two phases change.

A similar argument can be made for the hafnia-erbia system, the anomalous behavior being related to the formation of continuous domains based on the pyrochlore structure. The existence of similar domains has already been postulated by Carter and Roth (58) in calcia-stabilized zirconia and Bauerle and Hrizo (60) in the zirconia-yttria system. The grain boundary layer suggested by Bauerle and Hrizo provides a convenient region for a second, continuous, domain to form.

If the electrical conductivity is assumed to occur by migration of oxygen ions as has been reported in analogous systems (56,57), the lowering of the activation energy can be related to the formation of the pyrochlore structure in a qualitative manner. (The question of oxygen ion migration in this system will be discussed later.) The activation energy

may be estimated by Eyring's empirical rule that it is about 1/4 of the energy of the bonds broken in forming the activated complex (78, p. 476). In order to apply this rule, it is necessary to obtain expressions for the relative bonding energies of the oxygen ions in the pyrochlore and random fluorite structures. According to Pauling's (87) electronegativity criterion, bonding in the hafnia-erbia system is predominantly ionic. Pace et al.(88) have found that an ionic model closely characterizes the binding forces in the analogous zirconia-yttria system. If this is true, one approach to estimating the relative bond energies of the oxygen ions involves the concept of the electrostatic bond strength (87) which is defined as

$$S = \frac{n_i}{CN} . \qquad (5)$$

Here S is the bond strength, $n_i$ is the valence of atom i, and CN is its coordination number.

In the following discussion, only first nearest neighbors will be considered in comparing the fluorite and pyrochlore structures at the pyrochlore composition, 33.3 m/o erbia.

In the random fluorite structure, each cation will be surrounded by 7 oxygen ions. Thus the $Hf^{4+}$ electrostatic bond strength is 4/7. In a similar manner, the $Er^{3+}$ electrostatic bond strength is 3/7. For this structure, each oxygen ion is coordinated by four cations, two $Hf^{4+}$ and two $Er^{3+}$ ions on the average, and therefore, each oxygen ion will have four

first nearest neighbor bonds, two of 4/7 and two of 3/7 strength.

In the pyrochlore structure, there are two distinct oxygen sites. The (f) set oxygen (f-oxy) are 6 coordinated about the $Hf^{4+}$ cation and are bonded to two $Hf^{4+}$ and two $Er^{3+}$ cations. The (a) set oxygen (a-oxy) and the $Er^{3+}$ cations are in the holes between the $Hf^{4+}O_6$ octahedra. The $Er^{3+}$ cations are 8 coordinated by two types of oxygen; six f-oxy and two a-oxy. The a-oxy are 4 coordinated by $Er^{3+}$ cations. As above, the electrostatic bond strength of each oxygen bond is found by considering the coordination of oxygen about the cation. In this manner, the f-oxy are found to have two bonds of 2/3 and two bonds of 3/8 strength. The a-oxy have four electrostatic bonds of 3/8 strength.

Since each of the bond strengths is an approximate measure of the cation contribution to the positive potential seen by the oxygen ion (87), a clue to the relative stability of each oxygen site can be obtained by summing the respective electrostatic bonds ($S_i$) to each oxygen ion:

$$\text{f-oxy; } \Sigma S_i = 2[2/3 + 3/8] = 50/24 > 2$$

$$\text{F-oxy; } \Sigma S_i = 2[4/7 + 3/7] = 2$$

$$\text{a-oxy; } \Sigma S_i = 4(3/8) = 12/8 < 2,$$

where F-oxy is used to represent the average oxygen site in the fluorite structure. According to Pauling (87), the sum of the electrostatic bond strengths to an oxygen ion should be

equal to or nearly equal to two. The relative hierarchy of the positive electrostatic potentials at the different sites is a direct indication of the relative stability of the oxygen ions in those sites. The pyrochlore structure contains both the most stable oxygen site (f-oxy) and the least stable oxygen site (a-oxy). The relative stability of the average oxygen site in the random fluorite structure lies between those of the two pyrochlore oxygen sites, but substantially closer to the f-oxy level.

The deviation of the positive potential of the a-oxy site from two is significant (87) and is probably due to the mixed coordination of the $Er^{3+}$ ion; that is, two a-oxy at a distance $d_1$ and six f-oxy at a distance $d_2$ where $d_1 < d_2$. The existence of the $Er^{3+}$ ion and the a-oxy in holes between $HfO_6$ octahedra makes the rigorous application of the electrostatic valence principle difficult. A second approach is to calculate the electrostatic bond strength of the a-oxy in terms of its valence and the four coordinating $Er^{3+}$ ions. In this case, the a-oxy are found to have four bonds of 1/2 strength. Turning to the remaining six f-oxy coordinating the $Er^{3+}$ ion, it is seen that the erbium ion now has an unsatisfied charge of 2+ (since each $Er^{3+}$ ion is coordinated by two a-oxy). Thus the bond strengths of the $Er^{2+}$ to each f-oxy is 1/3, and the f-oxy thus has two bonds of 2/3 strength (from the $Hf^{4+}$ ion as before) and two bonds of 1/3 strength. This is consistent with Pauling's principles since the sum of the electrostatic

bond strengths to each oxygen site is equal to two. The effect of the bond length on the bond strength has also been demonstrated. Of the eight oxygen ions coordinating the $Er^{3+}$ ion, the two closer a-oxy have a stronger bond than the farther-removed f-oxy (1/2 vs 1/3).

The relative hierarchy between the different sites is no longer apparent. However, if it is assumed that the electrostatic bond strengths are approximately proportional to the bond energy, then the bond strengths can be converted to bond energy by a conversion factor $B_i$ and the total bond energy can be obtained by summing the individual values as before. The constants $B_1$ and $B_2$ identify a Hf-O bond and an Er-O bond respectively. The constants can include such quantities as covalency contributions and polarizability as well as repulsion terms required to achieve stability. Furthermore, it is assumed that $B_i$ is characteristic of the cation-anion bond and not the structure. Thus, it is equally applicable in the fluorite or pyrochlore structure. It is also assumed that $|B_1| > |B_2|$. That this is probably true is indicated by comparing such energetic quantities as heats of formation (-266 kcal (89) vs -226.8 kcal (90)), melting points (2825°C vs 2400°C) and the dissociation energies of the gaseous monoxides (7.9 eV (91) vs 6.58 eV (92)) for hafnia and erbia respectively. Thus, the total bond energy of the individual oxygen ions is

$$\text{f-oxy:} \quad E_f = \frac{4}{3} B_1 + \frac{2}{3} B_2,$$

$$\text{F-oxy:} \quad E_F = \frac{8}{7} B_1 + \frac{6}{7} B_2,$$

$$\text{a-oxy:} \quad E_a = 2B_2.$$

The differences between the relative bond energies is given as

$$\Delta E_{f-F} = 4/21 \ (B_1-B_2),$$

$$\Delta E_{F-a} = 8/7 \ (B_1-B_2),$$

$$\Delta E_{f-a} = 4/3 \ (B_1-B_2).$$

Thus, the bond strength hierarchy is established in the same order as before.

The results suggest that the a-oxy are less tightly bound in the pyrochlore structure than either the f-oxy or the oxygen ions in the random fluorite structure, which would account for the observed lower activation energy for conduction. The relative ease with which other anions are substituted for the a-oxy, as discussed earlier (25,26), further supports the idea of a relatively weakly-bound a-oxy.

The anomaly in the conductivity vs composition measurements can also be explained by ordering. In the random fluorite structure, the decrease in the conductivity as stabilizer content increases has been related (52) to the increasing probability of a migrating oxygen ion coming under the influence of an $Er^{3+}$ ion. In the case of ordering of the pyrochlore

type, the migrating oxygen ions will usually be a-oxy type. The surroundings of these oxygen ions are not changed much by varying the erbia content. If the ordering takes place in continuous domains throughout the sample (58,60), then the increasing erbia content would merely increase the extent of the ordered region until, at the pyrochlore composition (33.3 m/o erbia), the entire structure would be ordered. Moreover, increasing the erbia content increases the number of a-oxy as a relatively mobile conducting species. This would be expected to cause an arrest in the conductivity vs composition relation such as was observed experimentally.

It must be emphasized that the foregoing analysis of the relative bond energies is highly artificial and that it is in no way an attempt to develop a bonding scheme. However, as a simple indication of the relative bond strengths of the non-equivalent oxygen sites in the two structures, the analysis presents a useful picture that is consistent with the observed data.

As the erbia content increases above 33.3 m/o, the activation energy was observed to resume its rapidly increasing behavior while the conductivity again decreased. Whether the structure at these compositions is a random fluorite or retains some ordering is not apparent from these data.

The conductivity and its activation energy in the erbia solid solution region are given as a function of composition in Figure 21. The measurements were made in pure oxygen at

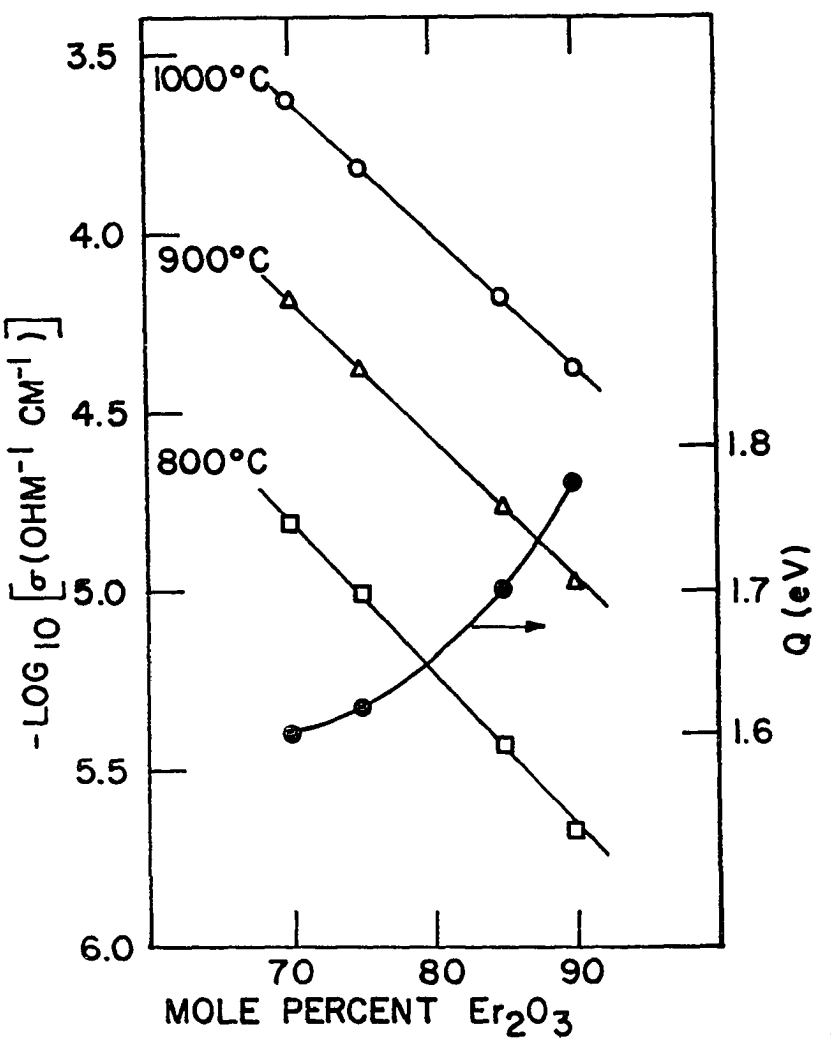


Figure 21. Total conductivity and activation energy for conduction as a function of composition in the erbia solid solution domain

1 atm pressure. In Figure 21, it is seen that the total conductivity increases and the activation energy decreases as the hafnia content increases. In view of the massively defective anion lattice in the C-type structure, the introduction of interstitial anions via hafnia might be expected to decrease the conductivity by blocking the migration paths. Such is not the case. However, the observed behavior is consistent with that discussed for the pyrochlore structure. As in the pyrochlore structure, the C-type structure is composed of oxygen octahedra, but the C-type structure does not contain any additional anions. As the hafnia content increases, the additional oxygen ions occupy interstitial positions as was determined by the density measurements. In fact, however, the interstitial sites in the erbia lattice are like the sites occupied by the a-oxy in the pyrochlore. (Note, however, that the interstitial sites in erbia are not necessarily described by the same spatial coordinates as the (a) positions in the pyrochlore.) Thus, the conductivity increases and activation energy decreases as the interstitial oxygen (pseudo a-oxy) concentration increases. A secondary effect on the observed behavior is probably the dilution of the larger $Er^{3+}$ cations by the smaller $Hf^{4+}$ cations ($r_c$ = 0.89 and 0.78Å respectively).

Implicit in the preceding discussion is the assumption that the total conductivity is due to oxygen ions (no significant electronic contribution) and, therefore, that the con-

ductivity observations can be explained by the oxygen ion behavior in a particular structure. This assumption can be tested by measuring the pressure dependence of the total conductivity. If the total conductivity is insensitive to the oxygen partial pressure in the ambient atmosphere, it is primarily ionic (4).

Figure 22 shows the pressure dependence of the total conductivity at 1000°C. In the fluorite domain (8.6 to 50 m/o erbia) a slight pressure dependence at high oxygen partial pressures is noted at the boundary compositions. However, within the fluorite domain, the conductivities remained unchanged as the oxygen partial pressures were varied. The conductivity of all of the compositions in the erbia solid solution domain exhibited some pressure dependence at high oxygen partial pressures, thus indicating some electronic contribution.

Conductivities measured in controlled $CO_2$-CO mixtures ($\log_{10}P_{O_2}$ = -10 and -14) were lower than those measured with the other gas mixtures. A similar effect was noted previously in the hafnia-yttria system (7). The effect is particularly significant in compositions containing 8.6 and 12.5 m/o erbia. As the erbia content of the samples increases, the effect lessens, until at 90 m/o erbia, it is virtually absent. In general, the effect appears to be more prevalent in the fluorite solid solutions than in the erbia solid solutions.

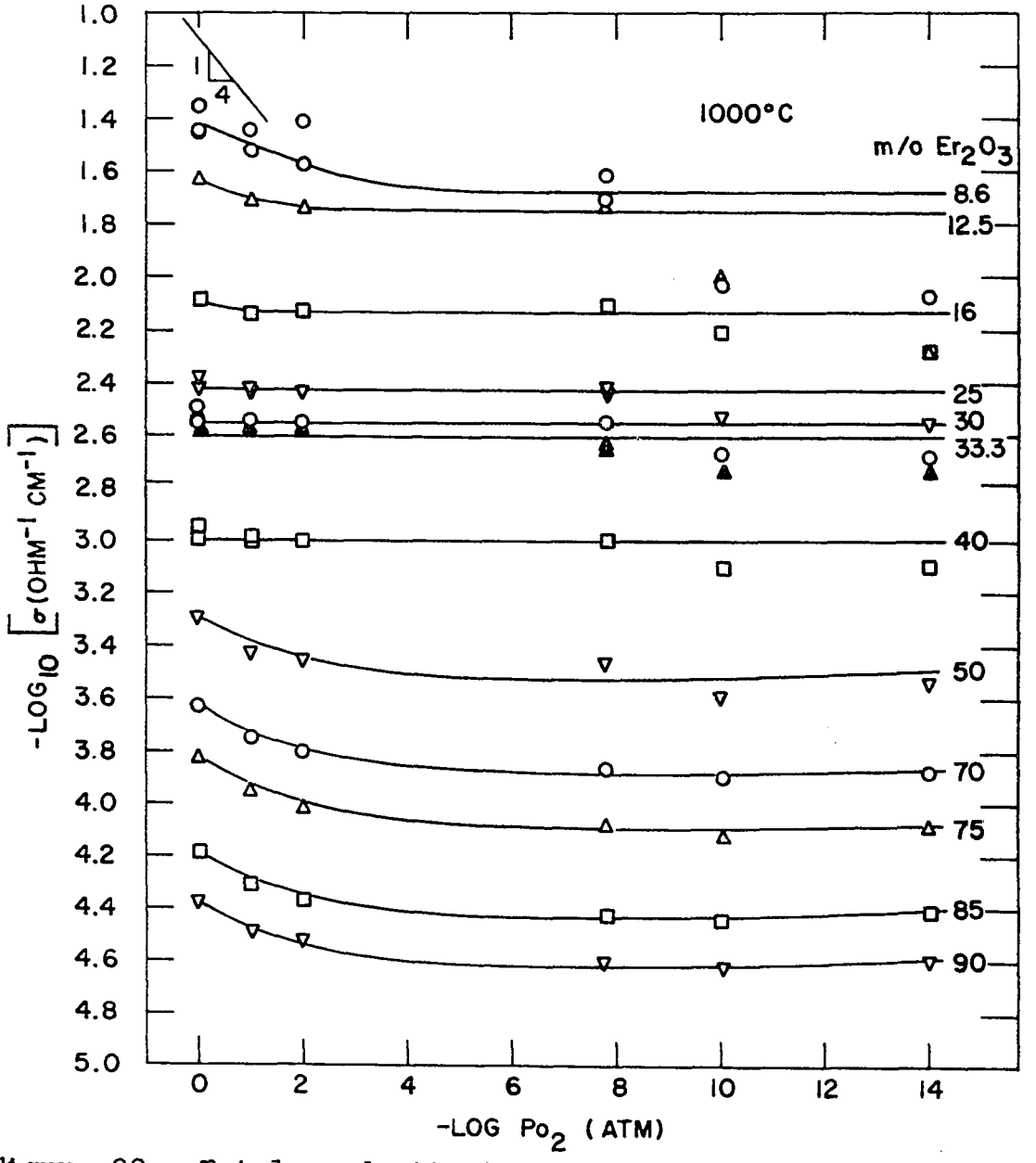


Figure 22. Total conductivity as a function of oxygen partial pressure for fluorite and erbia solid solutions

To determine if the effect truly signaled a departure from ionic conduction, simple open circuit emf measurements (4) were made on samples containing 8.6, 33.3, 50, and 90 m/o erbia. The oxygen partial pressures at the two faces of each sample were fixed at $10^{-6.24}$ and $10^{-10.34}$ atm at 1000°C with $Cu\text{-}Cu_2O$ (93) and Ni-NiO (94) electrodes. The results of these measurements as a function of temperature are given in Figure 23. The measured emfs at 1000°C are slightly lower than the thermodynamic values. There is no evidence of an anomalous effect in the emfs, in particular for the 8.6 m/o erbia sample. The decay in the emf generated by the sample containing 50 m/o erbia is characteristic of the loss of two phase equilibrium at one of the reference electrodes and not a property of the material. The near theoretical emf indicates that the conductivity is virtually all ionic. Finally, according to the X-ray and density studies, only the anion sublattice possesses significant defect (vacancy) concentrations whereas the cation sublattice is completely filled. Hence, cation conductivity must be negligible compared to anion conductivity in this case so that the total conductivity is due only to oxygen ion conduction.

The reason for the decrease in conductivity observed when the oxygen partial pressure is fixed by $CO\text{-}CO_2$ gas ratios is not known. The values obtained for the 8.6 and 33.3 m/o erbia samples suggest that they are solid electrolytes ($t_{ion} > 0.99$)

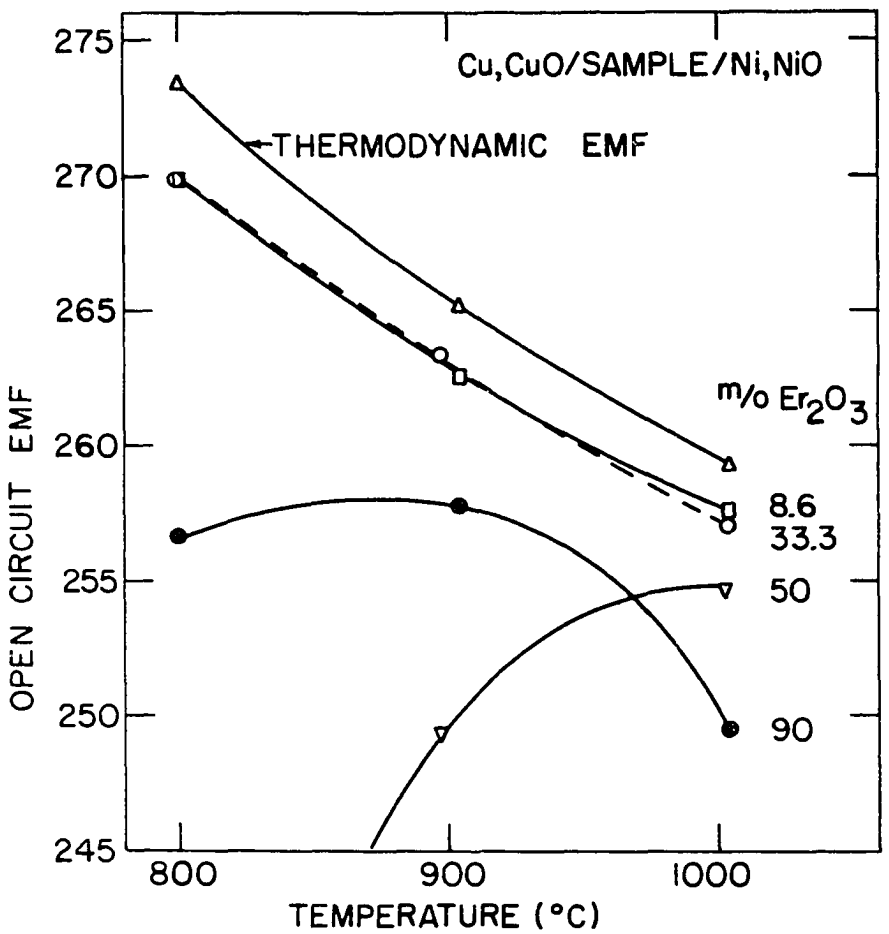


Figure 23. Open circuit emfs as a function of temperature for selected samples

within the oxygen partial pressure range fixed by the electrodes, and may deserve further attention in the future.

# CONCLUSIONS

1. The solubility of erbia in hafnia is less than 1 m/o erbia. The limited solubility that does exist lowers the upper limit of the hafnia monoclinic to tetragonal crystallographic transformation from 1825°C to 1725°C.

2. The hafnia-erbia system is dominated by fluorite and C-type (erbia) solid solutions separated at low temperatures by a two-phase domain. At 1450°C the fluorite solid solution extends from about 9 m/o to 50 m/o erbia. The lower boundary of the erbia solid solution lies at about 73 m/o erbia, but is indefinite. At 1900°C, the fluorite domain extends from 6 m/o to 60 m/o erbia. The boundary on the erbia solid solution domain at this temperature was not determined.

3. The intermediate two-phase domain is composed of fluorite and erbia solid solutions. The evidence suggests that this domain is a domed region and that a continuous solid solution spans the diagram at higher temperatures (>2000°C).

4. The liquidus curve exhibits a maximum of about 2845°C at 20 m/o erbia. A simple eutectic exists at 85 m/o erbia and 2340°C. The melting points of pure hafnia and erbia are 2825 $\pm$ 20°C and 2400 $\pm$ 20°C respectively.

5. As erbium replaces hafnium in the fluorite phase, charge neutrality is maintained by an anion vacancy defect structure. As hafnium is substituted for erbium in the erbia solid solution, charge neutrality is maintained by an anion

interstitial defect structure.

6. X-ray structural analysis of the fluorite phase confirmed ordering on the anion sublattice at 33.3 m/o erbia related to the pyrochlore structure. Evidence also suggests that some residual order remains in the fluorite phase for erbia contents greater than 33.3 m/o.

7. A previously unrecognized anomaly in the activation energy for electrical conduction is indicative of ordering of the pyrochlore type and is related to the oxygen ions in the (a) positions of the pyrochlore structure.

8. Ordering in the fluorite domain is also evidenced by anomalous behavior in the total conductivity vs composition relation.

9. Compositions within the fluorite domain exhibit predominantly ionic conductivity at elevated temperatures as evidenced by the oxygen pressure independence of the total conductivity and also by open circuit emf measurements.

# BIBLIOGRAPHY


1. Wagner, C. Uber den Mechanismus der electrischin Stromleitung im Nernotstift. Naturwissenschaften 31: 265-268. 1943.

2. Hund, F. Die fluoritphase im System $ZrO_2$-CaO. Zeitschrift fur Physikalische Chemie, Leipzig 199: 142-151. 1952.

3. Hund, F. Anomale Mischkristalle im System $ZrO_2$-$Y_2O_3$. Zeitschrift fur Elektrochemie 55: 363-366. 1951.

4. Kiukkola, K. and Wagner, C. Measurements on galvanic cells involving solid electrolytes. Electrochemical Society Journal 104: 379-387. 1957.

5. Buckley, J. D. Deterioration of calcia-stabilized zirconia. NASA TN(Technical Note) D-1595 [National Aeronautics and Space Administration, Washington, D.C.]. 1962.

6. Curtis, C. E., Doney, L. M., and Johnson, J. R. Some properties of hafnium oxide, hafnium silicate, calcium hafnate, and hafnium carbide. American Ceramic Society Journal 37: 458-465. 1954.

7. Schieltz, J. D. Electrolytic behavior of yttria and yttria stabilized hafnia. Unpublished Ph.D. thesis. Ames, Iowa, Library, Iowa State University of Science and Technology. 1970.

8. Buckley, J. D. and Wilder, D. R. Effects of cyclic heating and thermal shock on hafnia stabilized with calcia, magnesia, and yttria. NASA TN (Technical Note) D-5279 [National Aeronautics and Space Administration, Washington, D.C.]. 1969.

9. Ruh, R. and Corfield, P. W. R. Crystal structure of monoclinic hafnia and comparison with monoclinic zirconia. American Ceramic Society Journal 53: 126-129. 1970.

10. Smith, D. K. and Newkirk, H. W. The crystal structure of badeleyite (monoclinic $ZrO_2$) and its relation to the polymorphism of $ZrO_2$. Acta Crystallographica 18: 983-991. 1965.

11. McCullough, J. D. and Trueblood, K. N. The crystal structure of baddeleyite (monoclinic $ZrO_2$). Acta Crystallographica 12: 507-511. 1959.

12. Adam, J. and Rogers, M. D. The crystal structure of $ZrO_2$ and $HfO_2$. Acta Crystallographica 12: 951. 1959.

13. Wolten, G. M. Diffusionless phase transformations in zirconia and hafnia. American Ceramic Society Journal 46: 418-422. 1963.

14. Baun, W. L. Phase transformations at high temperatures in hafnia and zirconia. Science 140: 1330-1331. 1963.

15. Ohnysty, B. and Rose, F. K. Thermal expansion measurements on thoria and hafnia to 4500°F. American Ceramic Society Journal 47: 398-400. 1964.

16. Ruh, R., Garrett, H. J., Domagala, R. F., and Tallan, N. M. The system zirconia-hafnia. American Ceramic Society Journal 51: 23-27. 1968.

17. Teufer, G. Crystal structure of tetragonal $ZrO_2$. Acta Crystallographica 15: 1187. 1962.

18. Stansfield, O. M. Thermal expansion of polycrystalline $HfO_2$-$ZrO_2$ solid solutions. American Ceramic Society Journal 48: 436-437. 1965.

19. Boganov, A. G., Rudenko, V. S., and Makarov, L. P. X-ray investigation of zirconium and hafnium oxides at temperatures up to 2750°. Academy of Sciences of the U.S.S.R. Proceedings Chemistry Section 160: 146-148. 1965.

20. Roth, R. S. and Schneider, S. J. Phase equilibria in systems involving the rare earth oxides. Part 2: Polymorphism of the oxides of the trivalent rare earth ions. National Bureau of Standards Journal of Research 64A: 309-316. 1960.

21. Hyde, B. G., Bevan, D. J. M., and Eyring, L. A structural model of the rare-earth oxides. In International Conference on Electron Diffraction and the Nature of Defects in Crystals. Pp. II C-4-5. New York, New York, Pergamon Press. 1965.

22. Henry, N. F. M. and Lonsdale, K., eds. International tables for X-ray Crystallography. Vol. I. Kynoch Press, Birmingham, England. 1952.

23. Fert, A. Structure of some rare earths. Societe Francaise de Mineralogie et de Cristallographie Bulletin 85: 267-270. 1962. Original not available; abstracted in Chemical Abstracts 58: 3973b. 1963.

24. Foex, M. and Traverse, J. Etude a haute temperature des transformations allotropiques des sesquioxydes d'yttrium, d'erbium et de thulium. Academie des Sciences Comptes Rendus, Serie C, 267: 2490-2493. 1965.

25. Aleshin, E. and Roy, R. Crystal chemistry of pyrochlore. American Ceramic Society Journal 45: 18-25. 1962.

26. Palache, C., Berman, H., and Frondel, C. Dana's System of Minerology. 7th ed. Vol. I. Pp. 748-757. John Wiley and Sons, Inc., New York, New York. 1944.

27. Klee, W. E. and Weitz, G. Infrared spectra of ordered and disordered pyrochlore-type compounds in the series $RE_2Ti_2O_7$, $RE_2Zr_2O_7$ and $RE_2Hf_2O_7$. Journal of Inorganic Nuclear Chemistry 31: 2367-2372. 1969.

28. Roth, R. S. Pyrochlore-type compounds containing double oxides of trivalent and tetravalent ions. National Bureau of Standards Journal of Research 56: 17-25. 1956.

29. Bradley, F. N. $Pb_2Ti_2O_5F_2$, a new pyrochlore. American Ceramic Society Journal 52: 114. 1969.

30. Bystrom, A. X-ray analysis of $Ca_2Sb_2O_7$ and compounds of similar composition. Arkiv For Kemi, Mineralogi Och Geologi 18A (N:O 21): 1-8. 1944.

31. Rouanet, A. Diagrammes de solidification et diagrammes de phases de haute temperature des systemes zircone-oxyde d'erbium, zircone-oxyde d'yttrium et zircone-oxyde d'ytterbium. Academie des Sciences Comptes Rendus, Serie C, 267: 1581-1584. 1968.

32. Stewart, R. K. and Hunter, O., Jr. Stabilization of zirconia by erbia additions. To be published in the American Ceramic Society Journal. 1970.

33. Spitsbergen, U. and Houpt, P. M. Zirconia solid solutions with rare earth oxides. In Steward, G. H., ed. Science of Ceramics. Vol. 4. Pp. 247-254. Original not available; abstracted in Chemical Abstracts 70: 60408m. 1969.

34. Kalinovskaya, G. A., Spiridonov, F. M., and Komissarova, L. N. Phase equilibria in the $HfO_2$-$Sc_2O_3$ system. Journal of the Less-Common Metals 17: 151-159. 1969.

35. Radzewitz, H. Festkverperchemische untersuchungen ueber die systeme $SeO_{1.5}$-$ZrO_2(HfO_2)$, $AmO_{1.5}$-$ZrO_2(HfO_2,ThO_2)$ - $O_2$ und $TiO_2$-$NpO_2(PuO_2)$. U.S. Atomic Energy Commission Report KFK-433 [Kernforschungszentrum, Karlsruhe (West Germany)]. 1966.

36. Delamarre, C. and Perez y Jorba, M. Le systeme chaux-oxyde de hafnium. Revue Internationale des Hautes Temperatures et des Refractaires 2: 313-315. 1965.

37. Komissarova, L. N., Ken-shih, W., Spitsyn, V. I., and Simanov, Yu. P. The $HfO_2$-$La_2O_3$ system. Russian Journal of Inorganic Chemistry 9: 383-386. 1964.

38. Isupova, E. N., Glushkova, V. B., and Keler, E. K. Study of the $HfO_2$-$Sm_2O_3$ system in the solid phases, in the $HfO_2$-enriched region. Inorganic Materials 4: 334-339. 1968.

39. Warshaw, I. and Roy, R. Polymorphism of the rare earth sesquioxides. Journal of Physical Chemistry 65: 2048-2051. 1961.

40. Spiridinov, F. M., Stepanov, V. A., Komissarova, L. N., and Spitsyn, V. I. The binary system $HfO_2$-$Gd_2O_3$. Journal of Less-Common Metals 14: 435-443. 1968.

41. Isupova, E. N., Glushkova, V. B., and Keler, E. K. Study of the $Gd_2O_3$-$HfO_2$ system in the region rich in hafnium dioxide. Inorganic Materials 4: 1511-1515. 1968.

42. Perez y Jorba, M. Contribution a l'etude des systemes zircone-oxydes de terres rares. Annales de Chimie 7: 479-511. 1962.

43. Isupova, E. N., Glushkova, V. B., and Keler, E. K. The $Y_2O_3$-$HfO_2$ system in the region rich in hafnium dioxide. Inorganic Materials 5: 1658-1661. 1968.

44. Caillet, M., Deportes, C., Robert, G., and Vitter, G. Etude structurale dans le systeme $HfO_2$-$Y_2O_3$. Revue International des Hautes Temperatures et des Refractaires 4: 269-271. 1967.

45. Besson, J., Deportes, C., and Robert, G. Conductibilite electrique dans le systeme oxyde de hafnium-oxyde d' yttrium a haute temperature. Academie des Sciences Comptes Rendus, Serie C, 262: 527-530. 1966.

46. Komissarova, L. N., Spiridonov, F. M., and Spitsyn, V. I. Regularities in changes of composition and structure of compounds in the systems $HfO_2(ZrO_2)$-$M_2O_3$. Academy of Sciences of the U.S.S.R. Proceedings Chemistry Section 181: 691-693. 1968.

47. Belyaev, I. N. and Artamonova, S. M. Certain physical-chemical properties of combined precipitated hydroxides of holmium and zirconium and holmium and hafnium. Inorganic Materials 5: 76-77. 1969.

48. Roth, R. S. Pyrochlore-type compounds containing double oxides of trivalent and tetravalent ions. National Bureau of Standards Journal of Research 56: 17-25. 1956.

49. Komissarova, L. N., Spitsyn, V. I., and Ken-Shih, W. Lanthanum and neodymium hafnates. Academy of Sciences of the U.S.S.R. Proceedings Chemistry Section 150: 464-466. 1963.

50. Komissarova, L. N., Ken-Shih, W., and Spitsyn, V. I. Reaction of hafnium hydroxide with the hydroxides of yttrium, lanthanum, neodymium and ytterbium. Academy of Sciences of the U.S.S.R. Bulletin Division of Chemical Science No. 1: 1-7. 1965.

51. Strickler, D. W. and Carlson, W. G. Electrical conductivity in the $ZrO_2$-rich region of several $M_2O_3$-$ZrO_2$ systems. American Ceramic Society Journal 48: 286-289. 1965.

52. Tien, T. Y. and Subbarao, E. C. X-ray and electrical conductivity study of the fluorite phase in the system $ZrO_2$-CaO. The Journal of Chemical Physics 34: 1041-1047. 1963.

53. Subbarao, E. C. and Sutter, P. H. Order-disorder and ionic conductivity in cubic $ZrO_2$-CaO. Journal of Physics and Chemistry of Solids 25: 148-150. 1964.

54. Garvie, R. C. The cubic field in the system CaO-$ZrO_2$. American Ceramic Society Journal 51: 553-556. 1968.

55. Pyatenko, Yu. A. The crystal-chemical interpretation of some intermediate phases in the CaO-$HfO_2$ ($ZrO_2$) and $TR_2O_3$-$TiO_2(ZrO_2)$ systems. Academy of Sciences of the U.S.S.R. Proceedings Chemical Technology Section 173: 39-41. 1967.

56. Dixon, J. M., LaGrange, L. D., Merten, U., Miller, C. F., and Porter, J. T., II. Electrical resistivity of stabilized zirconia at elevated temperatures. Electrochemical Society Journal 110: 276-280. 1963.

57. Strickler, D. W. and Carlson, W. G. Ionic conductivity of cubic solid solutions in the system $CaO-Y_2O_3-ZrO_2$. American Ceramic Society Journal 47: 122-127. 1964.

58. Carter, R. E. and Roth, W. L. Conductivity and structure in calcia-stabilized zirconia. In Alcock, C. B., ed. Electromotive force measurements in high-temperature systems. Pp. 125-144. New York, New York, American Elsevier Publishing Company, Inc. 1968.

59. Smith, D. K. The nonexistence of yttrium zirconate. American Ceramic Society Journal 49: 625-626. 1966.

60. Bauerle, J. E. and Hrizo, J. Interpretation of the resistivity temperature dependence of high purity $(ZrO_2)_{0.90}(Y_2O_3)_{0.10}$. Journal of Physics and Chemistry of Solids 30: 565-570. 1969.

61. Barker, W. W. Statistical aspects of gross anion substoichiometry in fluorite-related systems. Materials Science and Engineering 2: 208-212. 1967.

62. Berard, M. F., Wirkus, C. D., and Wilder, D. R. Diffusion of oxygen in selected monocrystalline rare earth oxides. American Ceramic Society Journal 51: 643-647. 1968.

63. Hess, J. B. A modification of the Cohen procedure for computing precision lattice constants from powder data. Acta Crystallographica 4: 209-215. 1950.

64. Vogel, R. E. and Kempter, C. P. A mathematical technique for the precision determination of lattice parameters. Acta Crystallographica 14: 1130-1134. 1961.

65. Cullity, B. D. Elements of X-ray diffraction. Reading, Massachusetts, Addison-Wesley Publishing Company, Inc. 1956.

66. Busing, W. R., Martin, K. O., and Levy, H. A. OR FLS, a FORTRAN crystallographic least-squares program. U.S. Atomic Energy Commission Report ORNL-TM-305 [Oak Ridge National Laboratory, Tenn.]. 1962.

67. Cromer, D. T. and Waber, J. T. Scattering factors computed from relativistic Dirac-Slater wave functions. U.S. Atomic Energy Commission Report LA-3056 [Los Alamos Scientific Laboratory, N.M.]. 1964.

68. Tokonami, M. Atomic scattering factor for $O^{2-}$. Acta Crystallographica 19: 486. 1965.

69. Cromer, D. T. Anomalous dispersion corrections computed from self-consistent field relativistic Dirac-Slater wave functions. Acta Crystallographica 18: 17-23. 1965.

70. Intrater, J. and Hurwitt, S. High temperature, high vacuum, diffractometer attachment. Review of Scientific Instruments 32: 905-906. 1961.

71. Smith, D. K. Techniques of high-temperature X-ray diffraction using metal ribbon furnaces. Norelco Reporter 10: 19-29. 1963.

72. Ostertag, W. and Fischer, G. R. Temperature measurements with metal ribbon high temperature X-ray furnaces. Review of Scientific Instruments 39: 888-889. 1968.

73. Sherwood, E. M. Determination of thermophysical properties. In Campbell, I. E. and Sherwood, E. M., eds. High-temperature materials and technology. Pp. 880-988. New York, New York, John Wiley and Sons, Inc. 1967.

74. Stimson, J. F. International Practical Temperature Scale of 1948. Text revision of 1960. National Bureau of Standards Journal of Research, Section A, 65: 139-145. 1961.

75. Statton, W. O. The phase diagram of the $BaO$-$TiO_2$ system. The Journal of Chemical Physics 19: 33-40. 1951.

76. Gubareff, G. G., Janssen, J. E., and Torborg, R. H. Thermal radiation properties survey. 2nd ed. P. 181. Minneapolis, Minnesota, Honeywell Research Center. 1960.

77. Schneider, S. J. Compilation of the Melting Points of the Metal Oxides. U.S. National Bureau of Standards Monograph 68. 1963.

78. Darken, L. S. and Gurry, R. W. Physical chemistry of metals. New York, New York, McGraw-Hill Book Company, Inc. 1953.

79. Yvon, K., Jeitschko, W., and Parthe, E. A FORTRAN IV program for the intensity calculation of powder patterns. (1969 version). Laboratory for Research on the Structure of Matter, University of Pennsylvania, Philadelphia, Pennsylvania. 1969.

80. Fehrenbacher, L. L. and Jacobson, L. A. Metallographic observations of the monoclinic-tetragonal phase transformation in $ZrO_2$. American Ceramic Society Journal 48: 157-161. 1965.

81. Foex, M. Etude des points de solidification des oxydes et des chromites de terres rares. Academis des Sciences Comptes Rendus, Serie C, 260: 6389-6392. 1965.

82. Noguchi, T., Mizuno, M., and Kozuka, T. Freezing point measurements on metal oxides with a solar furnace. Kogyo Kagaku Zasshi 69: 1705-1709. 1966. Original not available; abstracted in Chemical Abstracts 68: 98960q. 1968.

83. Bratton, R. J. Defect structure of $Y_2O_3$-$ZrO_2$ solid solutions. American Ceramic Society Journal 52: 213. 1969.

84. Diness, A. Phase equilibria and point defect description in the systems $La_2O_3$-$ThO_2$, $Gd_2O_3$-$ThO_2$, $Yb_2O_3$-$ThO_2$ and CaO-$ZrO_2$. Unpublished Ph.D. thesis. University Park, Pennsylvania, Library, Pennsylvania State University. 1967.

85. Hamilton, W. C. Significance tests on the crystallographic R factor. Acta Crystallographica 18: 502-510. 1965.

86. Tien, T. Y. Electrical conductivity in the system $ZrO_2$-$CaZrO_3$. American Ceramic Society Journal 47: 430-433. 1964.

87. Pauling, L. The nature of the chemical bond. 3rd ed. Ithaca, New York, Cornell University Press. 1960.

88. Pace, N. G., Saunders, G. A., Sumengen, Z., and Thorp, J. S. The elastic constants and interatomic binding in yttria-stabilized zirconia. Journal of Materials Science 4: 1106-1110. 1969.

89. Wicks, C. E. and Block, F. E. Thermodynamic properties of 65 elements--their oxides, halides, carbides and nitrides. U.S. Bureau of Mines Bulletin 605. 1963.

90. Westrum, E. F. and Justice, B. H. Thermophysical properties of the lanthanide oxides. III. Heat capacities, thermodynamic properties, and some energy levels of dysprosium(III), holmium(III), and erbium(III) oxides. Journal of Physical Chemistry 67: 659-665. 1963.

91. Panish, M. B. and Reif, L. Thermodynamics of the vaporization of Hf and $HfO_2$: dissociation energy of HfO. Journal of Chemical Physics 38: 253-256. 1963.

92. Ames, L. L., Walsh, P. N., and White, D. Rare earths. IV. Dissociation energies of the gaseous monoxides of the rare earths. Journal of Physical Chemistry 71: 2707-2718. 1967.

93. Rizzo, F. E., Bidwell, L. R., and Frank, D. E. The standard free energy of formation of cuprous oxide. Metallurgical Society of the American Institute of Mining, Metallurgical, and Petroleum Engineers Transactions 239: 593-596. 1967.

94. Steele, B. C. H. High-temperature thermodynamic measurements involving solid electrolyte systems. In Alcock, C. B., ed. Electromotive Force Measurements in High-temperature Systems. Pp. 3-27. New York, New York, American Elsevier Publishing Company, Inc. 1968.

## ACKNOWLEDGEMENTS

The author wishes to thank Dr. D. R. Wilder who has guided both the experimental work and the preparation of this dissertation. Sincere gratitude is extended to Dr. J. W. Patterson and Dr. J. D. Schieltz for their helpful discussions during the course of this investigation. Thanks are due to Miss Verna Thompson who did an excellent job of typing this dissertation within a stringent time schedule. Most of all, the author thanks his wife, Carolyn.